A PULSE COMPRESSION RADAR SYSTEM

FOR HIGH-RESOLUTION IONOSPHERIC SOUNDING

A thesis presented for the degree of

Doctor of Philosophy in Physics

in the University of Canterbury,

Christchurch, New Zealand.

by

S.H. Krenek

1977

CONTENTS

LIST OF FIGURES

ABSTRACT

A low frequency pulse compression radar system, capable of
0.75 km spatial resolution, has been developed. This system
utilizes a linear frequency-modulated signal, and yields an
effective peak power enhancement of 14.5 dB, over a conventional
radar of equivalent resolution.

The required instrumentation, as well as the development
of the necessary signal processing software, are described in
detail. It is shown that the resolution and peak power enhance-
ment achieved by the system are consistent with those predicted
by theory.

The effectiveness of the pulse compression radar as a tool
for ionospheric observation is demonstrated by comparing its
performance to that of a conventional radar operating simul-
taneously.

LIST OF TABLES

CHAPTER 1

INTRODUCTION

1.1 IONOSPHERIC OBSERVATION RADARS

Radar techniques have been widely used in the study of the ionosphere for many years, principally as a means of obtaining data relating to electron density profiles in the D-, E- and F-regions of the ionosphere. Conventional ionosondes presently in use employ pulsed radio-frequency emissions with peak powers typically in the tens of kilowatts, this power being sufficient to provide total reflection echoes having an adequate signal-to-noise ratio.

There are, however, certain applications which require the sounding pulses to contain substantially greater energy. One example concerns studies of the D-region, where the echo is caused by partial reflection processes (Gardiner and Pawsey, 1953). The total energy contained in a pulse is clearly the product of the peak power of the pulse, and its temporal length (or 'pulse width'). This energy may therefore be increased by increasing either, or both, of these factors.

To increase the peak power output of a transmitter is always expensive, and, in extreme instances, is not technically feasible. Further, the use of transmitters having very high peak powers can result in cross modulation effects which alter the structure of the ionosphere itself.

On the other hand, an increase in the width of the transmitted pulse is easily accomplished; however, the spatial resolving power, σ, of a pulse is directly related to its width,

according to the relation

$$\sigma = \frac{c\tau}{2} \qquad (1.1)$$

where τ is the pulse width

c is the speed of electromagnetic radiation.

Thus an increase in the pulse width effects a corresponding degradation in the spatial resolution of the radar system.

Radar studies of the ionosphere are conducted at a field station of the University of Canterbury, situated at Birdling's Flat, near Christchurch. Interest has been shown in investigating the fine structures of electron density irregularities which give rise to radar echoes from the ionospheric D-region. Such a study would require a radar system capable of a high resolution. Also, since D-region partial reflections are characteristically weak, the energy contained in the sounding pulses should be maximised. These two requirements are clearly in conflict, and a project was initiated to resolve this dilemma.

1.2   THE DEVELOPMENT OF PULSE COMPRESSION

The conflict between high pulse-energy and good resolving power is by no means restricted to ionospheric sounding radars, and in fact was first investigated by engineers faced with the shortcomings of the military radars in use during World War II. It was well known that the bandwidth, Δf, of a pulsed radio-frequency signal was directly related to its pulse width, according to the Fourier relationship

$$\Delta f \approx \frac{1}{\tau} \qquad (1.2)$$

An inverse relationship thus exists between the resolving power and bandwidth of a radar signal, of the form

$$\sigma = \frac{c}{2\Delta f} \qquad\qquad (1.3)$$

The key to the solution of the energy-versus-resolution dilemma lay in the realisation that it is the bandwidth, and not the pulse width, which <u>fundamentally</u> determines the potential resolving power of a signal. This fact was recognised independently by several workers serving on both sides of the war. In this regard, Hüttman (1940) was issued a German patent covering his work during the late 1930's. Sproule and Hughes (1948) were granted British patents, and later Dicke (1953) and Darlington (1954) received American patents, all of these relating to work accomplished during the final years of the war.

The methods described in these patents all proposed the transmission of a wide pulse, the frequency of which was varied linearly throughout its duration. By virtue of its width, this 'linear frequency-modulated' pulse would contain a high energy. Moreover, it seemed intuitively obvious that, as a consequence of the wide bandwidth over which the frequency was 'swept', good resolving power should be attainable with this signal.

There are two instances which are known to occur in nature which lend support to this hypothesis. The following is paraphrased from a report on the ultrasonic emissions of bats (Griffin, 1950)

"The bat emits a series of ultrasonic pulses about two milliseconds

in width, at a repetition frequency of 10 to 20 Hz. The most striking

feature is that the frequency of the pulse is not constant, but

varies over the pulse width from typically 78 KHz to 30 KHz. Moreover

the length of a two millisecond pulse in air is about 70 cm,

suggesting that the bat must make use of the frequency modulation

inherent in the pulse to indicate target distance, since bats have no

difficulty locating food and obstacles by accoustic means even at

5 cm."

In his book "The Mind of the Dolphin" (Lilly, 1967) the author

describes the complex sonar of *Tursiops truncatus*, a species of

dolphin possessing a level of intelligence approaching, if not

surpassing that of *Homo sapiens*. Experiments with these animals

indicate that they employ a number of different sonar signals,

one in particular consisting of a pulse about 0.3 seconds long,

rising in frequency from about 5 KHz to 25 KHz. The dolphin is

observed to use this signal for observing close objects, making

the transmitted pulse long enough to overlap with the received

echoes. Lilly suggests that such a situation would produce beat

notes of a constant frequency between the transmitted and

received signals, enabling the dolphin to make an accurate

determination of target range. Though the transmitted pulse

is hundreds of meters in length, resolutions as low as 7 cm

would be obtainable using this technique.

Early workers in the field intended that the latent high

resolving power inherent in the linear frequency-modulated

pulse be exploited by passing the received radar echo through a

filter having a linear time-delay versus frequency character-

istic. This filter would delay one end of the received pulse

more than the other, causing the pulse to 'compress' in time,

and hence increase in amplitude due to conservation of energy.

This last effect was responsible for the name 'Pulse Compression'

becoming generally used to describe the technique outlined in

this section.

A complete description of the theory of pulse compression was originally published in a comprehensive paper by Klauder et al. (1960). Included in this report were treatments of both optimum ('matched filter') and practical means for compressing the received radar echoes. Klauder also introduced the appellation 'chirp' to describe a linear frequency-modulated pulse, and this terminology will be adopted throughout this thesis.

1.3 SCOPE OF THIS WORK

Pulse compression techniques have previously been employed to enhance ionospheric observation radars. A comprehensive study (Wipperman, 1967) established the feasibility of utilising pulse compression techniques to enhance radars used in ionospheric work. Barry and Fenwick (1965), and more recently Rinnert et al. (1976) used a pulse compression method enabling the use of low transmitter powers for D-region studies, while as early as 1954, Gnanalingum (1954) used what is effectively a pulse compression system, later adopted by Titheridge (1962).

It seems clear, therefore, that the use of pulse compression would be a viable means of overcoming the energy-versus-resolution problems associated with a study of the fine structure of ionospheric irregularities. Since the configuration of any pulse compression radar system is dependent both on the intended application, and practical factors relating to the particular installation, much of the specific design work must be done from first principles; this in itself is a task of considerable magnitude. The primary aim of this work was therefore to design and construct a pulse compression radar system suitable for ionospheric work, which would make best use

of the available resources at the Birdling's Flat field station.
Part of the design philosophy adopted was that the system be,
as far as possible, compatible with the instrumentation already
existing at that site.

A major achievement during the course of this work was the
design of a highly-linear frequency-modulated pulse generator,
which utilized only digital circuit elements. A novel approach
to the implementation of the compression filter was also
developed, offering distinct advantages over previously reported
systems.

In the next chapter a rigorous mathematical treatment of
pulse compression is presented. This is followed by a brief
description of the field station at Birdling's Flat, and a
statement of the design goals for the proposed system. The
design and construction of the instrumentation and software
required to implement the system are then reported in detail.
Finally, an evaluation of the completed system is given,
including the presentation of a number of ionospheric returns
obtained with the pulse compression system.

CHAPTER 2

MATHEMATICAL FOUNDATION OF PULSE COMPRESSION

2.1 INTRODUCTION

This chapter contains the formal mathematics of the pulse compression method. Underlying the development which follows is the premise that the potential resolving power of a radar signal is dependent solely on the bandwidth of the transmitted signal (and thus independent of its pulse width).

The signal considered during the development is the linear frequency-modulated, or 'chirp' pulse, introduced in the previous chapter. It should, however, be recognised that linear frequency modulation is only one of a number of modulation schemes capable of producing a pulse of the required bandwidth. The signal is also assumed to have a rectangular amplitude envelope, since this maximises the energy contained in each pulse.

The treatment of pulse compression first considers the frequency content of the linear FM pulse (often called the 'expanded' pulse, to distinguish it from the 'compressed' pulse appearing after signal processing). From this frequency content is derived the form of the optimum signal processing filter. Finally, an expression for the signal at the output of this filter (i.e. the compressed pulse) is developed.

2.2 THE LINEAR FM EXPANDED PULSE

The expanded pulse is shown diagrammatically in Fig. 2.1. The instantaneous frequency of the pulse is centred upon f_0, varying linearly throughout the duration of the pulse from
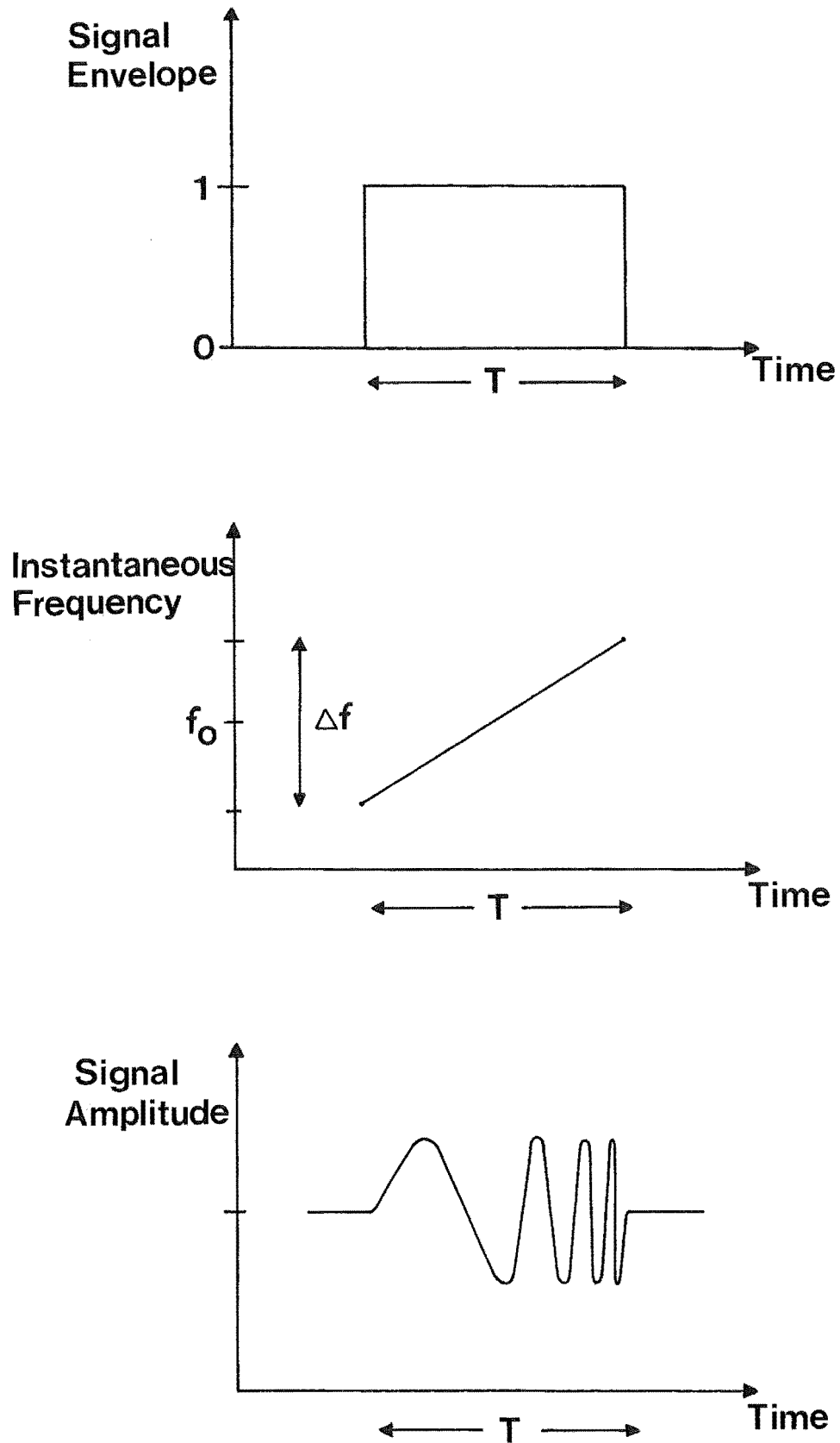
Fig. 2.1: Characteristics of a linear FM pulse.

$f_0 - \Delta f/2$ to $f_0 + \Delta f/2$. The mathematical expression for such a signal is

$$e(t) = rect(\frac{t}{T}) \; exp\{2\pi i (f_0 t + \frac{kt^2}{2})\} \qquad (2.1)$$

where f_0 is the centre frequency of the signal

  T is the pulse width in seconds

  k is the rate of frequency modulation.

The function rect(z) (Woodward, 1953) is defined as

$$rect(z) = 1 \quad if \quad |z| \leq \frac{1}{2}$$

$$rect(z) = 0 \quad if \quad |z| > \frac{1}{2}$$

This function provides the signal with a rectangular envelope between $t = -T/2$ and $t = +T/2$. The signal is arbitrarily chosen to have unit amplitude.

As usual the actual signal is obtained by taking the real part of the complex expression given in equation (2.1). The phase, ϕ, of e(t) is of course given by

$$\phi = 2\pi(f_0 t + \frac{kt^2}{2}) \qquad (2.2)$$

and the instantaneous frequency, f_i, at any particular time is found from

$$f_i = \frac{1}{2\pi} \frac{d\phi}{dt} = f_0 + kt \qquad (2.3)$$

Equation (2.3) shows that the signal contains the desired linear FM property, since during the T-second interval of the pulse, the frequency varies linearly from $f_0 - \frac{kT}{2}$ to $f_0 + \frac{kT}{2}$.

The frequency deviation (or 'swept bandwidth'), Δf, of the signal is just the difference between these two limits, i.e.

$$\Delta f = kT \qquad (2.4)$$

It is thus demonstrated that the signal $e(t)$ possesses the characteristics shown in Fig. 2.1. However, since the signal is limited in time, the actual frequency content of each pulse will not be adequately specified by equation (2.3); a complete description of the spectrum of the signal can only be obtained by Fourier analysis.

If $A(f)$ denotes the Fourier transform of some arbitrary time function $a(t)$, then the Fourier transform of equation (2.1) will be given by

$$E(f) = \int_{-\infty}^{\infty} e(t) \exp\{-2\pi i f t\} dt$$

$$= \int_{-T/2}^{T/2} \exp\{2\pi i (f_o - f) t + \frac{kt^2}{2}\} dt \qquad (2.5)$$

It can be shown (Chin and Cook, 1959) that this integral has a solution

$$E(f) = \sqrt{\frac{T}{2\Delta f}} \exp\{-i\pi(f-f_0)^2/k\} [Z(u_2) - Z(u_1)] \qquad (2.6)$$

where $Z(u)$ is the complex Fresnel integral, defined as

$$Z(u) = C(u) + iS(u) = \int_0^u \exp\{i\pi\alpha^2/2\} d\alpha \qquad (2.7)$$

The arguments of the Fresnel integrals are

$$u_1 = -2(f-f_0)\left[\sqrt{\frac{T}{2\Delta f}} - \sqrt{\frac{T\Delta f}{2}}\right]$$

$$u_2 = -2(f-f_0)\left[\sqrt{\frac{T}{2\Delta f}} + \sqrt{\frac{T\Delta f}{2}}\right] \qquad (2.8)$$

The amplitude spectrum of e(t) is obtained by taking the absolute value of equation (2.6):

$$|E(f)| = \sqrt{\frac{T}{2\Delta f}}\,|Z(u_2) - Z(u_1)| \qquad (2.9)$$

Some further algebraic manipulations (Cook, 1960) of the Fresnel integral arguments yield the result

$$u_1 = \sqrt{\frac{D}{2}}\left[1 + \frac{2(f-f_0)}{\Delta f}\right]$$

$$u_2 = \sqrt{\frac{D}{2}}\left[1 - \frac{2(f-f_0)}{\Delta f}\right] \qquad (2.10)$$

where $D = T\Delta f$.

This quantity D is called the 'time-bandwidth product' of the signal. It is also variously known as the 'dispersion factor' or the 'compression ratio' of the system; the significance of these alternate terminologies will become apparent later. The time-bandwidth product is the most important factor relating to the performance of a pulse compression radar system.

Inspection of equations (2.10) and (2.9) yields the important result that the shape of the amplitude spectrum of e(t), when plotted against $(f-f_0)/\Delta f$, is dependent only on the time-bandwidth product, and not the absolute frequency deviation, Δf. Equation (2.9) has been evaluated for various values of D, and the normalised results plotted in Fig. 2.2 (from Klauder et al., 1960). It can be seen that as the time-bandwidth product increases, the spectrum becomes more nearly rectangular,
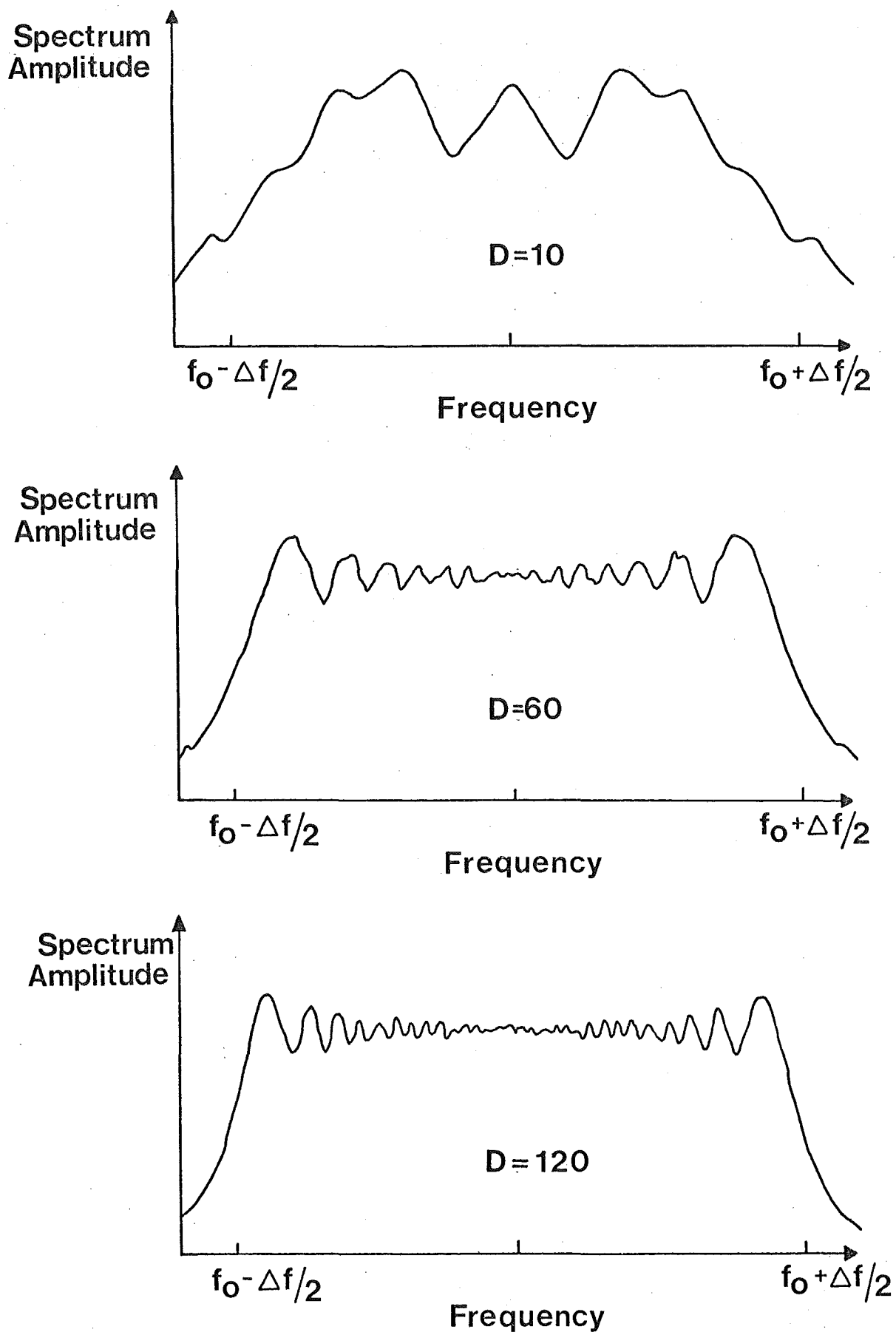
Fig. 2.2: Amplitude spectra for chirp pulses of various time-bandwidth products.

and more clearly contained in the frequency interval $f_0 \pm \Delta f/2$. However, it has been calculated (Klauder et al., 1960) that even for values of D as low as ten, ninety-five percent of the spectral energy is contained within the band of interest.

This completes the description of the linear FM expanded pulse, which is a suitable signal for emission by the transmitter of a pulse compression radar system. In the next sections it is shown how an echo received from a transmission of this nature may be 'compressed' in time by passing it through a suitable filter.

2.3 OPTIMUM SIGNAL PROCESSING AND THE MATCHED FILTER

The received radar return should be processed in such a manner as to maximise the information which can be extracted from it. It is not immediately obvious what philosophy must be pursued to achieve this goal. Woodward (1953) discusses several criteria for just which quantity should be maximised. Since the presence of noise is the major factor contributing to the degradation of signal quality, it is usual, though not universal, to attempt to maximise the signal-to-noise ratio of the radar return. Specifically, a processing filter will be designed which maximises the ratio of peak signal power to the mean noise power.

So far, only linear FM signals have been considered; for the following discussion, the treatment will be broadened to apply to any time function.

As before, the Fourier transform of an arbitrary time function a(t) will be denoted by A(f). Let this arbitrary time signal be passed through a filter having an equally arbitrary

network admittance function, $Y(f)$. If it is assumed that the noise contaminating the signal is Gaussian, the signal-to-noise ratio at the filter output may be expressed as (Klauder et al., 1960):

$$\frac{S}{N} = \frac{|\int Y(f) \cdot A(f) \, \exp\{2\pi i f t_m\} df|^2}{\int |A(f)|^2 \, df \, \int |Y(f)|^2 \, df} \qquad (2.11)$$

where t_m is the time at which the right hand side of the equation is a maximum. t_m will, in general, be a function of both $Y(f)$ and $A(f)$.

Since the signal, $A(f)$, is normally already specified, the problem reduces to finding a $Y(f)$ which maximises equation (2.11). This is a problem in the calculus of variations, whose solution is summarised in the Schwartz inequality, which states that for two arbitrary functions, $f(z)$ and $g(z)$,

$$\frac{|\int f(z) \, g(z) \, dz|^2}{\int |f(v)|^2 dv \int |g(w)|^2 dw} \leq 1 \qquad (2.12)$$

The equality holds only when $f(z)$ is proportional to $g^*(z)$ (where the * operator indicates complex conjugation). Application of the inequality to equation (2.11) indicates that the maximum signal-to-noise ratio at the output of the filter occurs when

$$Y(f) \propto A^*(f) \, \exp\{-2\pi i f t_m\} \qquad (2.13)$$

The exponential factor represents only a gross time delay in the filter, and as such can be ignored in this discussion. A filter of the form given in equation (2.13) is called a <u>matched filter</u> for the signal, $A(f)$, and will be denoted by $Y_m(f)$. Thus

the matched filter for any time signal a(t) is defined by

$$Y_m(f) \equiv A*(f) \qquad\qquad (2.14)$$

where the constant of proportionality has been arbitrarily chosen to be unity.

It is important to realise that the preceeding development is valid irrespective of the signal configuration; any signal passed through its own matched filter maximises equation (2.11) to unity.

An expression for the output of a filter which is matched to its input signal will now be developed. The frequency domain representation of the filter output is given by

$$A_o(f) = Y_m(f) . A_i(f) \qquad\qquad (2.15)$$

where $A_o(f)$ is the spectrum of the output signal
$\quad\quad A_i(f)$ is the input signal spectrum.

This follows directly from the definition of the admittance function of a filter. Substituting equation (2.14) into equation (2.15) yields the important result:

$$A_o(f) = A_i*(f) . A(f)$$

$$\text{or} \qquad A_o(f) = |A_i(f)|^2 . \qquad\qquad (2.16)$$

The corresponding time domain relationship follows from the well-known property of Fourier transforms: multiplication of two functions in the frequency domain is equivalent to convolution in the time domain.

Hence

$$a_o(t) = Y_m(t) {}^\times a_i(t) \qquad\qquad (2.17)$$

where $y_m(t)$ is the impulse response of the filter and $\times$ is the convolution operator, defined such that for two arbitrary functions, $f(z)$ and $g(z)$,

$$f(z) \times g(z) = \int_{-\infty}^{\infty} f(z-w)g(w)\,dw \qquad (2.18)$$

Taking the inverse Fourier transform of equation (2.14) leads to the relation

$$y_m(t) = a*(-t) \qquad (2.19)$$

Substituting equation (2.19) into equation (2.17) then gives the result

$$a_o(t) = a_i*(-t) \times a_i(t) \qquad (2.20)$$

$$\text{or} \qquad a_o(t) = \int_{-\infty}^{\infty} a*(\tau-t)\,a_i(\tau)\,d\tau \qquad (2.21)$$

Equations (2.16) and (2.21) describe the output from a matched filter in the frequency and time domains respectively, and each embodies a result of fundamental significance. Equation (2.16) shows that the output signal from a matched filter is the Fourier transform of the power spectrum of the input signal. Equation (2.21) demonstrates that the filter response is the autocorrelation of the input signal. Consequently matched filter processing is equivalent to autocorrelation processing.

2.4 PROCESSING THE LINEAR FM SIGNAL

An expression for the output of a filter matched to a linear FM pulse may now be developed. It will be recalled that this signal is described by

$$e(t) = rect(\tfrac{t}{T}) \exp\{2\pi i(f_0 t + kt^2/2)\} \qquad (2.1)$$

The form of the matched filter for this signal follows directly from the definition given in equation (2.14):

$$Y_m(f) = E^*(f) \qquad (2.22)$$

where $E^*(f)$ can be readily obtained from equation (2.6). Substituting leads to

$$Y_m(f) = \sqrt{\tfrac{T}{2\Delta f}} \exp\{i\pi(f-f_0)^2/k\} \left[Z^*(u_2) - Z^*(u_1) \right] \qquad (2.23)$$

The output of this matched filter, $e_o(t)$, may be obtained from equation (2.21):

$$e_o(t) = \int_{-\infty}^{\infty} e_i^*(\tau-t) \, e_i(\tau) d\tau$$

$$= \int_{-\infty}^{\infty} rect(\tfrac{\tau-t}{T}) rect(\tfrac{\tau}{T}) \exp\{2\pi i(f_0 t + \tfrac{k\tau^2}{2} - \tfrac{k(\tau-t)^2}{2}\} d\tau \qquad (2.24)$$

This integral is readily evaluated (Cook, 1961) to give

$$e_o(t) = \tfrac{1}{\pi t \sqrt{k}} \exp\{2\pi i f_0 t\} \sin \pi(ktT-kt^2) \qquad (2.25)$$

This may be rearranged to show that the matched filter output is the product of a sinusoidal time function, $\exp\{2\pi i f_0 t\}$, and a term

$$\sqrt{D} \; \frac{\sin \pi (\Delta f |t| - \Delta f^2 t^2/D)}{\pi \Delta f |t|} \qquad (2.26)$$

This term represents the amplitude envelope of the filter output. As before, D is the time-bandwidth product of the chirp pulse. Fig. 2.3 shows the shape of this envelope for various values of D. It can be seen, and indeed it is obvious from inspection of (2.26) that this envelope approximates a $\frac{\sin x}{x}$ function, and that this approximation improves as D increases.

The shape of the envelope described by (2.26) is of paramount importance, for embodied in it is the realization of the aims of pulse compression. The following points should be noted:

a) The amplitude of the output pulse has been increased by a factor of $\sqrt{D}$.

b) The width of the 'compressed' pulse, τ, taken at the -3 dB points of the main lobe, is given approximately by

$$\tau = \frac{1}{\Delta f} \qquad (2.27)$$

The effective resolution achieved is thus dependent <u>only</u> on the bandwidth of the transmitted pulse. Further, the ratio of the expanded to the compressed pulse widths is given by

$$\frac{T}{\tau} = T\Delta f = D \qquad (2.28)$$

The significance of describing D as the 'compression ratio' of the system now becomes apparent.

Thus the compression process effects an increase in the resolution of the radar, the magnitude of which is equal to the time-bandwidth product, D. Also, the peak power in each pulse is increased, again by a factor of D.

Response Amplitude

D=10

Time (Seconds)
-10 -8 -6 -4 -2   2 4 6 8 10

Response Amplitude

D=50

Time (Seconds)
-10 -8 -6 -4 -2 0 2 4 6 8 10
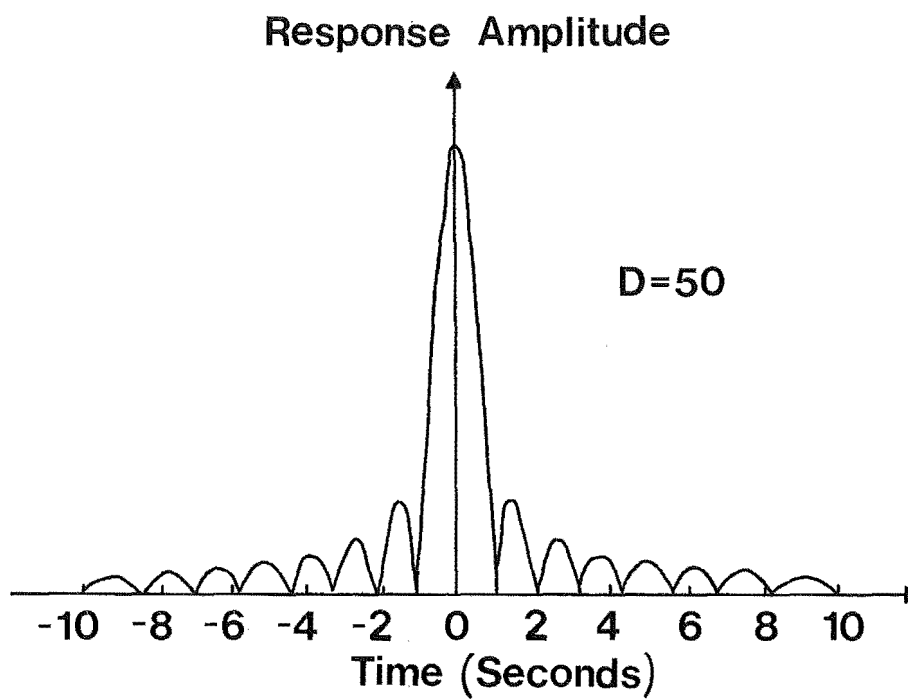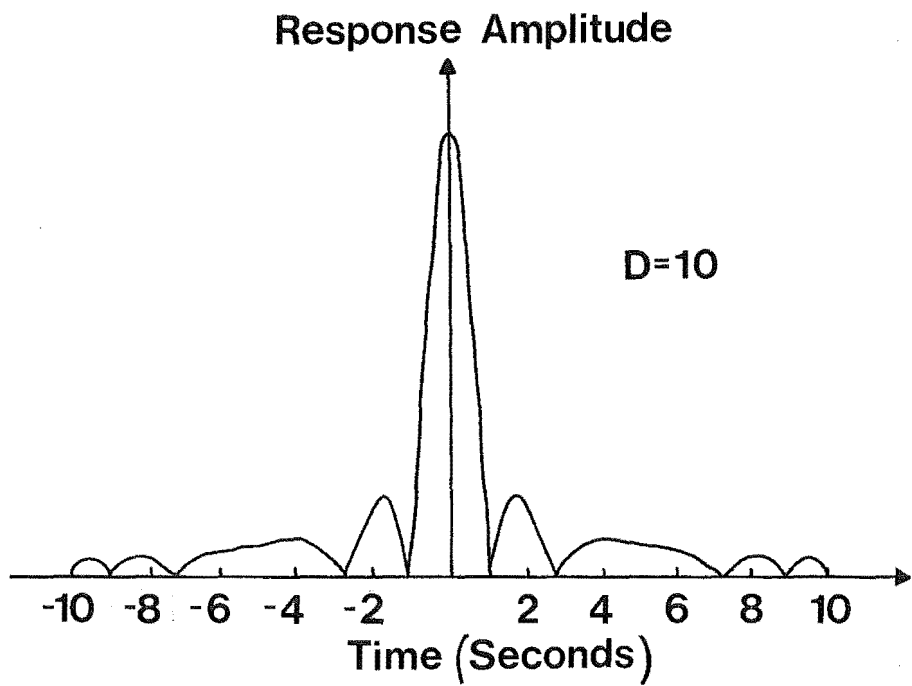
Fig. 2.3: Linear FM matched filter output
envelopes ($\triangle$f normalised to unity).

2.5   RANGE SIDELOBE SUPPRESSION

Consider again the envelope of the matched filter output, shown in Fig. 2.3.   The major lobe, of course, represents the position of the radar echo; the minor lobes, since the X-axis is a time axis, occur before and after the main response, and accordingly are referred to as range sidelobes.   For a true $\frac{\sin x}{x}$ function, the closest of these have an amplitude of -13 dB relative to the main lobe.   Clearly, in a multitarget environment, or, as in the ionosphere, with a distributed target, there is a problem with data interpretation, when the sidelobes from a strong echo could easily mask the main lobe of an adjacent weaker echo.   A number of methods have been used to reduce the amplitude of these sidelobes, all based upon tailoring the frequency response of the receiving system according to some particular "weighting function".

A weighting function is a function, defined over a finite frequency range, possessing a Fourier transform with a $\frac{\sin x}{x}$ -like envelope.   This envelope, however, differs from a $\frac{\sin x}{x}$ function in some important aspects:

a) It has vastly reduced sidelobe amplitudes (typically around -40 dB relative to the main lobe)

b) The main lobe is somewhat broader than that of a $\frac{\sin x}{x}$ function

c) The amplitude of the main lobe is about one dB less than that of the $\frac{\sin x}{x}$ function.

Some of the most useful weighting functions are the Dolph-Chebyshev function (Dolph, 1946) (an optimum but often physically unrealizable function), the Taylor approximation to the Dolph-Chebyshev function (Taylor, 1955), and the generalised cosine-power functions.   Optimum is defined here as the

condition of lowest sidelobe levels for a given amount of main
lobe broadening. The generalised cosine-power functions are
given by the formula

$$W(f) \quad = \quad k + (1-k) \cos^n \pi (\frac{f-f_0}{\Delta f}) \tag{2.29}$$

which represents a cosine-power function, centred about f_0,
sitting on a 'pedestal' of height k.

The means by which a weighting function effects a
suppression of the range sidelobes is as follows. For the
purposes of this discussion, it will be assumed that the
spectrum of the chirp signal is rectangular, i.e.

$$E(f) \quad = \quad 1 \quad \text{for } f_0 - \Delta f/_2 \leq f \leq f_0 + \Delta f/2$$

$$= \quad 0 \quad \text{elsewhere.} \tag{2.30}$$

The frequency-domain representation of the output of a filter
matched to this signal may be obtained from equation (2.16):

$$E_O(f) \quad = \quad |E(f)|^2$$

$$= \quad 1 \quad \text{for } f_0 - \Delta f/2 \leq f \leq f_0 + \Delta f/2$$

$$= \quad 0 \quad \text{otherwise.} \tag{2.31}$$

The output signal will thus be a sinusoid of frequency f_0, with
a $\frac{\sin x}{x}$ - shaped envelope. If this output pulse is passed
through a filter having an admittance function W(f) (where W(f)
is some weighting function), then the output of this filter,
$E_{ow}(f)$, will be given by

$$E_{OW}(f) = E_O(f).W(f)$$

$$= W(f) \quad \text{for } f_0 - \Delta f/2 \leq f \leq f_0 + \Delta f/2$$

$$= 0 \quad \text{elsewhere} \tag{2.32}$$

The output of the filter in the time domain will thus be the Fourier transform of the weighting function. Note that the frequency range over which $W(f)$ is defined must be such that it encompasses the rectangular spectrum $E(f)$ exactly. Also, since $W(f)$ is centred upon f_0, the output of the weighting filter will be a sinusoid of frequency f_0, with an <u>envelope</u> dependent on $W(f)$. Fig. 2.4 will help clarify this.

Note that the output pulse from the weighting filter is broader than the unweighted signal; the magnitude of this broadening is known as the 'pulse widening factor' of the weighting factor. The amplitude decrease of the weighted pulse is often called the 'mismatch loss' introduced by the weighting filter.

Some of the most commonly used weighting functions and their effects on the matched filter output pulse are presented in Table 2.1.

<u>Table 2.1</u> Properties of certain weighting functions.

Function	Peak Sidelobe Level (dB)	Pulse Widening Factor	Mismatch Loss (dB)
Dolph-Chebyshev	-40	1.35	0
Taylor approximation	-40	1.4	-1.2
Generalised Cosine-power:			
Hamming (k = .08, n = 2)	-42.8	1.47	-1.34
Hanning (k = 0, n = 2)	-32.2	1.62	-1.76

In reality, of course, the spectrum of the chirp signal is not rectangular, but contains 'Fresnel ripples' at the band edges.
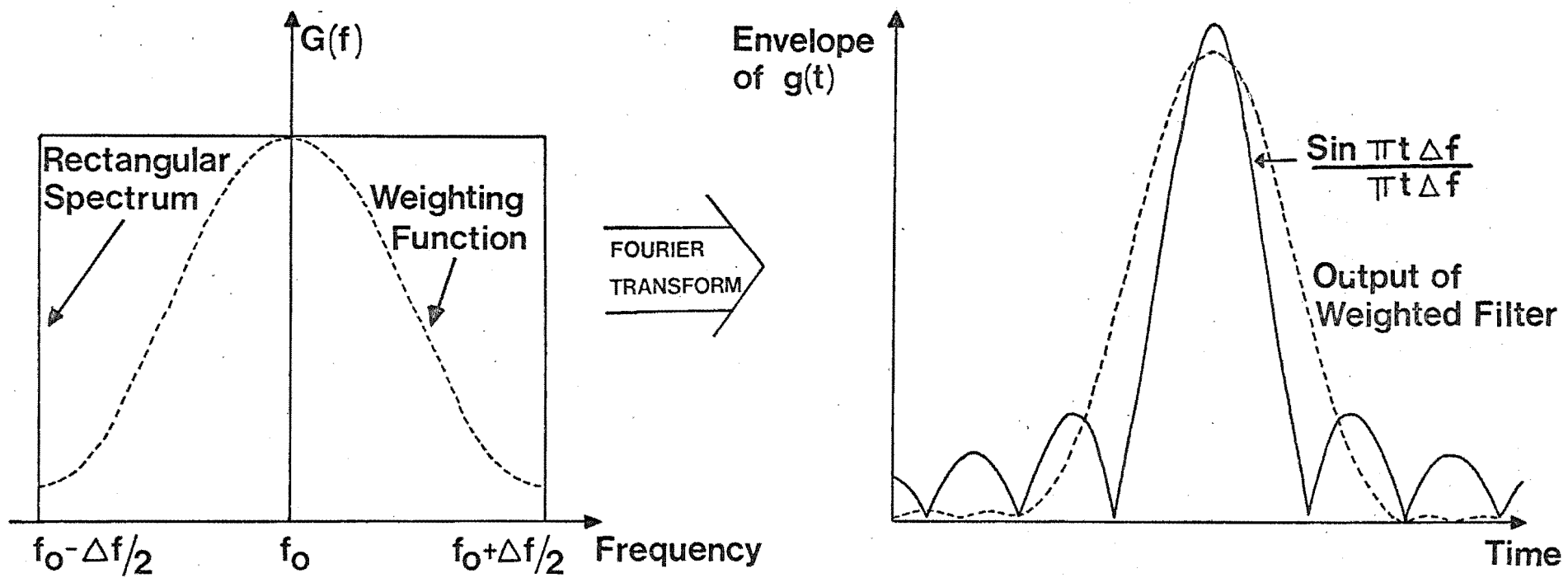
Fig. 2.4: Effect of frequency weighting on the matched filter output.

(see Fig. 2.2). Failure to allow for this fact during the design of a weighting filter results in considerable degradation of the attainable sidelobe levels, especially for low values of D (Klauder et al., 1960). This aspect is examined in more detail in chapter 4.

2.6 EFFECTS OF MOVING TARGETS

The mathematical development has so far implicitly assumed negligible doppler shifting of the radar signal due to radial velocity of the target. A more general derivation (Cook, 1961) shows that this assumption is justified only if the doppler frequency, f_d, is small compared to Δf, the 'swept bandwidth' of the chirp signal.

The doppler frequency may be obtained from the formula

$$f_d = \frac{2f_0 v_t}{c} \qquad (2.33)$$

where f_0 is the centre frequency of the signal

v_t is the radial velocity of the target

c is the velocity of electromagnetic radiation.

Rearrangement leads to the inequality

$$v_t \ll \frac{\Delta f c}{2f_0} \qquad (2.34)$$

which must be satisfied in order that target velocity may be neglected. Since vertical velocities of ionospheric irregularities are of the order of a few meters per second, their effects are clearly negligible in this context.

2.7 SUMMARY

In this chapter it has been demonstrated that the principle of pulse compression has a sound theoretical basis. The original premise that the potential resolving power of a radar signal is dependent only on its bandwidth has been validated. Further, it is shown that the compression process effects an increase in the peak power of each received pulse, the magnitude of which is equal to the compression ratio of the transmitted signal. It should be noted that the preceding development has been completely general, in the sense that no consideration has been required of the means of generating the chirp signal, or the method of implementing the matched filter. These factors would naturally vary for different installations.

CHAPTER 3

DESIGN GOALS FOR A PULSE COMPRESSION RADAR AT BIRDLING'S FLAT

3.1 A BRIEF HISTORY OF BIRDLING'S FLAT

Ionospheric research has been firmly established at Canterbury University for some decades, most of the early practical work being carried out at the University's field station at Rolleston. By about 1961 however, the available ground space there was becoming severely limited, especially for the large transmitting and receiving arrays required for work at lower frequencies. Accordingly, a search for a new site was conducted, and a lease eventually secured for the present field station at Birdling's Flat (location $172.7^{\circ}E$, $43.8^{\circ}S$; magnetic inclination, 22° to the vertical).

This area is well suited for use as an upper-atmosphere research installation for a number of reasons:

a) Situated on several square miles of flat land, it offers almost unlimited space for large antenna arrays.

b) Since it is located about 50 km from the city, man-made electrical noise is at a minimum.

c) It is a coastal site, a prerequisite for the use of atmospheric sounding rockets.

A grant from the U.S. National Science Foundation provided sufficient finance to install the initial equipment at the site. This included two 100 kw pulse transmitters, plus receiving and data recording equipment. All the instrumentation was originally housed in caravans; it was not until 1968 that the first permanent building was erected at the field station.

Early work at Birdling's Flat included electron-density measurements using the Differential Absorption technique (Gardiner and Pawsey, 1953). Data was recorded manually from measurements of the trace on a cathode ray tube displaying the ionospheric returns. This was a tedious process, and most workers in the field contributed something towards a more auto-mated data reduction system (Shearman, 1962; Manson, 1965; Austin, 1966). Studies of ionospheric winds were also conducted during the first few years of operation at Birdling's Flat. Dedicated hardware was utilized to produce a one-bit correlation of the signals from three antennae, the data being output to a paper tape punch (Fraser, 1965, 1968).

The instrumentation at the field station was substantially upgraded in 1972 with the purchase of a DEC PDP8e minicomputer. This initiated important progress in two distinct areas. Firstly, the field station could be placed entirely under soft-ware control, enabling routine data-collecting experiments to be performed in the absence of personnel. Secondly, full data processing could be undertaken in the field, with the conse-quent advantages of immediate evaluation of equipment perfor-mance and experimental techniques. An excellent description of on-line control of ionospheric sounding experiments may be found in Fraser (1973).

The only major change in the station hardware since 1972 has been the replacement of electron tube-based equipment with semiconductor units. With the exception of the transmitters, there is presently no valve-operated equipment in use at Birdling's Flat. A recent study of the D-region (Wratt, 1974) includes a description of most of the electronics existing at the station at the commencement of this project.

3.2 CHOICE OF SYSTEM PARAMETERS

The selection of the parameters for the proposed pulse
compression radar system is dependent to some extent on the
nature of the experimental work for which the system is intended.
It will be recalled (chapter 1) that this project was initiated
principally to assist an anticipated study of the fine structures
present in the D-region electron densities. Any decision
regarding the resolving power of the proposed system must
therefore be made with due regard to the physical size of the
electron density irregularities present in the ionosphere.

It was assumed (von Biel, 1975) that little structure
exists in the D-region of characteristic size less than about
1 km; accordingly, it was decided to attempt a system resolving
power of 0.75 km. A signal bandwidth of 200 kHz is required to
achieve this resolution (see equation (1.3)). For a convent-
ional radar, this is equivalent to a pulse width of 5 micro-
seconds. The transmitting licence for Birdling's Flat requires
the signal frequency to be centred on 2.4 MHz; the chirp signal
must therefore vary in frequency between 2.3 and 2.5 MHz.
The direction of frequency modulation is arbitrarily chosen to
be positive.

Optimum performance of a pulse compression radar is contin-
gent on making the compression ratio, or time-bandwidth product,
as large as possible. Once the bandwidth has been specified,
therefore, this requirement reduces to maximising the pulse
width. Though in theory overlapping expanded pulses can be
separated by the compression filter, attempting to process a
signal which contains ionospheric returns mixed with a direct
signal from the transmitter (i.e. the 'ground pulse') places

unrealistic demands on the linearity and dynamic range of the
receiving and processing system. The restriction is thus
created that the transmitted pulse must have ceased before
radar returns from the closest target of interest arrive. It
can safely be assumed that ionospheric returns will not be
received from below about 60 km; this height is equivalent to
an echo time of 400 μsec. This figure hence provides an upper
limit for the transmitted pulse width.

There are, however, technical factors which also govern
the range of permissible pulse widths. For example, the output
tubes in the transmitter will have a certain maximum period of
continuous operation, which, if exceeded, will result in rapid
deterioration of the tube cathodes. For the transmitter at
Birdling's Flat, this constraint is far more severe than that
discussed in the previous paragraph; consultations with the
designer of the transmitter indicated that it would be most
unwise to attempt a pulse width greater than 150 μsec. This
value was therefore adopted.

The following list summarises the proposed parameters for
the pulse compression radar system.

Type of signal = linear FM ('chirp')

Swept bandwidth, Δt = 200 kHz

Centre frequency = 2.4 MHz

Expanded pulsewidth, T = 150 μsec

Compression ratio, $T\Delta f$ = 30.

The actual resolution achieved by the system is expected
to be somewhat larger than 0.75 km, due to 'main lobe
broadening' introduced by the weighting filter (see section
2.5). Also, hardware considerations required the pulsewidth to
be altered to 142 μsec (see chapter 5); this has the effect
of reducing the compression ratio to 28.

CHAPTER 4

DEVELOPMENT OF THE SIGNAL PROCESSING FILTER

4.1 INTRODUCTION

In general, the radar return from a linear FM pulse transmission consists of a number of overlapping expanded pulses, each with some particular amplitude and phase. This return requires some form of processing in order that the resolution potential inherent in the signal may be fully realised. It was shown in chapter 2 that the optimum processing network which achieves this is a matched filter. Although the theory of matched filtering was fully understood early in the development of pulse compression, it was not until recently that the technology was of a sufficiently high standard to permit realisation of a true matched filter. Previously, workers were forced to substitute various approximations.

One of the most common early implementations of the compression filter propagated the expanded pulse down an ultrasonic delay line, which exhibited a linear time delay-versus-frequency characteristic (Fitch, 1960; Wipperman, 1967). Such a device, if the parameters were chosen correctly, presented a filter function to the incoming signal of the form

$$Y(f) = \exp\{i\pi(f-f_0)^2/k\} \qquad (4.1)$$

It can be seen that this will approximate the matched filter function, given in equation (2.23), reasonably well if the term $[Z^*(u_2) - Z^*(u_1)]$ is small. It can be shown (Klauder et al., 1960) that the response of such a 'dispersive delay' filter to

a linear FM pulse is similar to the matched filter response, with the exceptions that

a) The envelope of the output pulse is a true $\frac{\text{Sin } X}{X}$ function,

b) The frequency inside this envelope is linearly modulated at the same rate as the input signal, but in the opposite direction.

It is most instructive to consider this example of the dispersive delay line, as it can give a clear intuitive picture of how a compression filter operates. Since the velocity of propagation in the line is a linear function of frequency, it may be readily appreciated that the trailing edge of the expanded pulse can be made to propagate faster than the leading edge, causing the two to reach some point in the line simultaneously. A compression of the pulse is thus effected.

Other devices are known to exhibit dispersive delay characteristics, for example lumped constant bridged T networks. If a number of these all-pass time delay equalisers are designed for different delays and then cascaded, the resulting filter can be made to exhibit a linear delay-versus-frequency characteristic over a restricted range with reasonable accuracy (O'Meara, 1959; Brandon, 1965).

Alternative methods exist for implementing the processing filter which do not make use of dispersive delay characteristics. One such method, an optical technique, achieved a convolution between a signal and a reference by imprinting the reference on an optical mask, and using the signal to set up acoustic waves in a liquid immediately in front of the mask. Use was made of the Fourier transform property of a lens imaging system in

performing the convolution (Cutronoa et al., 1960; Reich and Slobodin, 1961; Slobodin, 1963).

Another method first introduced in 1971 propagated a chirp signal and its time inverse as surface acoustic waves from opposite ends of a Lithium Niobate plate, to achieve a convolution of the two directly. In initial experiments, bandwidths of up to 400 MHz were demonstrated (Bongianni, 1971; Grasse, 1971).

The discovery of the Fast Fourier Transform (Cooley and Tukey, 1965; Brigham and Morrow, 1967) initiated a new approach to signal processing. Techniques were developed by which filters could be implemented arithmetically, using digital computers. Two distinctly different approaches are in general use:

a) Processing in the time domain with recursive or non-recursive digital filters (Rader and Gold, 1967; Helms, 1968; Echard and Boorstyn, 1972; Gray and Nathanson, 1971).

b) Transforming a time series into the frequency domain with a Fast Fourier Transform (FFT), multiplying the spectrum by the filter function, and transforming the product back into the time domain (Hart and Sheats, 1971; Halpern and Perry, 1971).

The second method is more useful for complicated filter functions, since the filter can be implemented as soon as its frequency response (whatever form it may take) is known. This aspect will be dealt with in greater detail later in this chapter.

In the past, many processing methods which were perfectly valid mathematically were unuseable because of technological limitations. However, with the availability of the computational filters just described, it may be assumed that such restrictions no longer apply.

4.2 MATHEMATICAL ANALYSIS OF THE PROPOSED FILTER

The mathematical treatment of range sidelobe suppression (section 2.5) clearly indicated that the optimum form of the output from a pulse compression signal processing network was the Fourier transform of the chosen weighting function. For a simple weighting filter, this situation only occurs if its input has a rectangular spectrum. Since the spectrum of the matched filter output is not rectangular, use of a simple weighting filter will cause some signal degradation, which is manifested as an increase in the sidelobe levels of the filter output. Cook and Paolillo (1964) have calculated that the magnitude of this increase is about 10 dB; clearly, this results in unacceptably large range sidelobes. Even so, the presence of Fresnel spectral ripples is often neglected in the design of a pulse compression signal processing filter. It was, however, determined that this would not be the case in the present work.

The frequency domain output of a filter matched to the chirp waveform is by definition

$$E_o(f) = E(f) \cdot Y_m(f) \tag{4.2}$$

where $E(f)$ is the spectrum of the input signal, taken to be

a chirp pulse centred aroung $t = 0$

and $Y_m(f)$ is the admittance function of the matched filter.

The matched filter is defined by

$$Y_m(f) \equiv E*(f) \tag{2.22}$$

which leads to

$$E_O(f) = E(f) \cdot E*(f) \tag{4.3}$$

Introducing the signal $E_O(f)$ into a weighting filter gives

$$E_{OW}(f) = E_O(f) \cdot W(f)$$

$$= E(f) \cdot E*(f) \cdot W(f) \tag{4.4}$$

where $W(f)$ is a weighting function

and $E_{OW}(f)$ represents the output of the weighting filter.

The width and position of the weighting function is chosen, of course, so that it encompasses the usable portion of the chirp spectrum (see Fig. 2.4). It will be recalled that optimum output from the weighting filter is predicated upon the fact that its input has a rectangular spectrum. This may be ensured by preceding the weighting filter with a filter $V(f)$, which is specified such that when applied to the matched filter output, it transforms the signal into one with a rectangular spectrum of similar bandwidth. Let $W'(f)$ denote the filter found by cascading $V(f)$ and $W(f)$. That is,

$$W'(f) = V(f) \cdot W(f) \tag{4.5}$$

If this filter $W'(f)$ is now applied to the matched filter output, the output from the composite filter so formed will be expressed by

$$E_{ow'}(f) \quad = \quad E(f).Y_m(f).V(f).W(f)$$

$$= \quad E(f).E^*(f).V(f).W(f) \tag{4.6}$$

Inspection of equation (4.6) shows that if V(f) is to perform its specified function, it must be of the form

$$V(f) \quad = \quad \frac{1}{E(f).E^*(f)} \quad \text{for } f_0 - \Delta f/2 \leq f \leq f_0 + \Delta f/2$$

$$= \quad 0 \qquad \text{elsewhere} \tag{4.7}$$

The output of the composite filter then becomes simply

$$E_{ow'}(f) \quad = \quad W(f) \tag{4.8}$$

as desired.

Inspection of equations (4.5) and (4.7) shows that optimum signal processing will be achieved if the simple weighting filter W(f) is replaced by a filter W'(f), given by

$$W'(f) \quad = \quad \frac{W(f)}{E(f).E^*(f)} \tag{4.9}$$

If this is the case, the time domain output of the processing filter will be the Fourier transform of the weighting function.

Let $Y_c(f)$ be defined as the network admittance function of a complete signal processing filter, formed by cascading $Y_m(f)$ and W'(f).

Then, by definition

$$E_{ow'}(f) \quad = \quad E(f).Y_c(f) \tag{4.10}$$

Comparing this with equation (4.8) leads to the fundamentally important result that

$$E(f) . Y_c(f) = W(f)$$

or $\qquad Y_c(f) = \dfrac{W(f)}{E(f)}$ (4.11)

Equation (4.11) gives an expression for the admittance function of a complete signal processing filter, $Y_c(f)$, which compresses the chirp signal, compensates for Fresnel ripples in its spectrum, and applies frequency weighting to reduce the sidelobes. This filter function may be readily obtained knowing only the spectrum of the chirp signal, and form of the chosen weighting function.

4.3   REALISATION OF THE PROCESSING FILTER

This section describes how the proposed signal processing filter, $Y_c(f)$, is physically realised. Earlier in this chapter, it was indicated that given the availability of digital computing power, a mathematical rather than an electronic implementation would be most appropriate.

Time domain digital filtering was studied carefully as a possible means of realising the filter. This technique, though storage requirements are modest, often necessitates large numbers of multiplications, and in general is more suited to installations where dedicated multiplying hardware is available. Also, it is by no means certain that the implementation of a given filter function will be straightforward, or even at all possible.

These disadvantages do not apply to frequency domain filtering, though this method does require considerably more computer storage. However, the PDP8 at Birdling's Flat was equipped with a large memory (16K words), and since an efficient FFT routine was available (Rothman, 1968) it seemed clear that implementing the processing filter in the frequency domain would be the superior approach.

The operation of the Fast Fourier Transform is well known and has been reported widely in the literature (Cooley and Tukey, 1965; Brigham and Morrow, 1967; Brigham, 1974), and will not be described here. It should, however, be understood that the transform operates on a sequence of time samples (usually some power of two in number) and returns an equal number of coefficients, representing the magnitudes of the frequency components present in that sequence.

Implementation of a filter in the frequency domain requires first that the input signal be sampled at fixed intervals, and that these samples be converted to digital form. These digital samples are then transformed into the frequency domain by an FFT. The resulting spectrum is multiplied point by point by the filter function, and the product transformed back into the time domain. Two points concerning this process should be noted.

a) The FFT coefficients in both the time and frequency domains are in general complex (representing amplitude and phase), as is the filter function.

b) The input signal, its spectrum, and the filter function are all discretely specified.

A discrete function is formed as a result of sampling a continuous function. It may be written in the form a(j), where j may have only integral values. For example, a sinusoidal signal of frequency f_0, expressed in continuous form by

$$g(t) = \exp\{2\pi i f_0 t\} \qquad (4.12)$$

would be described after sampling by

$$g(j) = \exp\{2\pi i f_0 j t_s\} \qquad (4.13)$$

where $j = 0, 1, 2, \ldots$

and t_s is the sampling interval.

A selection of a finite number of these samples, say those with $0 \leq j \leq 255$, would provide a set of 256 complex amplitudes which would be in a suitable form to be processed by a discrete Fourier transform.

The actual sampling is performed by an analogue-to-digital converter, which converts an electrical voltage into an equivalent digital word which can be read by the computer. Care must be exercised in the selection of the sampling frequency, since a series can only represent a continuous function accurately if there are at least two samples per period of the highest frequency present in that function. An inadequate sampling rate will result in the well-known phenomena of aliasing and spectral foldover (Brigham, 1974; Blackman and Tukey, 1958).

Since analogue-to-digital (A-D) converters are inherently bandwidth limited, a proceedure known as baseband mixing (Gray and Nathanson, 1971) is often employed prior to sampling. This

technique keeps the frequencies present in a signal as low as possible by mixing the signal with that of a local oscillator tuned to the signal's centre frequency. For example, if a signal contains frequencies between $f_0 - \Delta f/2$ and $f_0 + \Delta f/2$, then this signal is heterodyned with a sinusoid of frequency f_0. If the bandwidth of the original signal is Δf, the maximum frequency present after mixing is of course $\Delta f/2$. This is shown diagrammatically in Fig. 4.1. Normally, such a process results in distortion of the signal, as it becomes impossible to separate positive and negative frequencies after mixing. However, if both the real and imaginary components of the original signal (i.e. both the amplitude and phase) are preserved, this problem of <u>spectral foldover</u> may be avoided. Fig. 4.2 illustrates a method by which this can be accomplished.

This arrangement operates as follows. A local oscillator is provided with two outputs, both at a frequency of f_0, but differing in phase by 90°. The chirp signal is mixed with each of these outputs, and the products are lowpass filtered to retain only the difference terms. The outputs of these filters will be of the same form, but differing in phase by 90°, and may be envisaged as the real and imaginary parts of the original signal, shifted down to zero frequency. The ability to distinguish positive and negative frequencies will not be lost, since an input to the mixer of $\exp 2\pi i (f_0 + f_1)$ will appear at the outputs as

$$e_i(t) = \cos(2\pi f_1)$$

and $$e_q(t) = \sin(2\pi f_1)$$

whereas an input of $\exp 2\pi i (f_0 - f_1)$ will appear as

AMPLITUDE SPECTRUM
OF SIGNAL

SPECTRUM AFTER
BASEBAND MIXING

$f_0 - \Delta f/2$ f_0 $f_0 + \Delta f/2$

FREQUENCY

$-\Delta f/2$ 0 $\Delta f/2$
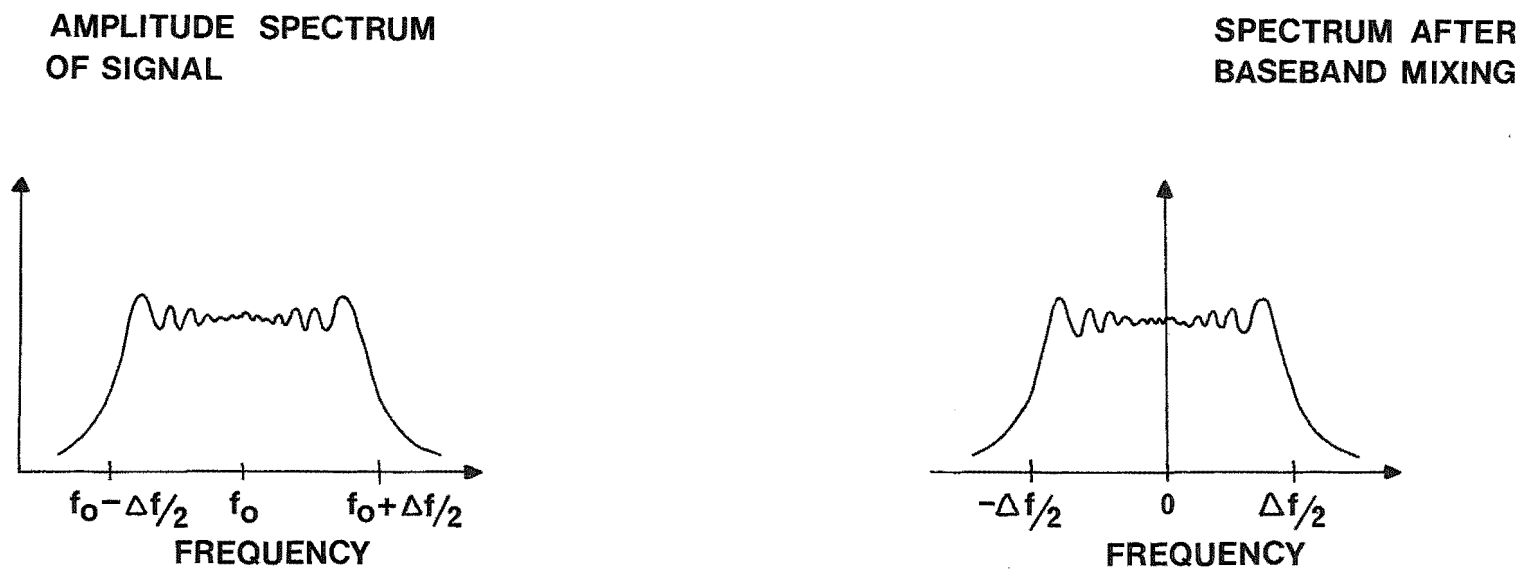
FREQUENCY

Fig. 4.1: Effect of baseband mixing on signal spectrum.

Signal Input

$$\cos 2\pi i \left(f_0 t + kt^2/2\right)$$

multiplier $\bigotimes$ $\cos 2\pi f_0 t$ | local oscillator | $\sin 2\pi f_0 t$ $\bigotimes$ multiplier

low pass filter

low pass filter

'in phase' output

$$e_i(t) = \cos \pi k t^2$$

'quadrature' output

$$e_q(t) = \sin \pi k t^2$$
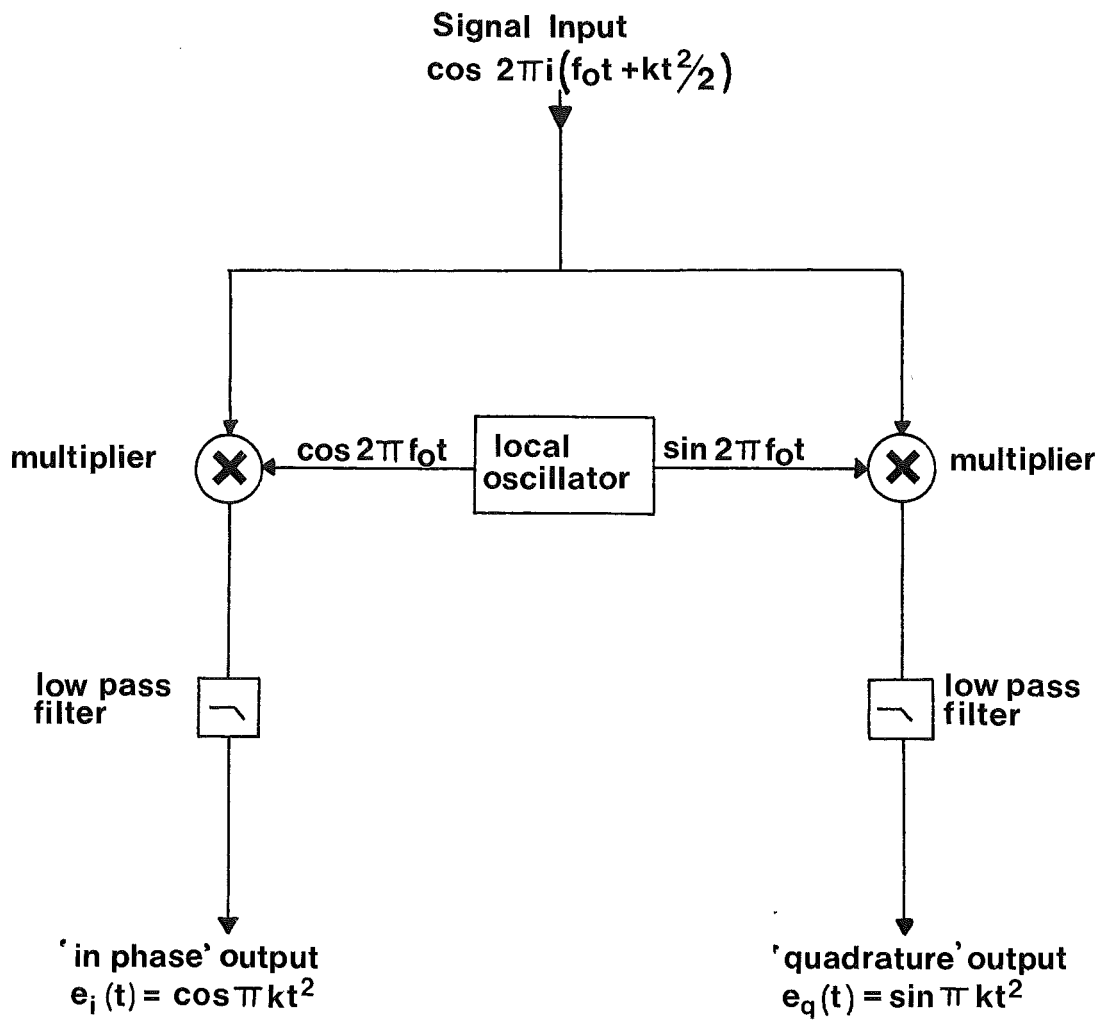
Fig. 4.2: Baseband mixing technique.

$$e_i(t) \quad = \quad \cos(2\pi f_1)$$

$$\text{and} \quad e_q(t) \quad = \quad -\sin(2\pi f_1)$$

the negative sign in the quadrature, or imaginary channel indicating a negative frequency.

The two outputs from the mixer may thus be regarded as the real and imaginary parts of a complex signal, i.e.

$$e(t) \quad = \quad e_i(t) + ie_q(t) \tag{4.14}$$

If these outputs are sampled simultaneously, the pairs of samples so obtained would form a set of complex numbers, which would be suitable for processing by the computer.

The operation of the computational filter may now be described in more detail. The input signal to the filter will be of the form

$$e(j) \quad = \quad \exp 2\pi i \left\{ \frac{k[(j-N/2)t_s]^2}{2} \right\} \tag{4.15}$$

where k is the rate of frequency modulation of the chirp signal

$j = (0,1,2 \ldots N-1)$

t_s is the sampling interval.

Note that this signal is at 'baseband', and that the samples, $e(j)$, are complex.

The discrete spectrum of this signal will be denoted by $E(n)$, where $0 \leq n \leq N-1$. The filter function, given in continuous form in equation (4.11) will be described in discrete form by

$$Y_c(n) \quad = \quad \frac{W(n)}{E(n)} , \qquad 0 \leq n \leq N-1 \tag{4.16}$$

where $Y_c(n)$ and $W(n)$ are the discrete formulation equivalents of the functions $Y_c(f)$ and $W(f)$. The spectrum of the filter output, given in continuous form in equation (4.10) will become

$$E_{ow}{}'(n) \ = \ Y_c(n).E(n)$$

$$= \ W(n) \qquad 0 \le n \le N-1 \qquad (4.17)$$

and of course the corresponding time-domain relationship is

$$e_{ow}{}'(j) \ = \ w(j) \qquad 0 \le j \le N-1 \qquad (4.18)$$

Operation of the processing filter first requires that the outputs from the baseband mixer be sampled by the A-D converter, and an FFT performed on these samples. The complex spectral weights $E(n)$ produced by the transform are then each multiplied by the corresponding complex $Y_c(n)$ to yield $E_{ow}{}'(n)$ (i.e. $E_{ow}{}'(1) = E(1).Y_c(1)$ etc.). These products are then transformed by an inverse FFT to give the processed time series $e_{ow}{}'(j)$. Fig. 4.3 should help clarify this description.

Another important effect of baseband mixing should be recognised. Whereas without mixing, the weighting function needed to be centred about f_0 in order to encompass the signal spectrum, it now requires to be centred about zero frequency. This implies that rather than being a pulse at frequency f_0 with an envelope of $w(t)$, the output is now simply a single 'blip' in time of the shape $w(t)$ (see Fig. 4.4). In other words, baseband mixing has provided a detection of the input signal.
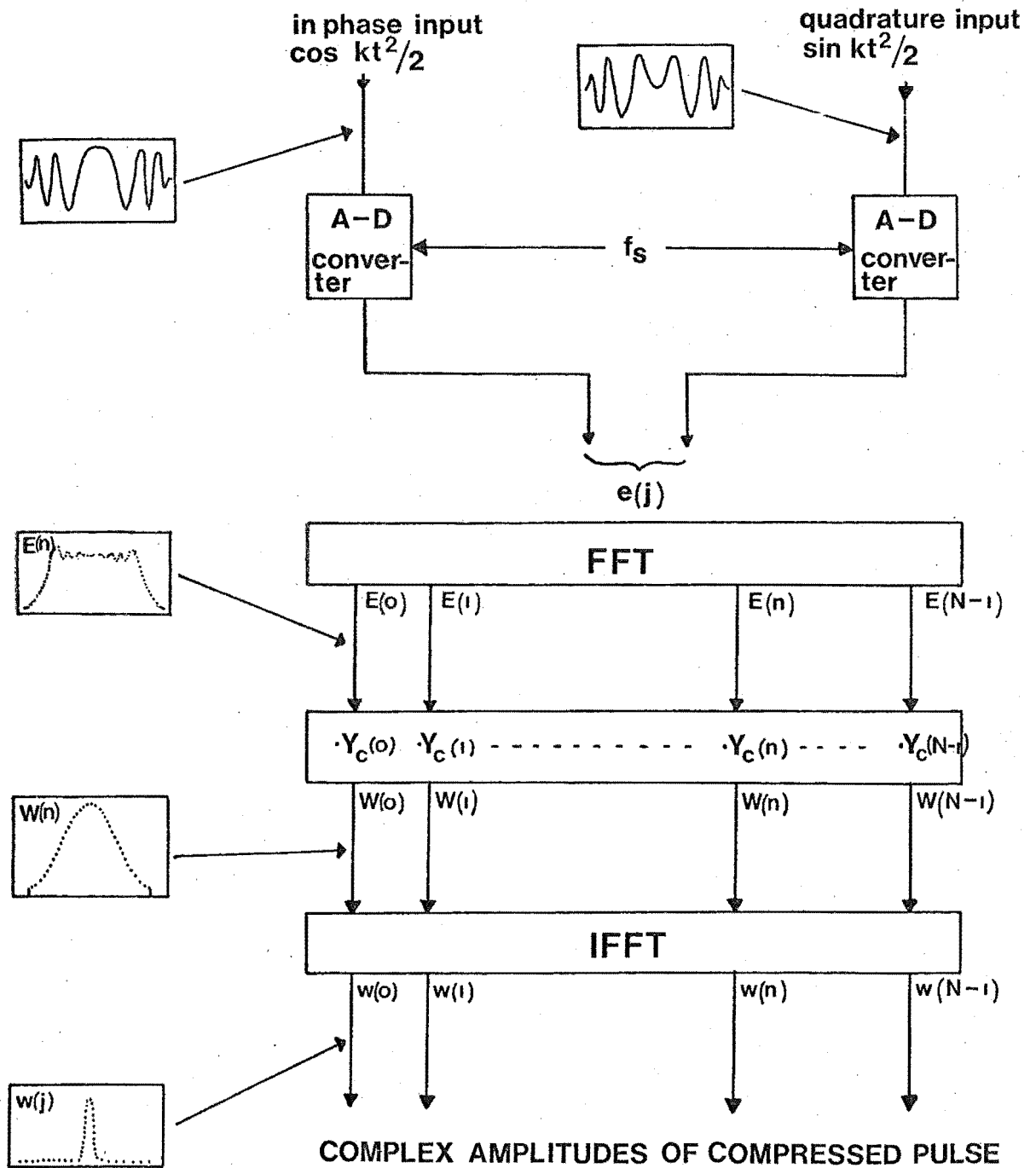
Fig. 4.3: Block diagram of signal processing method.

FREQUENCY DOMAIN   **TIME DOMAIN**
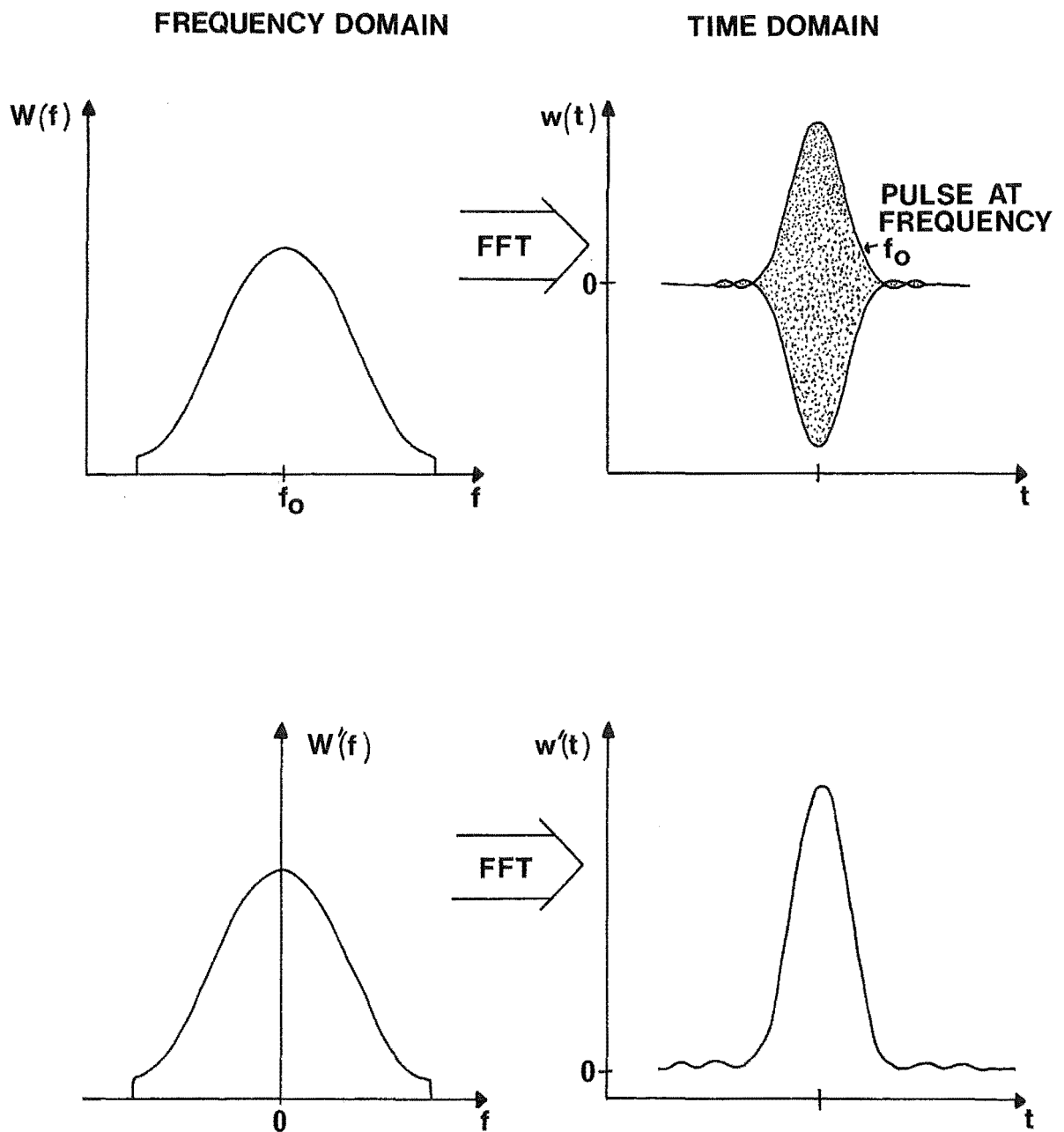
Fig. 4.4: Effect of baseband mixing on filter output.

4.4 APPLICATION TO REAL TARGETS

The preceding analysis has always used, as an input to the processing filter, a signal e(t) consisting of a single chirp of unit amplitude and zero phase, centred about time t = 0. Now, of course, a real radar return consists of a number of overlapping chirps, each having its own amplitude, phase, and time of arrival. A limiting case of this occurs in the ionosphere, where the target is often of a distributed nature. For any signal processing method to be viable, it must preserve these three parameters of each chirp throughout the processing filter.

Before an analysis of how the proposed filter will handle real radar returns can be made, certain aspects of discrete Fourier transforms must be understood. If H(n) denotes the Fourier transform of an arbitrary time series h(j), then the following properties hold:

1. A delay, or shift, in the time domain is equivalent to a linear added phase in the frequency domain. That is,

$$h(j-k) \quad \xrightarrow{\text{DFT}} \quad H(n) \; \exp\{-2\pi i k n/N\} \qquad (4.19)$$

where in this case the time signal has been delayed by k
       sampling intervals

and   N is the total number of samples.

2. A constant phase change in the time samples produces an equivalent constant phase change in the frequency domain, i.e.

$$h(j) \cdot \exp i\theta \quad \xrightarrow{\text{DFT}} \quad H(n) \cdot \exp i\theta \qquad (4.20)$$

where θ is a constant.

This follows directly from the linearity property of Fourier transforms.

An expression may now be derived for the output of the processing filter when excited by a simulated radar return from a point target, that is, a chirp of arbitrary amplitude and phase, delayed by an arbitrary amount of time, say m sampling intervals.

Such a signal would be described by

$$f(t) = A \text{ rect}\left[\frac{t-mt_s}{T}\right] \exp\{2\pi i[f_0(t-mt_s) + \frac{k(t-mt_s)^2}{2} + \phi]\}$$

(4.21)

where A is the amplitude of the signal

ϕ is the phase of the signal, taken with respect to an arbitrary zero

t_s is the sampling interval of the A-D converter.

Alternatively,

$$f(t) = Ae(t-mt_s) \cdot \exp(2\pi i\phi)$$

(4.22)

where e(t) is defined in equation (2.1).

If f(t) is mixed to baseband and sampled, the discrete function so obtained is given by

$$f(j) = A \cdot e(j-m) \cdot \exp(2\pi i\phi)$$

(4.23)

where e(j) is defined in equation (4.15).

The Fourier transform of this would be

$$F(n) = A \cdot \exp(2\pi i\phi) \cdot E(n) \cdot \exp(2\pi imn/N)$$

(4.24)

using properties 1 and 2 given earlier.

Multiplying this spectrum by the filter function gives

$$Y_c(n) \ F(n) \ = \ A.\exp(2\pi i\phi).\exp(2\pi imn/N).Y_c(n).E(n)$$

$$= \ A.\exp(2\pi i\phi).\exp(2\pi imn/N).W(n) \qquad (4.25)$$

since $Y_c(n).E(n) = W(n)$ from equation (4.16).
A final inverse Fourier transform on this will yield as an
output from the filter,

$$f_{ow'}(j) \ = \ Aw(j-m).\exp(2\pi i\phi) \qquad (4.26)$$

which is a replica of $e_{ow'}(j)$, the output pulse obtained from
an input of $e(t)$, except that it has been time-shifted by m
sampling periods, has an amplitude A, and a phase of ϕ.

Thus the composite filter, $Y_c(n)$, fulfils the conditions
required by a radar signal processing filter outlined at the
beginning of this section. It is easy to generalise the
preceding treatment to a case where the input to the filter
consists of radar returns from Q targets, each producing an
echo of amplitude A_q, a phase ϕ_q, and delayed by m_q sampling
intervals. The input signal would be a linear combination of
all these individual echoes, or

$$e_c(t) \ = \ \sum_{q=1}^{Q} A_q e(t-m_q t_s) \ \exp(2\pi i\phi_q) \qquad (4.27)$$

and by a reasoning similar to the preceding case, the output of
the processor would be

$$e_{cow'}(j) \ = \ \sum_{q=1}^{Q} A_q w(j-m_q t_s) \ \exp(2\pi i\phi_q) \qquad (4.28)$$

as required.

4.5 COMPUTER SIMULATION OF THE FILTER

The preceding mathematical analysis indicates the validity of the proposed signal processing method; however, as an additional confirmation of its performance a simulation of its use was implemented on the University's B6700 computer.

Firstly, the digitized expression for the chirp signal, given in equation (4.15) was evaluated over a range of j, and the numbers so obtained were transformed by an FFT routine to give the complex spectral coefficients, $E(n)$. A weighting function was then selected (the Hamming function in this case) and the coefficients of the filter function determined according to the equation

$$Y_c(n) = \frac{W(n)}{E(n)} \qquad (4.16)$$

where the division, it will be remembered, is complex. Various input signals were then treated by this filter according to the method depicted in Fig. 4.3.

A large number of different signals were processed, in order to test every aspect of the processing filter, and to try and find any problems which might occur in the processing of ionospheric returns. Some examples of these signals were:

signals with a number of overlapping and non overlapping chirp pulses (to test the resolution of the system)

signals of varying phase and amplitude

signals with delays that were non-integral multiples of the sampling frequency

signals with an added D.C. component (such as would occur if a receiver had an offset drift)

signals in which part of the chirp was truncated (receiver
gate opened part way through the chirp)

signals immersed in Gaussian noise

simulated returns from a diffuse target.

Some examples of the results of these simulations are reprod-
uced in Figs 4.5 to 4.10. On each of these diagrams the func-
tion plotted is the amplitude of the time-domain output from
the processing filter. Each point on the horizontal axis is
equivalent to 1 µsec.

Fig. 4.5 shows the filter output from a single chirp
pulse 150 µsec in length. The sidelobes are too small to be
resolved by the discrete plotting technique. Fig. 4.6 shows
that the filter clearly resolves two identical chirp pulses 10
µsec apart. The output shown in Fig. 4.7 was produced by a
signal contaminated by Gaussian noise of amplitude -12 dB with
respect to the signal. Whereas this represents an extremely
poor signal-to-noise ratio unlikely to be encountered in prac-
tice, it does show that, although there is obviously noise in
the filter output, the position and shape of the main response
is still accurate. Fig. 4.8 represents the filter output from
a signal with a simulated receiver offset of 2.5 volts in one
channel. Once again, this is an extreme example (the receiver
rarely drifts more than a few millivolts) but it does indicate
that the significant characteristics of the input signal
(amplitude and arrival time) are faithfully reproduced.

Fig. 4.9 is an important plot. It shows the output of the
filter excited by a chirp pulse of which the first 25% had been
truncated. Whereas the position of the output response is
correct, spurious output occurs between the start of the 'scan'
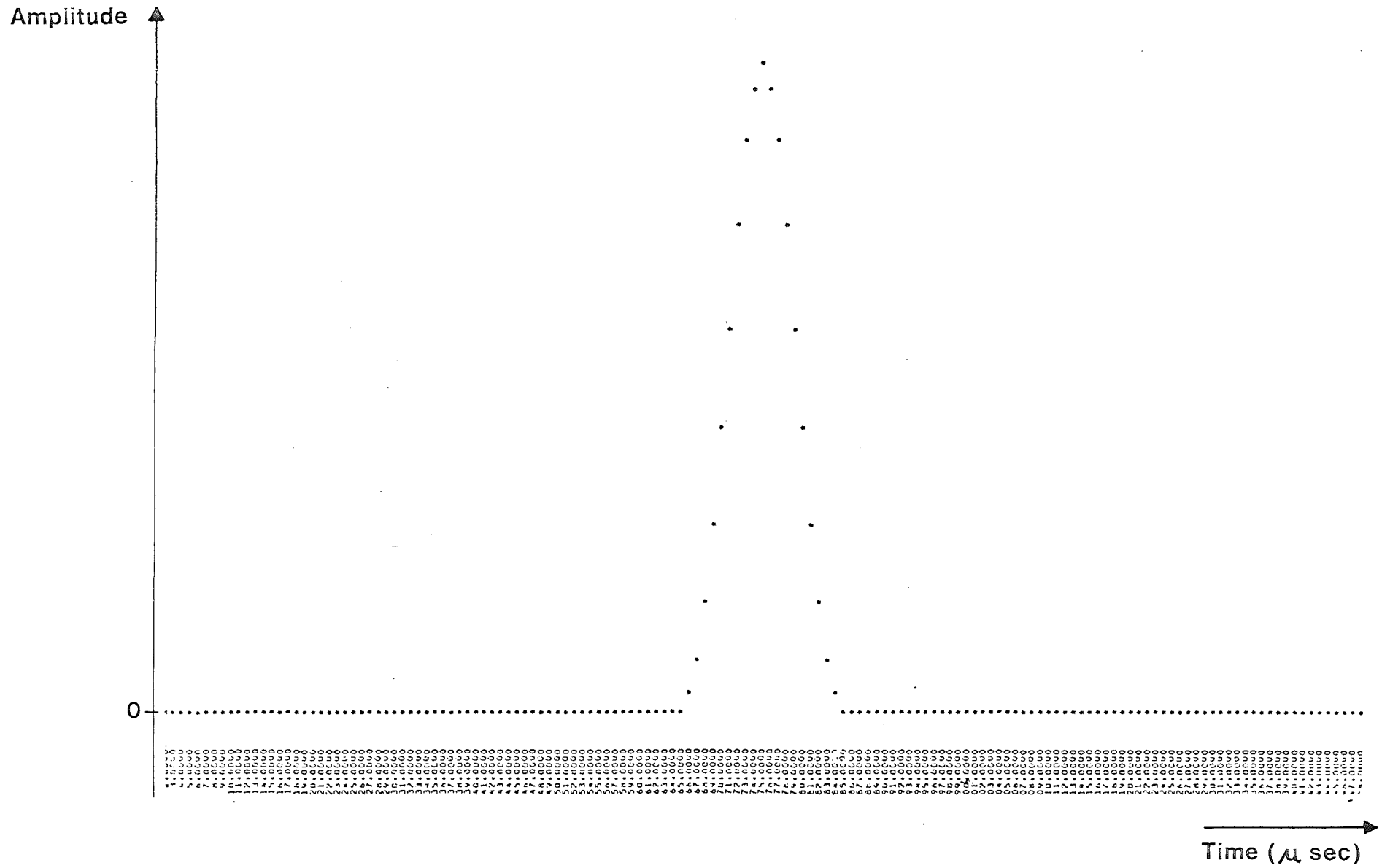
Fig. 4.5: Simulated processing of a single chirp pulse.

Amplitude

0

Time (μ sec)
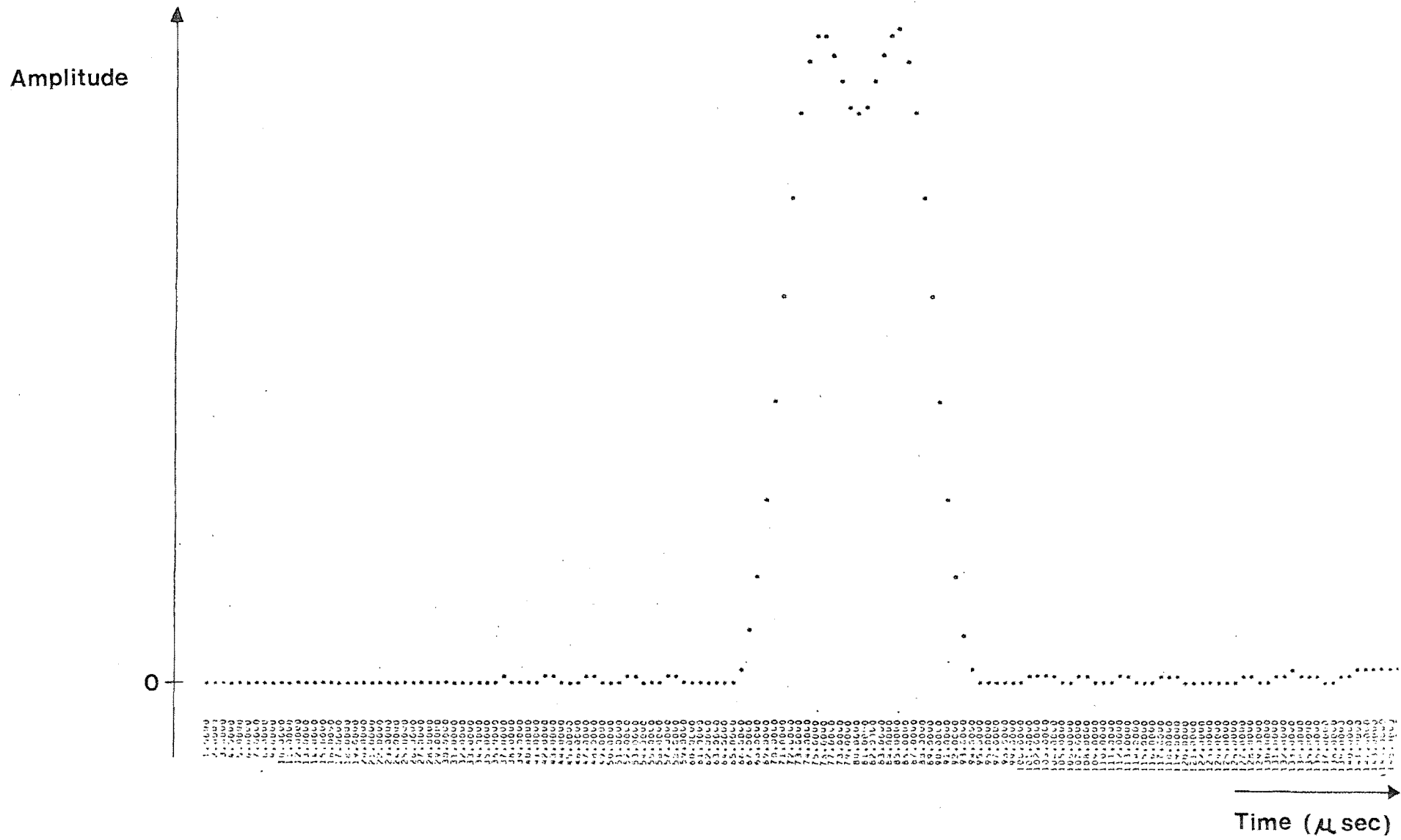
Fig. 4.6: Two chirp pulses 10 μsec apart.
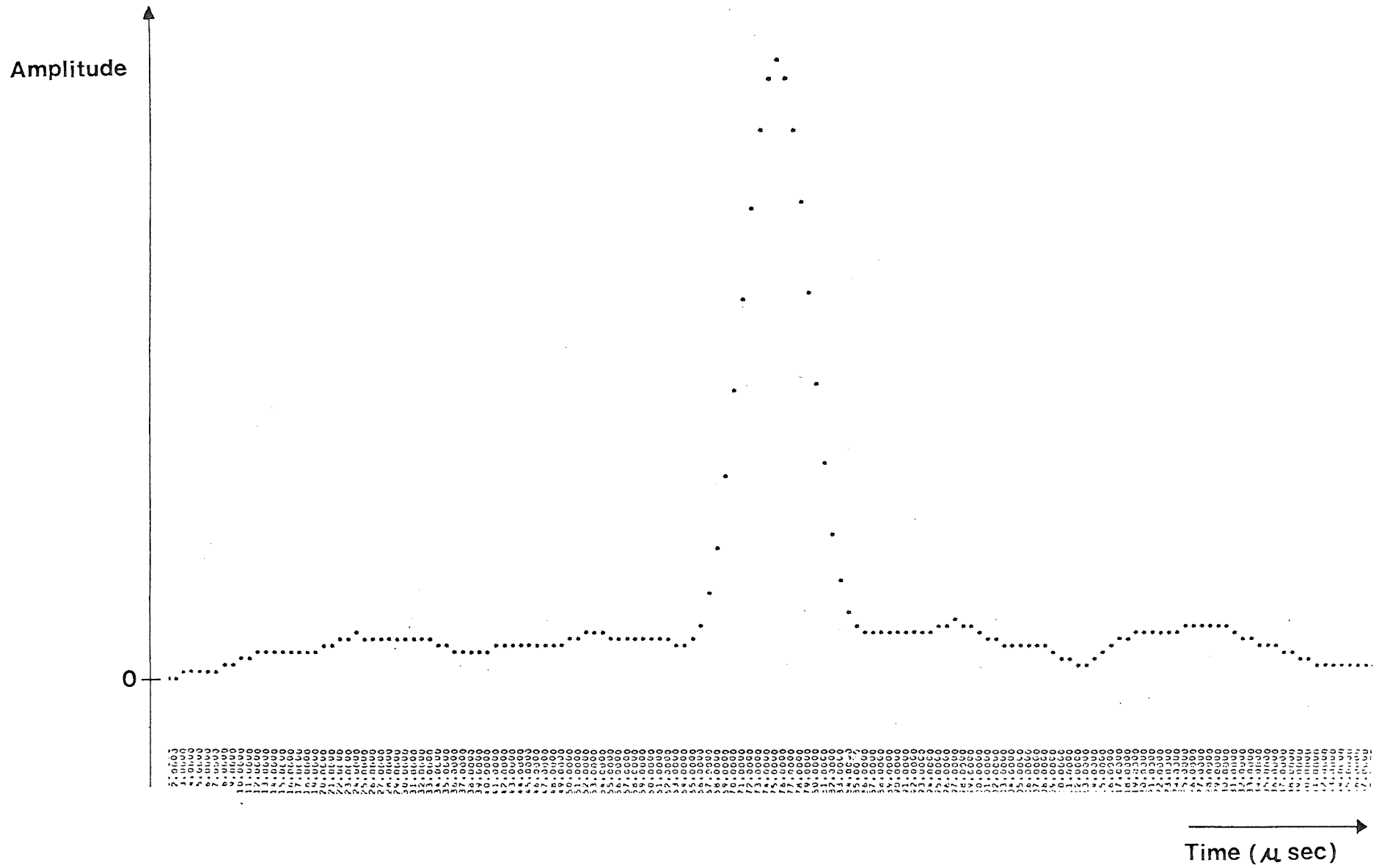
Fig. 4.7: Signal contaminated by gaussian noise.
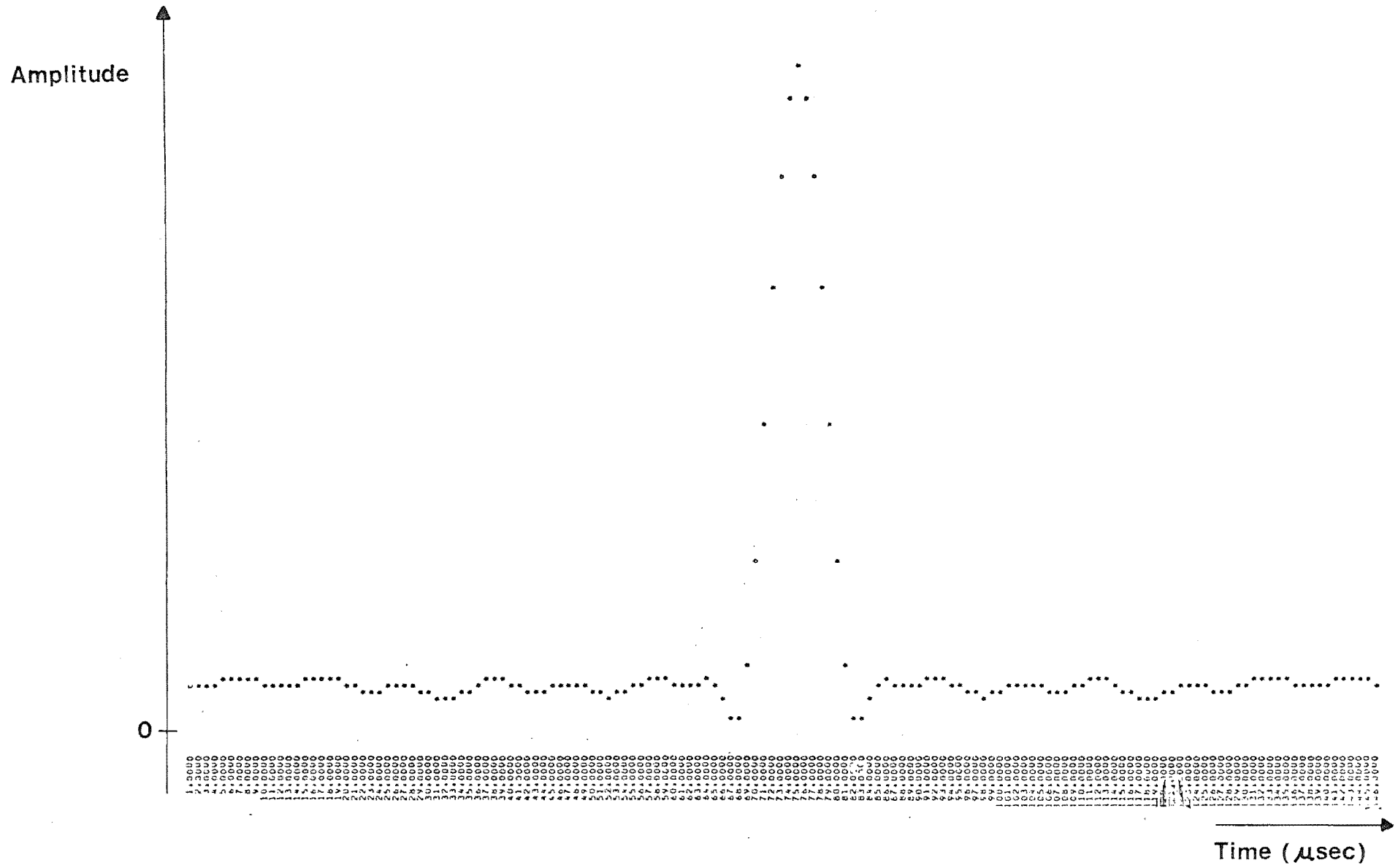
Fig. 4.8: Signal with offset in one channel.
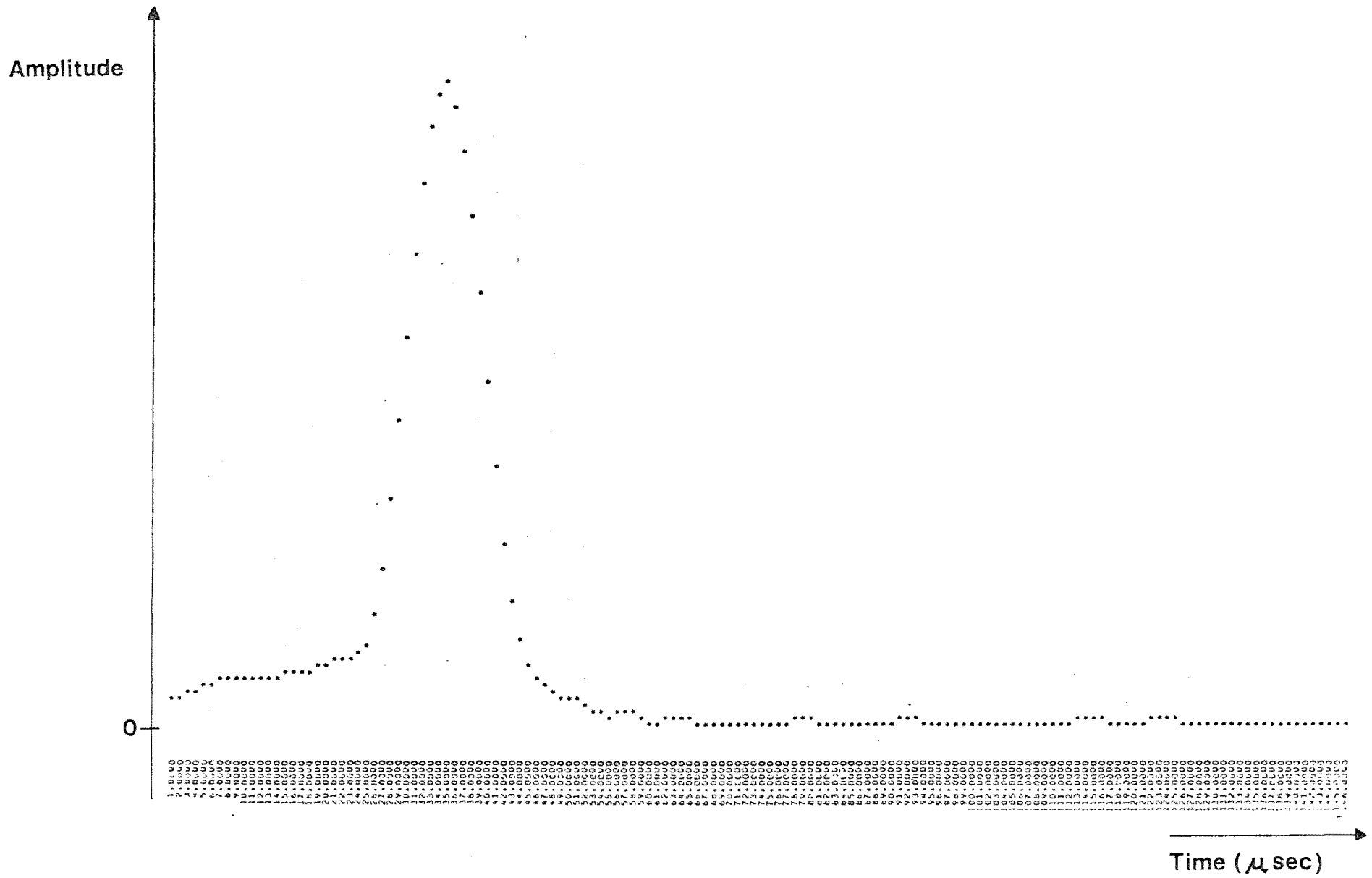
Fig. 4.9: Output from truncated chirp pulse.

and the output pulse itself. Care must thus be observed in the interpretation of any data appearing in the first and last 75 μsec of any ionospheric scan.

Fig. 4.10 shows the results from processing a simulated return from a diffuse target. A simple model was set up in which the amplitude of the 'echo' from 100 neighbouring points on the target could be programmed. This model 'ionosphere' is depicted by the unbroken line in the diagram. The dashed line represents the output from the processing filter. It can be seen that the filter presents an accurate picture of the function which gave rise to its input, to within the resolution capability of the signal.

The results of these simulations were encouraging, showing that the filter did not give any anomalous outputs for a wide variety of degradations from the ideal matched input. The limit of resolution appeared to be 7 μsec, rather than 5 μsec; this was an expected consequence of main lobe broadening intro-duced by the weighting function.

4.6 SUMMARY

This chapter has included a full description of the matched and weighted filter to be used for processing ionos-pheric returns, beginning with the theoretical derivation of the required filter function, and continuing with a description of how this is to be physically implemented. Some confirmation of the effectiveness of this filter is also deduced from a computer simulation of its performance.

Amplitude

reflection amplitudes
of ionospheric model

_ _ _ _ _ output of processing
filter

1Km

Height
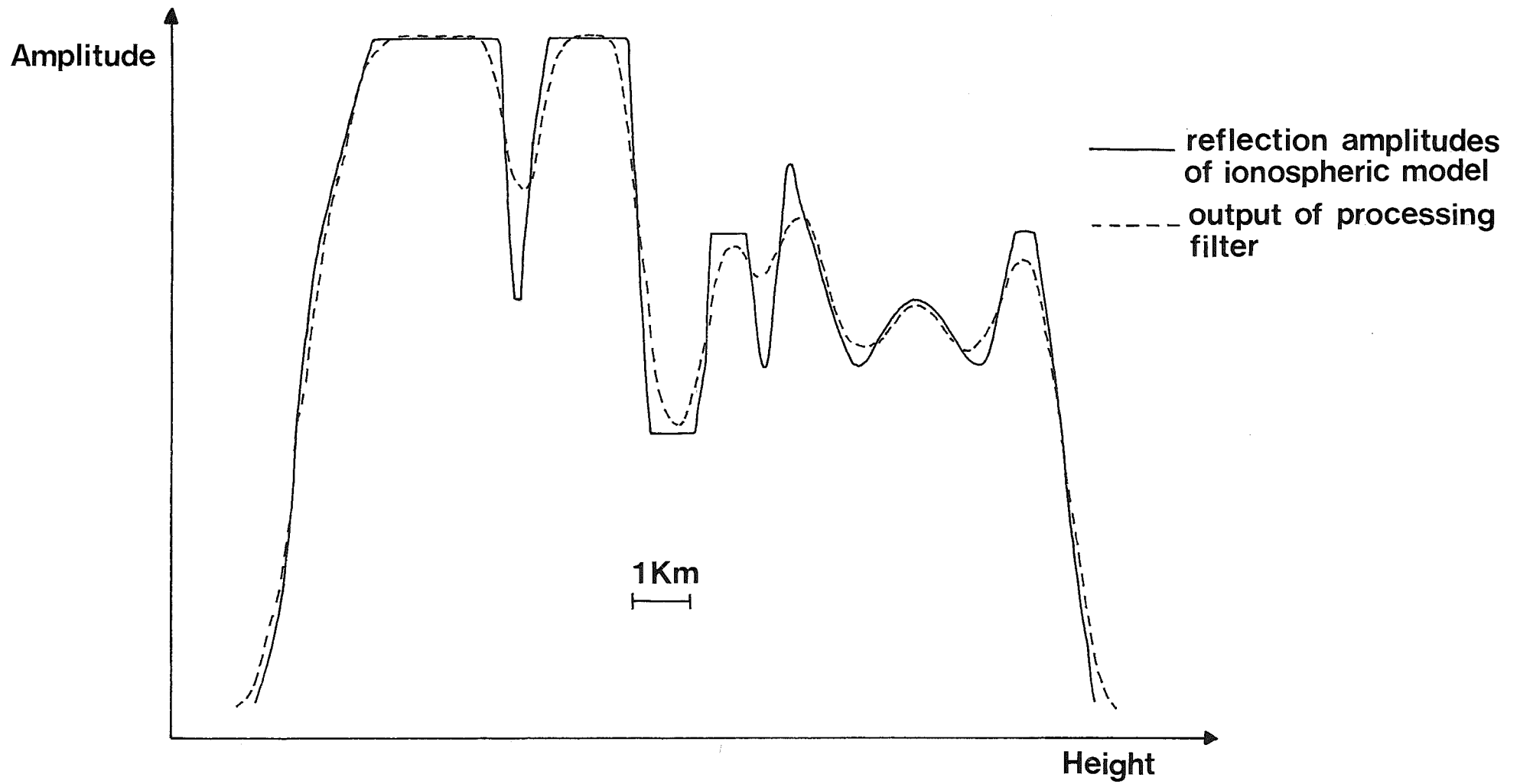
Fig. 4.10: Processing of a simulated ionospheric return.

The theoretical development of the pulse compression radar system is now complete, and subsequent chapters will deal with the specific hardware required for the installation of the system at Birdling's Flat.

CHAPTER 5

GENERATION OF THE LINEAR FREQUENCY MODULATED PULSE

5.1 INTRODUCTION

The design of a linear FM pulse generator has always been
one of the major tasks associated with the development of a
pulse compression radar system. The number of different
techniques in use is almost as great as the number of systems
themselves. Historically, 'chirp generators' fell into two
broad classes, designated 'active' and 'passive' generation
schemes. Passive systems derive the signal by exciting some
sort of dispersive filter with an impulse function (Klauder et
al., 1960; Wipperman, 1967). Such systems are not generally
used today, since small errors in the dispersive filter char-
acteristic can result in large amplitude variations in the
output and irregularities in the sweep rate. Also, active
systems are presently far more feasible and accurate than in
the past.

In an active generation system, the signal is produced by
an oscillator, the frequency of which is varied by external
control. Early examples of this type included voltage controlled
multivibrators, and similar techniques (Cook et al., 1964; Temes
et al., 1963). It is, however, difficult to achieve good lin-
earity of the frequency sweep with circuitry of this kind.

A number of techniques were developed in the 1960's to
improve the linearity of active generators. Peebles and Stevens
(1965) devised a method of synthesizing the sweep with a
number of smaller sweeps, the linearity of which could be more

easily controlled. Similarly, Fenwick and Barry (1965) approx-
imated a linear sweep by a succession of constant-frequency
pulses each of a slightly higher frequency than the previous.
In the late 1960's, Kibbler (1968) used a closed-loop generat-
ing system to correct for linearity errors in the generator, by
sampling the phase of the output signal, and comparing it to a
known reference. Also, Shirley (1968) independently developed
a similar system at about the same time. More recently,
Vettori (1971) devised a system for generating a linear FM
pulse using only digital circuit elements, and it is this system
which provided the basis for the method described in this
chapter.

The use of digital techniques in the application considered
here has a number of advantages. Firstly, the performance of
a digital circuit is not affected by component or environmental
variations, and as such the signal is repeatable, and free from
drift effects. Also, if arithmetic elements are used to
effectively calculate the frequency throughout the sweep,
errors in the sweep rate become practically non-existent. The
only deviation from linearity would be due to errors in the
clock frequency. There are, however, certain inherent disad-
vantages in the use of digital techniques, originating in the
fact that any circuit parameter (voltage, phase, time etc.)
must be quantized to some extent (though the level of
quantization can often be made arbitrarily small).

In the system described here, it is proposed to obtain
the required frequency modulation by phase modulating a fixed-
frequency carrier. This modulation is effected by abruptly

changing the phase of the carrier by a discrete amount at pre-
determined instants. Thus phase 'jumps' are inserted into the
signal at appropriate moments. The positions of these phase
jumps are controlled by arithmetic counting circuits, ensuring
excellent sweep linearity. The technique does, however, intro-
duce some 'noise', or spurious frequencies into the signal by
virtue of the discreteness of the phase jumps. It is shown,
though, that this noise can be reduced to an acceptable level.

5.2 THE MATHEMATICS OF DISCRETE PHASE MODULATION

In this section, the mathematical validity of approximating
a given signal with a discrete phase modulated signal will be
developed. As mentioned in the previous section, the technique
involves phase modulating a carrier by inserting phase 'jumps'
into the signal at certain 'sampling instants' throughout the
signal duration. These phase jumps are all of the same
magnitude; the degree of frequency modulation is controlled by
varying the frequency of occurrence of the phase increments.

Consider the case of a carrier signal at a frequency f_0,
phase modulated by an arbitrary phase function, $\psi(t)$. An
expression for such a signal would be

$$f(t) \quad = \quad \exp i\{2\pi f_0 t + \psi(t)\} \qquad\qquad (5.1)$$

Approximation of this function by a discrete phase modulated
signal first requires that the function $\psi(t)$ be sampled at
fixed intervals, giving a discrete phase function, $\psi(n)$. This
function is then quantized, that is, it may only take on values
of the form $p.\Delta\psi$, where p is an integer and $\Delta\psi$ is a fixed

quantization magnitude. This quantization is necessitated by the requirement that all phase jumps inserted into the signal be of the same magnitude. Fig. 5.1 shows the relationship between $\psi(t)$, $\psi(n)$, and the quantized function, $\psi_q(n)$ graphically. Note that in order to completely specify $\psi_q(n)$, all that is required is the knowledge, at each successive sampling instant, of whether to increment the function by $\Delta\psi$, to decrement it, or to leave it unaltered. It is essential that the reader understands this last point fully, as this is the principle on which the chirp generator operates.

Consider now the expression for a linear frequency-modulated pulse, given in equation (2.1). It may be re-written as

$$e(t) = \text{rect} \left[\frac{t}{T}\right] \exp i\{2\pi f_0 t + \phi(t)\} \tag{5.2}$$

where T is the duration of the signal

f_0 is the centre frequency

$\phi(t)$ is the modulating phase function.

The phase function is given by

$$\phi(t) = \pi k t^2 \tag{5.3}$$

where k is the rate of frequency modulation

which may be re-written as

$$\phi(t) = \frac{\pi \Delta f t^2}{T} \tag{5.4}$$

where Δf is the 'swept bandwidth' of the signal.

It is this phase function, $\phi(t)$, that is to be represented by a quantized, discrete function in the development which follows.
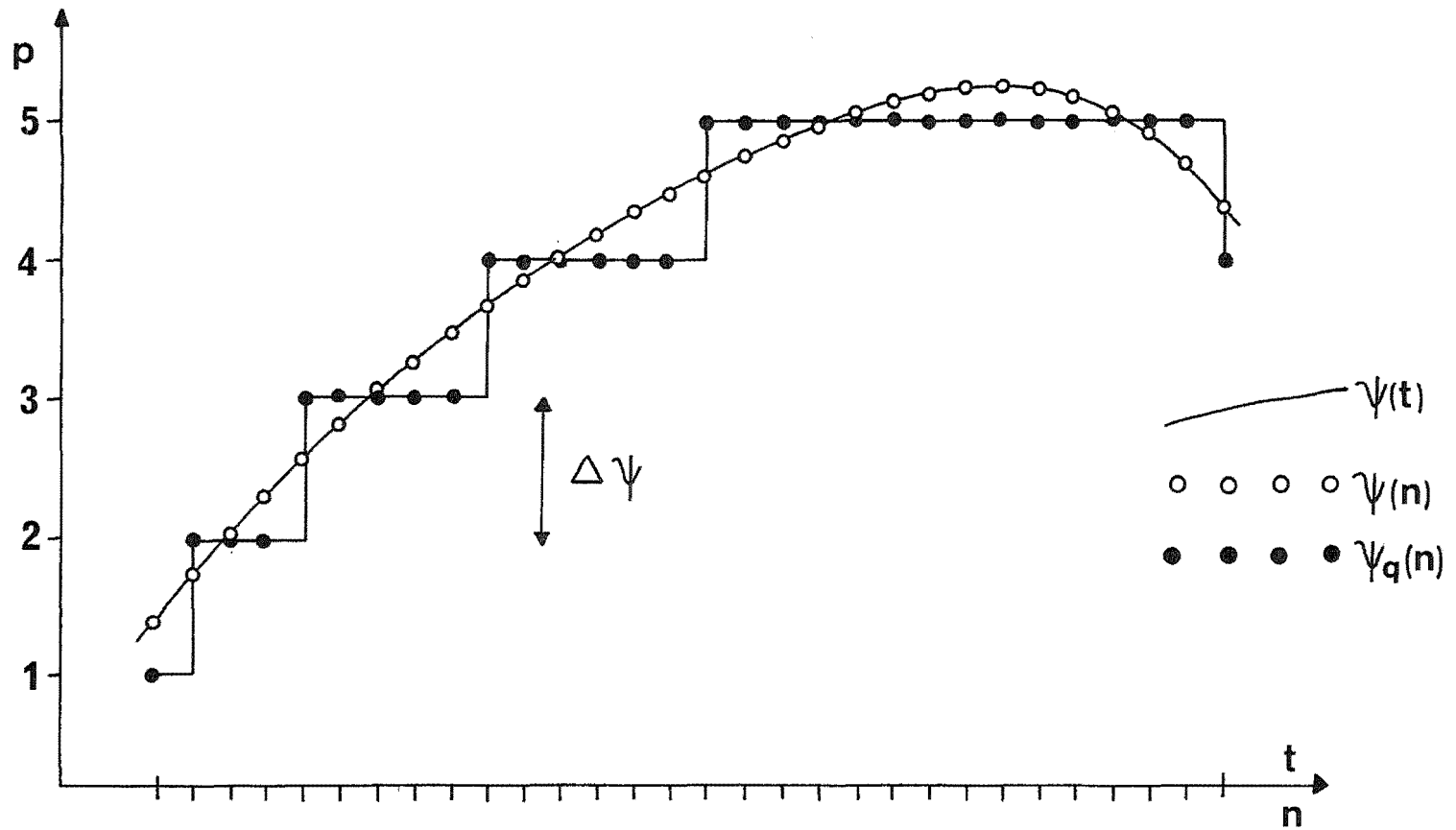
Fig. 5.1: Relationship between continuous, sampled, and quantised functions.

Suppose $\phi(t)$ is sampled at fixed intervals of Δt, giving a discrete function $\phi(n)$. If it is required that the difference between two adjacent samples is never greater than $\Delta\phi$, say, then an upper limit is created for the sampling interval, Δt. The magnitude of this maximum permissible Δt is, of course, dependent on the gradient of $\phi(t)$, according to the relation

$$\Delta t \leq \frac{\Delta\phi}{\left|\frac{d\phi(t)}{dt}\right|_{max}} \qquad (5.5)$$

where $\left|\frac{d\phi(t)}{dt}\right|_{max}$ is the maximum gradient of the function $\phi(t)$.

The gradient of $\phi(t)$ may be found directly from equation (5.4) as

$$\frac{d\phi(t)}{dt} = \frac{2\pi\Delta ft}{T} \qquad (5.6)$$

and the magnitude of this slope is clearly at a maximum when $t = -T/2$ or $T/2$, and is given by

$$\left|\frac{d\phi(t)}{dt}\right|_{max} = \pi\Delta f \qquad (5.7)$$

Substituting this into equation (5.5) leads to

$$\Delta t \leq \frac{\Delta\phi}{\pi\Delta f} \qquad (5.8)$$

which gives the maximum sampling interval permissible if the difference between two adjacent samples is to be no greater than $\Delta\phi$. Expressed in terms of the minimum sampling frequency, $f_{s_{min}}$, this is

$$f_{s_{min}} = \frac{\pi \Delta f}{\Delta \phi} \qquad (5.9)$$

If $\phi(t)$ is sampled throughout its duration at this minimum frequency, the total number of samples required, N, is given by

$$N = f_{s_{min}} \cdot T$$

$$\text{or} \qquad N = \frac{\pi D}{\Delta \phi} \qquad (5.10)$$

where $D = T\Delta f$, the time-bandwidth product of the chirp signal.

Thus if $\phi(t)$ is to be properly represented by $\phi(n)$, the range of $-T/2 \leq t \leq T/2$ must correspond to the range $0 \leq n \leq \frac{\pi D}{\Delta \phi}$. This will be accomplished if the variable t is replaced by n according to the relation

$$t = n\Delta t - T/2$$

$$\text{or} \qquad t = \frac{n\Delta \phi}{\pi \Delta f} - T/2 \qquad (5.11)$$

Substituting this into equation (5.4) gives

$$\phi(n) = \frac{\pi \Delta f}{T} \left[\frac{n\Delta \phi}{\pi \Delta f} - T/2 \right]^2$$

$$\text{or} \qquad \phi(n) = \frac{n^2 \Delta \phi^2}{\pi D} - n\Delta \phi + \theta \qquad (5.12)$$

where $\theta = \frac{\pi \Delta f T}{4}$, a constant phase factor.

This discrete function $\phi(n)$ must next be quantized. The quantized phase function, $\phi_q(n)$, is defined by

$$\phi_q(n) = q_n \Delta \phi \qquad (5.13)$$

where q_n is an integer

and $\Delta\phi$ is the 'quantization magnitude'.

The value of q_n may be obtained from the relation

$$q_n = \text{entier}[\phi(n)/\Delta\phi] \qquad (5.14)$$

where 'entier' has the meaning 'the nearest integer below'. Substituting equation (5.12) into equation (5.14) gives

$$q_n = \text{entier}\left[\frac{n^2\Delta\phi}{\pi D} - n + \frac{\theta}{\Delta\phi}\right]$$

or $q_n = \text{entier}\left[\frac{n^2\Delta\phi}{\pi D} + \frac{\theta}{\Delta\phi}\right] - n \qquad (5.15)$

since n is an integer.

The quantization magnitude, $\Delta\phi$, is chosen to have the same value as the maximum phase difference between adjacent samples of $\phi(n)$. This ensures that the difference between adjacent values of q_n is never greater than 1. The significance of this requirement is as follows. The chirp generator operates by computing the value of q_n at each sample instant throughout the signal duration. If this value differs from that at the previous sample point, a phase jump is inserted into the signal. Restricting the permissible values of $q_n - q_{n-1}$ to +1, 0, or -1 means that phase jumps of magnitude $+\Delta\phi$ or $-\Delta\phi$ only are required. This results in a considerable reduction of hardware requirements.

The linear FM pulse will thus be approximated by the function

$$e_q(t) \;=\; \text{rect}\left[\frac{t}{T}\right] \exp\, i\{2\pi f_0 t + \phi_q(n)\} \qquad\qquad (5.16)$$

which differs from e(t), given in equation (2.1) only in that it will contain some spurious frequency components introduced by the quantization of the phase function. (The locations and magnitudes of these components are investigated in section (5.4).)

The function $\phi_q(n)$ is a modulating phase applied to the carrier, $\exp\, i(2\pi f_0)$. Every Δt seconds, this function changes its value by $-\Delta\phi$, 0, or $+\Delta\phi$, and in such a manner, introduces a linear frequency modulation into $e_q(t)$. At the beginning of the chirp pulse, when maximum negative deviation from f_0 is required, a phase jump of $-\Delta\phi$ should occur at <u>each</u> sampling instant (since sampling takes place at the minimum possible frequency). As time progresses, there would exist a few sampling instants with zero phase jump, the incidence of these zeroes increasing towards the centre of the chirp, when <u>all</u> phase jumps would be zero. Later in the pulse, phase jumps of $+\Delta\phi$ would occur at some sampling points, the incidence of these increasing until, at the end of the chirp, all sample points would have positive phase jumps. A graph of $\phi_q(n)$ compared with $\phi(t)$ for N = 32 points is shown in Fig. 5.2, and should help make this description clear.

5.3 IMPLEMENTATION OF THE DISCRETE PHASE MODULATOR TECHNIQUE

The complexity of the circuitry required to implement the procedure described in the previous section may be considerably reduced if the phase quantization magnitude, $\Delta\phi$ is chosen to be of the form π/m, where m = $\{2,4,8,...\}$. The general
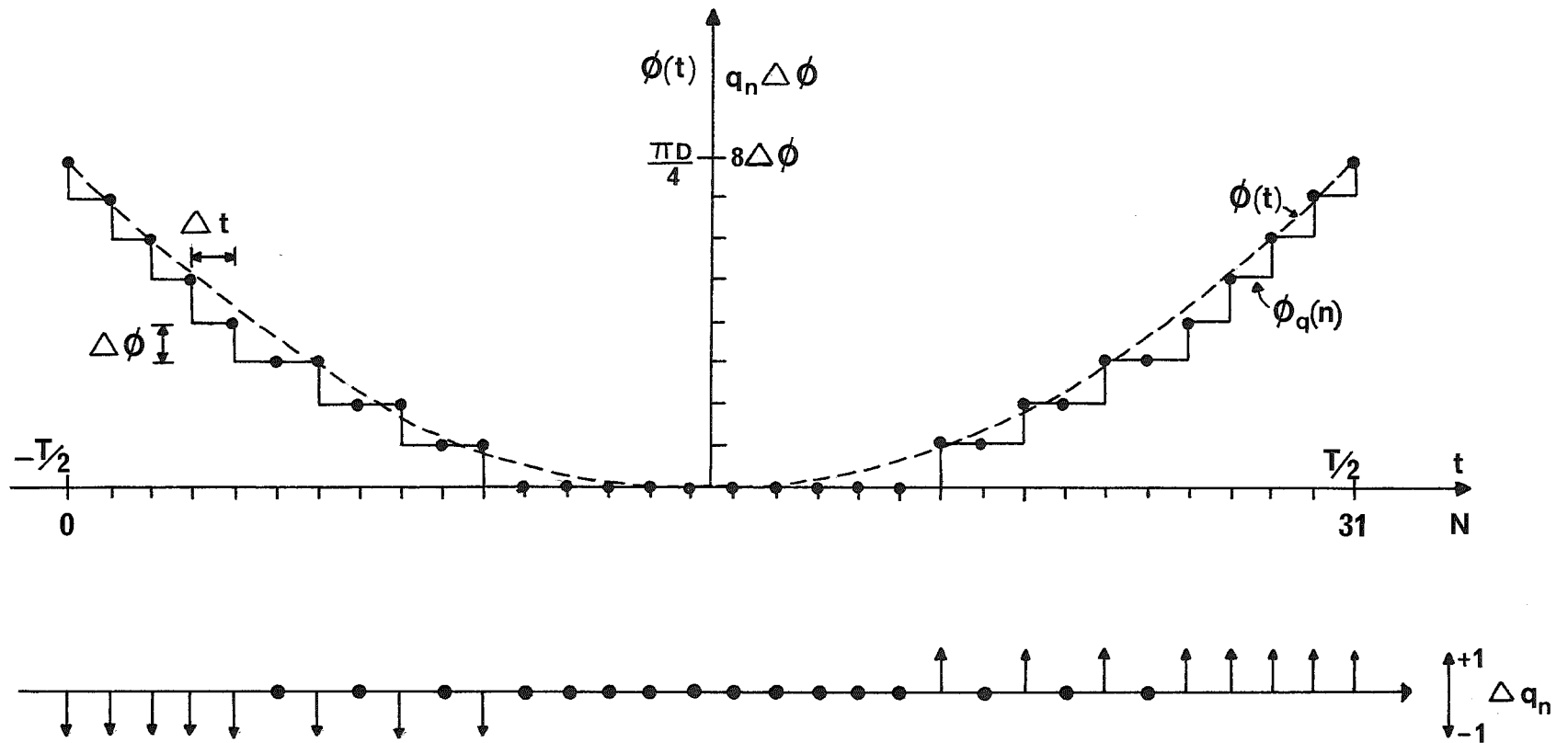
Fig. 5.2: Relationship between $\phi(t)$, $\phi_q(n)$, and q_n.

principle of the proposed implementation is depicted in Fig. 5.3. Here a number of networks are available, each providing a constant phase shift of π/m. Any number of these may be inserted progressively in series with the signal by means of a rotary switch. If the switch is rotated clockwise, a phase jump of $+\pi/m$ will result; if anticlockwise, a jump of $-\pi/m$.

A chirp pulse may be generated with this arrangement by computing q_n at each sampling point, and comparing it with the previous value, q_{n-1}. (It was earlier noted that the difference between these two values of q may only be -1, 0, or +1). If q_n is one larger than q_{n-1}, the rotary switch must be jumped clockwise; if smaller, it must be jumped anticlockwise, and if it is the same, the switch must be left alone.

q_n is computed using equation (5.15), which may be re-written, replacing $\Delta\phi$ by π/m and neglecting the constant phase factor, as

$$q_n = \text{entier} \left[\frac{n^2}{mD}\right] - n \qquad (5.17)$$

The total number of samples is given by equation (5.10) as $\frac{\pi D}{\Delta\phi}$, which becomes simply mD.

The desirability of using only digital circuitry in the construction of the chirp generator has already been stated. The consequences of utilising a square wave, rather than a sinusoidal carrier should therefore be investigated. The effect on the frequency content of the signal will be discussed in section 5.4; at this point, only the logistics of such a situation will be considered. Fig. 5.4 shows an unmodulated square wave, below which is an example of a similar waveform with one negative, and one positive phase jump inserted, both of magnitude $\pi/2$. It can readily be seen that if the magnitude
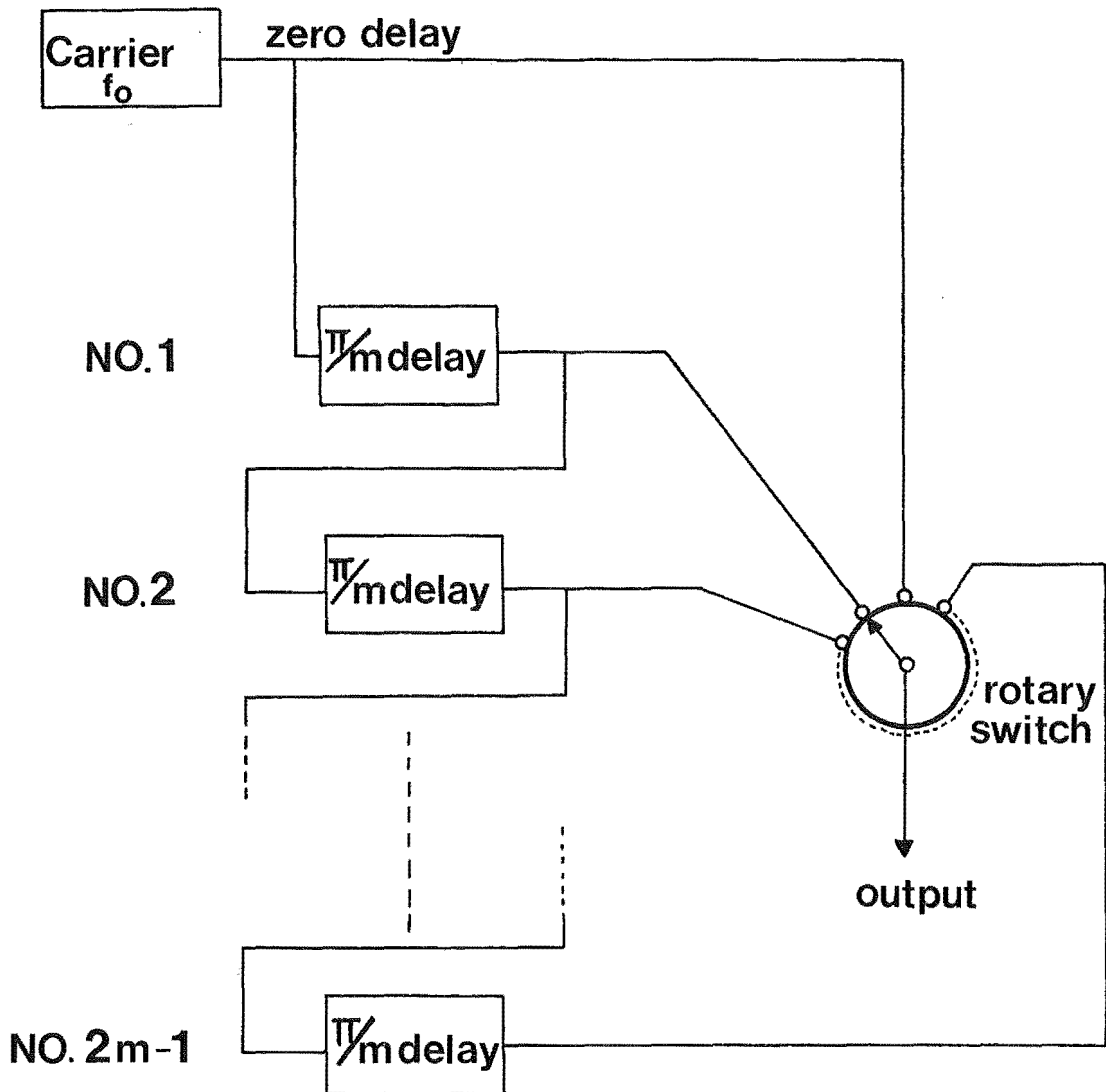
Fig. 5.3: Discrete phase modulation technique.

$\triangle \phi = -\pi/2$ $\triangle \phi = +\pi/2$
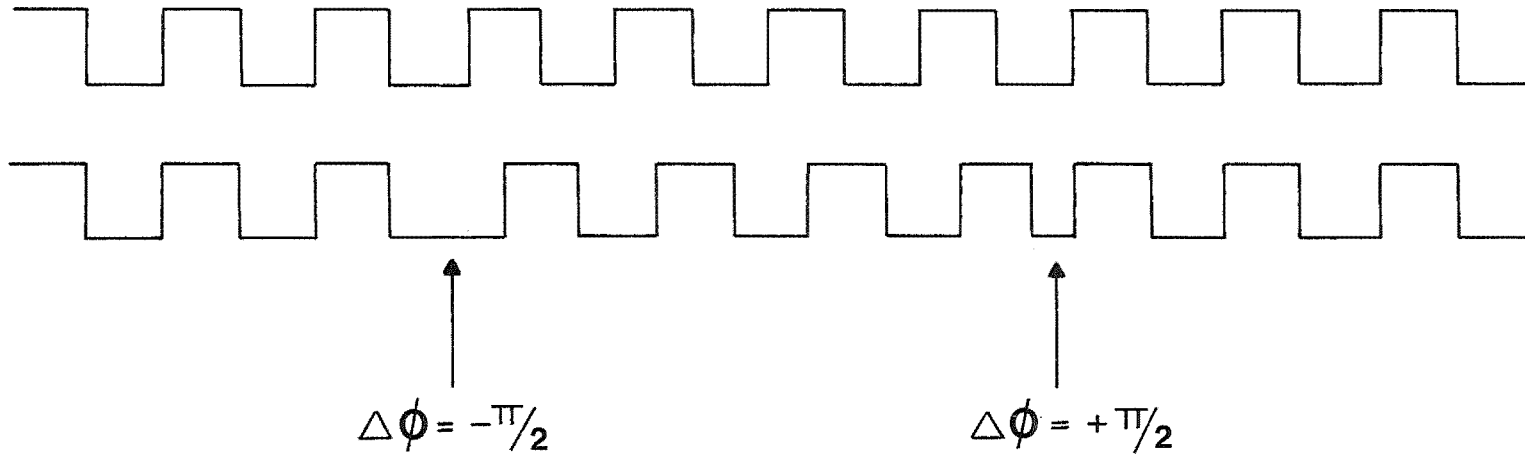
Fig. 5.4: A square wave containing phase jumps.

of the phase jumps is not to exceed the chosen value of π/m, only one jump may be inserted in any half cycle of the carrier waveform. Since the minimum frequency that will be present in the signal is $f_0 - \Delta f/2$, the maximum permissible sampling frequency is determined by

$$f_s \leq 2(f_0 - \Delta f/2) \qquad (5.18)$$

But from equation (5.9) the minimum sampling frequency is given by

$$f_{s_{min}} = m\Delta f \qquad (5.19)$$

(replacing $\Delta\phi$ in equation (5.9) by π/m). Combining equations (5.18) and (5.19) leads to

$$m\Delta f \leq f_s \leq 2(f_0 - \Delta f/2)$$

$$\text{or} \qquad Q \geq \frac{1+m}{2} \qquad (5.20)$$

$$\text{where} \qquad Q = \frac{f_0}{\Delta f}$$

Thus, the use of a square wave carrier limits the maximum bandwidth obtainable, once the factor m has been chosen.

5.4 FREQUENCY CONTENT OF A DISCRETE PHASE MODULATED CHIRP PULSE

A linear FM signal generated with the technique just described will contain a number of frequency components in addition to the desired signal. In order to investigate the frequencies and amplitudes of these spurious components, it is instructive to consider a carrier signal which is discretely phase modulated by phase jumps of constant magnitude, occurring

at a constant frequency. Such a signal could be produced by rotating the rotary switch in Fig. 5.3 at a constant rate in one direction. This procedure would result in the output being <u>shifted</u> from f_0 by some amount δf. Assuming that all phase jumps have a magnitude of π/m, and occur at fixed intervals of Δt, the frequency shift will be related to these by

$$\delta f = \frac{1}{2\pi} \frac{\Delta \phi}{\Delta t} = \frac{1}{2m\Delta t} \qquad (5.21)$$

Referring again to Fig. 5.3, it can be seen that the signal at the output will consist of a sum of 2m periodic signals, each at a frequency of f_0, with each signal being 'on' for Δt seconds, and 'off' for $(2m-1)\Delta t$ seconds. Each of these 2m signals could be expressed as a square wave carrier with some particular phase, amplitude modulated by a rectangular envelope of length Δt. If these 2m signals are summed, with due regard to their phases and times of occurrence, the result, after considerable re-grouping, may be written:

$$s(t) = \sum_{r=1}^{\infty} (-1)^{r+1} \frac{1}{2r-1} \left\{ \sum_{z=0}^{\infty} \frac{\sin \pi(\frac{2mZ+1}{2m})}{\pi(\frac{2mZ+1}{2m})} \cdot \cos 2\pi \left[(2r-1) f_1 + Z2m\delta f \right] t \right.$$

$$\left. + \sum_{Z=1}^{\infty} \frac{\sin \pi(\frac{2mZ-1}{2m})}{\pi(\frac{2mZ-1}{2m})} \cdot \cos 2\pi \left[(2r-1) f_1 - Z2m\delta f \right] t \right\} \qquad (5.22)$$

where $f_1 = f_0 + \delta f$.

If this signal is long-lasting in time, it may be represented by the line spectrum shown in Fig. 5.5. The sum over Z (in
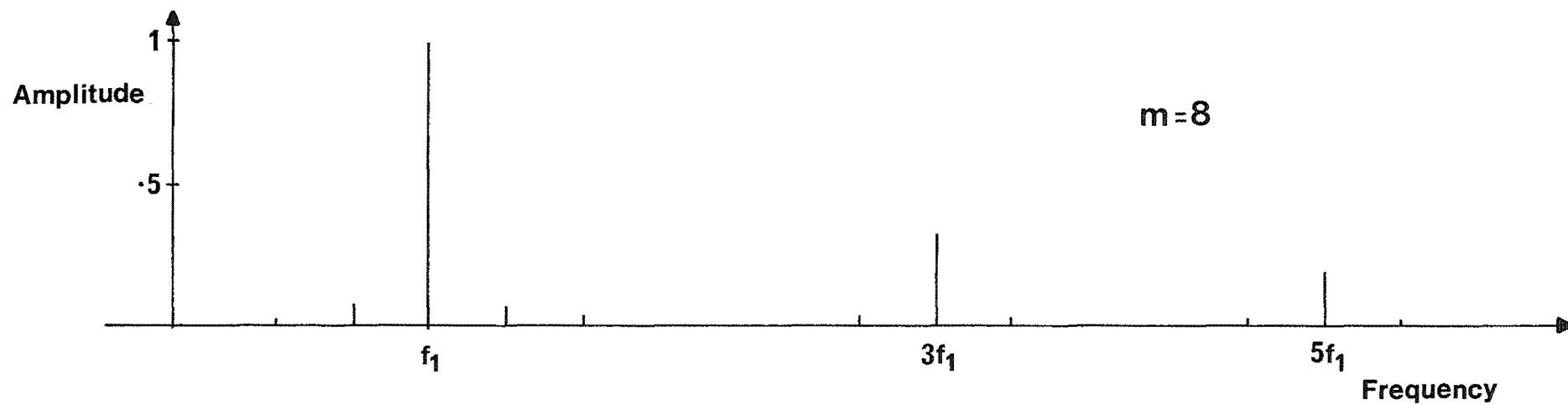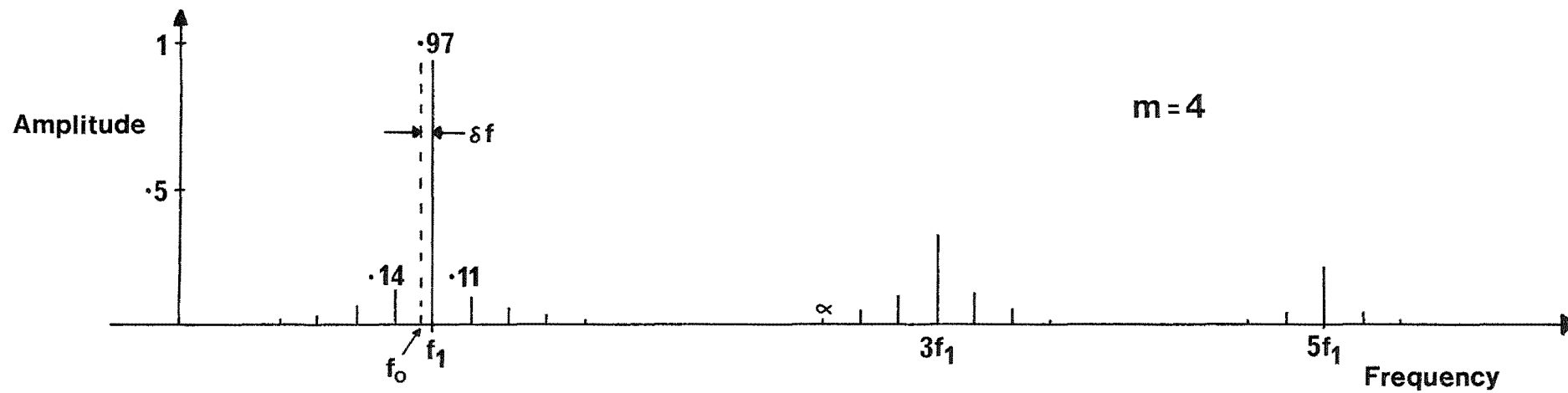
Fig. 5.5: Frequency content of a square wave with constant phase jump rate.

equation 5.22) represents a family of lines centred around the main component at f_1, the minor lines originating because the phase of the signal has been quantized. The sum over r represents attenuated replicas of this family centred about $3f_1$, $5f_1$, ..., occurring because the carrier is a square wave. The interline distance within a family is $2m\delta f$, and though the positions of the lines are centred about f_1, the ampltiude distribution of these lines is a $\frac{\sin x}{x}$ function centred on f_0. Hence the lines above f_1 will have different amplitudes from the corresponding lines below f_1, resulting in the two sums over Z in equation (5.22). The first term represents the main line and the higher frequency set; the second term is the lower frequency set. Note that by doubling the value of m, the number of spectral lines is halved, with a consequent increase in the energy of the main component.

The spectrum of a linear FM signal generated by the discrete phase modulation technique may be regarded as being of the form shown in Fig. 5.5, where the spectral lines move slowly along the frequency axis as the instantaneous frequency of the chirp pulse increases. Though a simplified model, it is useful in that it will give with reasonable accuracy the locations and amplitudes of the major spurious frequencies present in the chirp generator output.

5.5   CHOICE OF SIGNAL PARAMETERS

Before a detailed design of the chirp generator is attempted, the values of the various parameters associated with the discrete phase modulation technique must be fixed. In particular, the following criteria should be met as closely as possible.

1. In order to keep spurious frequency components at a minimum, the factor m should be made as large as possible (see Fig. 5.5). The selection must, however, be consistent with the constraint imposed by the use of a square wave carrier, i.e.

$$Q \geq \frac{1+m}{2}$$ (5.20)

2. The use of binary arithmetic in the calculation of q_n results in the restriction that the time-bandwidth product of the signal be some power of 2 (see section 4.6.2).

3. The use of a phase coherent receiving system puts some constraints on the frequencies available as inputs to the chirp generator.

4. Consider Fig. 5.5 again, bearing in mind how the spectral lines shift throughout the duration of the chirp pulse. Since the inter-line distance is directly proportional to δf, it may be appreciated that by generating a larger frequency sweep than is actually required, and utilizing only a portion of it, all spurious spectral lines in the fundamental family may be removed from the desired signal region. This effect will be discussed in detail shortly; at this stage, it need only be understood that it is a contributing factor in the following selection of signal parameters.

A large number of possible configurations was investigated, in an attempt to best satisfy the preceding conditions. It was found that a value of m=8 consistently violated condition 1, and hence m=4 was chosen. The most satisfactory compromise yielded the following parameters:

Carrier frequency = 2.2 MHz

Time-bandwidth product = 256

Extent of frequency deviation = 1.9 - 2.5 MHz

Length of signal = 426 μsec.

The time taken for the signal to sweep the range from 2.3 to 2.5 MHz at this modulation rate is given by

$$T = \frac{0.2}{2.5-1.9} \cdot 426 \text{ μsec}$$

or $\qquad T = 142$ μsec.

This is somewhat less than the originally specified pulse width of 150 μsec; the deviation originates principally as a consequence of condition 3 given earlier.

The sampling frequency which will provide sufficient deviation from f_0 may be found from equation (5.19):

$$f_{s_{min}} = m\Delta f = 4(2.5-1.9)$$

or $\qquad f_{s_{min}} = 2.4 \text{ MHz}.$ $\hfill (5.23)$

The mechanism by which the spurious frequencies in the immediate family of spectral lines are kept out of the range 2.3 to 2.5 MHz will now be investigated in detail. Consider a discrete phase modulated pulse with the parameters specified earlier, i.e. a frequency range from 1.9 to 2.5 MHz, and a length of 426 μsec. It is intended to utilize only the section of this signal which extends from 2.3 to 2.5 MHz. The line spectrum at some particular instant in the sweep is drawn in Fig. 5.6, for the case of m=4, where only the closest spectral lines in the immediate family are shown. Note that the lines are always separated by $2m\delta f$, or in this case $8\delta f$.
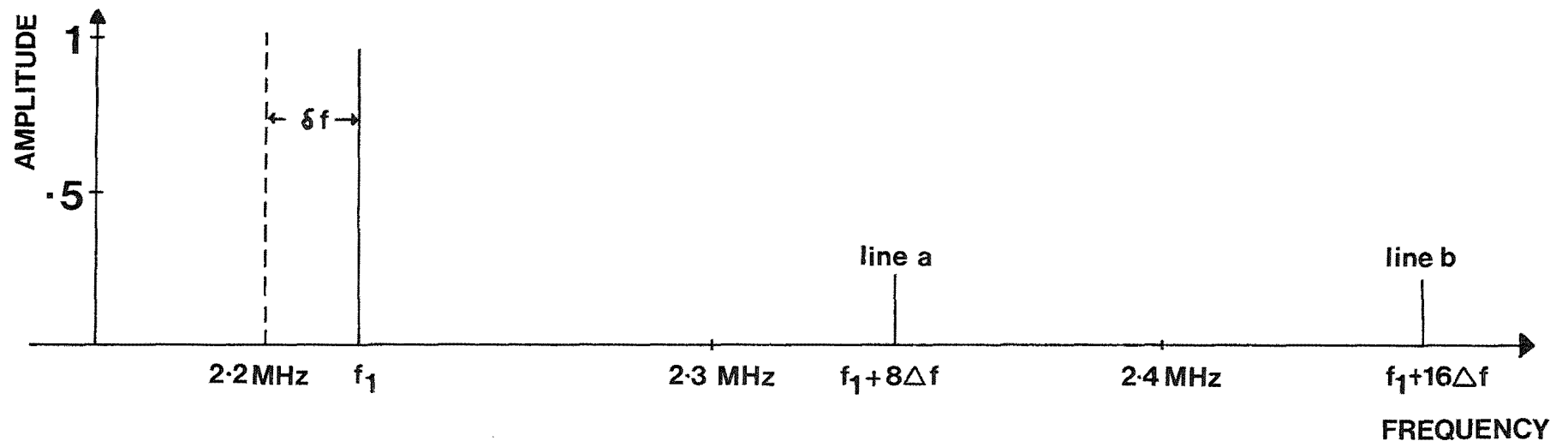
Fig. 5.6: Some lines in the chirp spectrum.

Now, when f_1 is in the range from 2.3 to 2.5 MHz, δf will be in the range $0.1 \leq \delta f \leq 0.3$ MHz, and consequently, line 'a' (Fig. 5.6) will move from 3.1 to 4.9 MHz, and hence will <u>never</u> fall inside the range 2.3 to 2.5 MHz. Similarly, line 'b' will be even further removed from the region of interest. Thus the only spurious spectral lines which could possibly come within the range 2.3 to 2.5 MHz are those which extend down from the second family of lines (grouped around $3f_1$) and higher families.

The line of largest amplitude which does cross the signal region is in fact the third line in the family below the component at $3f_1$ (this line is marked with an 'α' in Fig. 5.5). Its separation from the line at $3f_1$ will be $3(2m\delta f)$, or $24\delta f$. Thus the frequency of this line will be given by

$$f_\alpha = 3f_1 - 24(f_1 - f_0)$$

or $$f_\alpha = 52.8 - 21f_1 \text{ MHz} \tag{5.24}$$

The period that this line is present in the interval 2.3 to 2.5 MHz may be obtained from the inequality

$$2.3 \leq 52.8 - 21f_1 \leq 2.5$$

or $$2.395 \leq f_1 \leq 2.404 \text{ MHz} \tag{5.25}$$

In other words, during this interval of f_1, a component sweeps rapidly through the range 2.5 to 2.3 MHz, the amplitude of which is obtained from equation (5.22) as

$$A_\alpha = \frac{1}{2r-1} \left[\frac{\sin \pi (\frac{2mZ-1}{2m})}{\pi (\frac{2mZ-1}{2m})} \right] \tag{5.26}$$

where in this case r=2 and Z=-3. Evaluation yields

$$A_\alpha = 0.014$$

The component α is only present in the range 2.3 to 2.5 MHz for 4.5% of the duration of the chirp pulse; it thus has an average power during the signal interval of 0.001% of that of the main component. Other spurious components from higher order families will, of course, have even lower amplitudes, and hence the contribution of all these spurious components may safely be neglected.

5.6 PRACTICAL CONSIDERATIONS

This section deals with a number of separate issues. The first part describes a mechanism by which phase jumps of $\pi/4$ may be inserted into a square wave carrier at any given instant; this is followed by an indication of how circuitry may be devised which can compute the difference between q_n and q_{n-1} for any value of n. Certain control features of the chirp generator are also discussed.

5.6.1 The Discrete Phase Modulator

The discrete phase modulator inserts a phase jump of $\pi/4$ into a carrier signal whenever it receives a 'modulation command' from another section of the chirp generator. This is achieved by inserting two successive phase jumps of $\pi/2$ into a square wave carrier of frequency $4f_0$; that is, a total phase increment of π radians. The waveform so produced is then divided by four, resulting in a signal at a frequency f_0, containing phase jumps of $\pi/4$.

The mechanism by which the technique is realised is shown schematically in Fig. 5.7. The changeover switch is operated each time a 'modulation command' is received, the actual instant of switching being synchronised with the next falling edge of the signal at point 'A'. The waveforms which appear at various points in the circuit are shown graphically in Fig. 5.8. It may be seen that operating the switch produces one half-cycle of a signal at a frequency of f_0 which is shorter than adjacent half-cycles by $\pi/4$ radians. This would occur irrespective of the position of the 'modulation command' (dashed line), and for either switching direction. A circuit which performs this function using digital circuit elements is described in section 5.7.

It should be noted that the method of discrete phase modulation described in this section is only capable of inserting positive phase jumps into a carrier signal. However, since the entire range of signal frequencies utilized (2.3 to 2.5 MHz) is above the carrier frequency of 2.2 MHz, negative phase jumps are not required.

5.6.2 The Modulation Command Controller

The function of this section of the chirp generator is to compute the value of q_n at each sample instant, and determine whether or not this value differs from q_{n-1}. (It will be recalled that $q_n - q_{n-1}$ may only be +1, 0, or -1). If $q_n - q_{n-1}$ is ±1, a modulation command is sent to the discrete phase modulator circuit; if $q_n - q_{n-1}$ is zero, no action is taken.

The value of q_n is computed using the relation
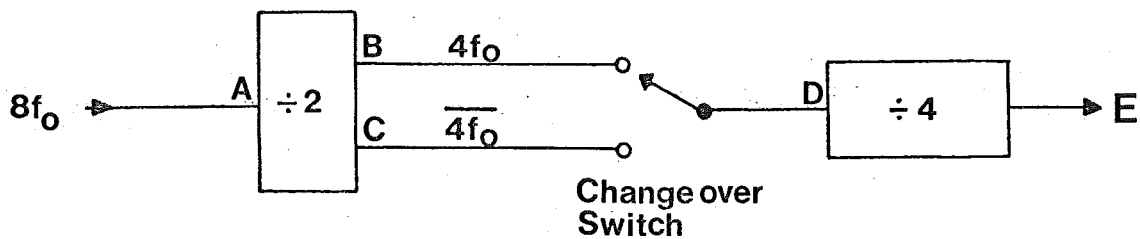
Fig. 5.7: A method of inserting phase jumps into a carrier.
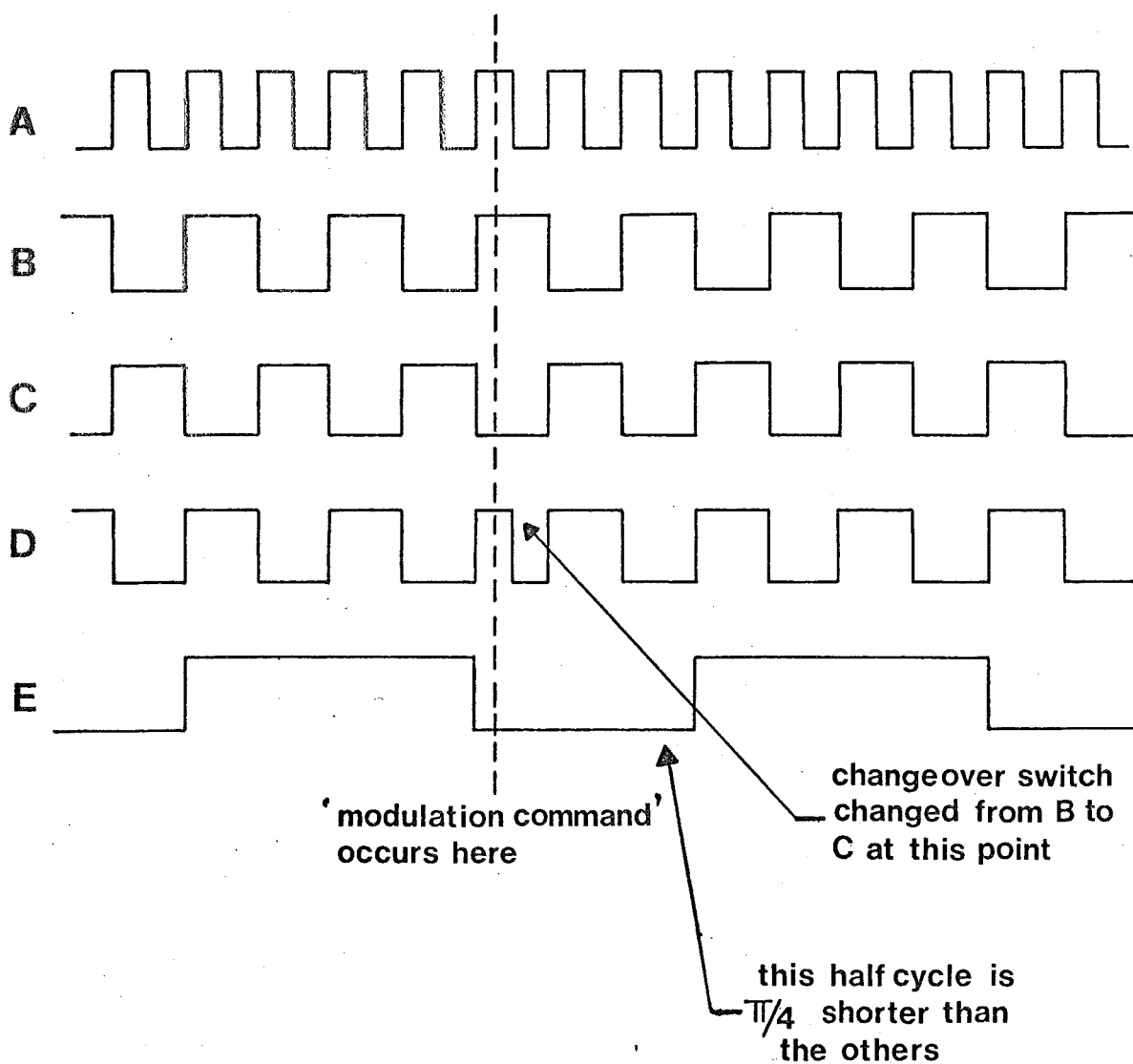
Fig. 5.8: Waveforms at various points in Fig. 5.7

$$q_n = \text{entier } [\frac{n^2}{mD}] - n, \quad 0 \le n \le mD \tag{5.17}$$

which for m=4 and D=256 becomes

$$q_n = \text{entier } [\frac{n^2}{1024}] - n, \quad 0 \le n \le 1024 \tag{5.27}$$

The criterion for sending a modulation command to the discrete phase modulator ($q_n - q_{n-1} = \pm1$) thus becomes

$$\text{entier}[\frac{n^2}{1024}] - n - \{\text{entier } [\frac{(n-1)^2}{1024}] - (n-1)\} = \pm1$$

$$\text{or} \quad \text{entier}[\frac{n^2}{1024}] - \text{entier } [\frac{(n-1)^2}{1024}] = 2 \text{ or } 0 \tag{5.28}$$

A circuit must thus be devised which can compute the value of entier $[n^2/1024]$ for any value of n in its range, and determine if it has changed, either by 2 or 0, or by 1, from its previous value.

A configuration which accomplishes this is sketched in Fig. 5.9. Suppose for the moment that the upper 20-bit binary register contains the value of n^2. Now, if the least significant k bits are ignored, the binary word formed by the remaining bits will contain the value entier $[n^2/2^k]$. More specifically, if only the upper ten bits are considered, they will contain the value of entier $[n^2/1024]$.

Consider bit 11 only. It is the least significant bit of the number entier $[n^2/1024]$. If entier $[n^2/1024]$ changes its value by 2 or 0, this bit will remain unchanged. If entier $[n^2/1024]$ changes its value by 1, bit 11 will be complemented. Hence if bit 11 does not change its state when the number in

| 0 | 1 | 1 | 0 | 0 | 1 | 0 | 1 | 1 | 0 | 1 | 1 | 0 | 1 | 1 | 0 | 0 | 1 | 0 | 0 |

20 bit register–contains n^2

ADD   ADD   ADD

10 bit register–contains n ⟶

| 0 | 1 | 1 | 1 | 0 | 1 | 1 | 0 | 1 | 0 |

10 9   8   7   6   5   4   3   2   1 bit number
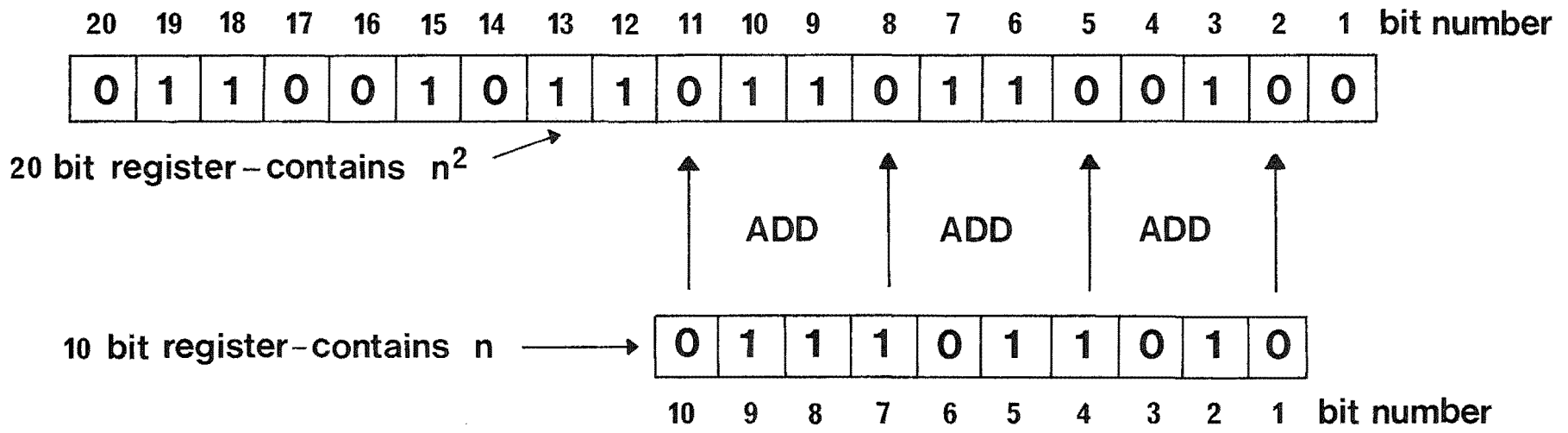
Fig. 5.9: Modulation command controller principle.

the upper register is altered from n^2 to $(n+1)^2$, a phase jump must be inserted into the signal at that point.

The upper register can be made to always contain n^2 by sequential computation from the formula

$$(n+1)^2 = n^2 + 2n + 1$$

in the following manner. Suppose that the lower register is to contain n, and that initially, both registers contain zero. At each sampling instant, the contents of the lower register are added to bits 2 to 11 of the upper register (this is equivalent to adding 2n to that register). The n^2 register is then incremented by 1, and will thus contain the number n^2+2n+1. Finally, the lower register is incremented, so that it contains the next value of n. Hence, at each sampling instant, the following operations must take place:

1. Add the contents of the lower register to bits 2 to 11 of the upper register.

2. Increment the upper and lower registers.

3. Test bit 11 of the upper register - if it has the same value as in previous samples, send a modulation command to the discrete phase modulator.

Strictly, all modulation commands which occur in the first half of the sweep ($0 \leq n \leq 512$) should produce negative phase jumps; however, since this part of the sweep is not used, this fact can be ignored without prejudicing the state of the registers, and hence the waveform of the later part of the sweep. Also, since bit 11 of the n^2 register is the most significant bit that affects the modulation process, bits 12 to 20 can actually be omitted from the circuitry, remaining present 'in spirit' only.

5.6.3 Control

Certain control functions must be included in the chirp generator if the proposed method is to be implemented effectively. For instance, it is desirable that upon receipt of a trigger pulse, the chirp generator instantly generate a linear FM pulse in the range 2.3 to 2.5 MHz. This is accomplished in the following manner, noting that the range $2.3 \leq f \leq 2.5$ MHz corresponds to the range $683 \leq n \leq 1024$. The two registers are initially both set to zero, and are taken through the sequence of adding and incrementing, outlined in the previous section, with the output of the generator inhibited. As soon as the lower register reaches a value of n = 683, this process is halted. When a trigger command is received, the output is enabled, and the modulation process re-started, continuing until n = 1024. The output is then again inhibited, and the procedure repeated.

Other minor control functions will be discussed in the next section when the full circuitry of the chirp generator is presented.

5.7 DETAILED CIRCUITRY

5.7.1 General Considerations

Since the signal processing method described in chapter 4 requires for its operation a phase coherent receiving system, all signals used in the generator and in the receiving system should be derived from a master clock. The stable frequency source resident at Birdling's Flat operates at 9.6 MHz; it would be desirable to derive all required signals from this by frequency synthesis. Two inputs to the chirp generator are required, one at $8f_0$, or 17.6 MHz for the carrier, and one at

2.4 MHz, the sampling frequency. Inspection of these numbers shows that both of them bear simple integer relationships to 9.6 MHz. Specifically,

$$17.6 = 9.6 \times 11/6$$

$$2.4 = 9.6/4$$

This is not accidental; the desirability of using these two frequencies instigated a slight compromise in the choice of signal parameters, resulting in the deviation from a 150 μsec pulse width.

The circuitry which performs the synthesis of 17.6 MHz from 9.6 MHz is described in detail in the Appendix.

5.7.2 The Discrete Phase Modulator Circuit

The complete circuit of this section of the chirp generator is presented in Fig. 5.10. This circuit performs the function described in section 5.6.1, and depicted in Fig. 5.7. It may assist the reader to refer back to these before proceeding.

The 17.6 MHz input is first buffered, and fed into a 'toggling' flip-flop. Either of the two complementary outputs is then selected, depending on the state of the D-type flip-flop. This flip-flop and the three associated gates comprise the 'changeover switch' shown in Fig. 5.7. According to the specification given in 5.6.1, this switch must be changed each time a modulation command is received, the actual instant of switching being synchronised with the falling edge of the signal at point 'A' in Fig. 5.7. The circuit realises this criterion, since the output of the flip-flop FF2 will change

AND Gate

OR Gate

Inverting Buffer

17·6 MHz

Ⓐ

FF1

Q̄

Q

D-type

Q

Q̄

D

clock

FF2

Q

T

Output
inhibit/enable

8·8 MHz
phase modulated

÷ 2

T

Q

4·8 mHz
chirp out

reset

'modulation command'
input

FF flip flop
T   toggling input
QQ̄ complimentary
    outputs
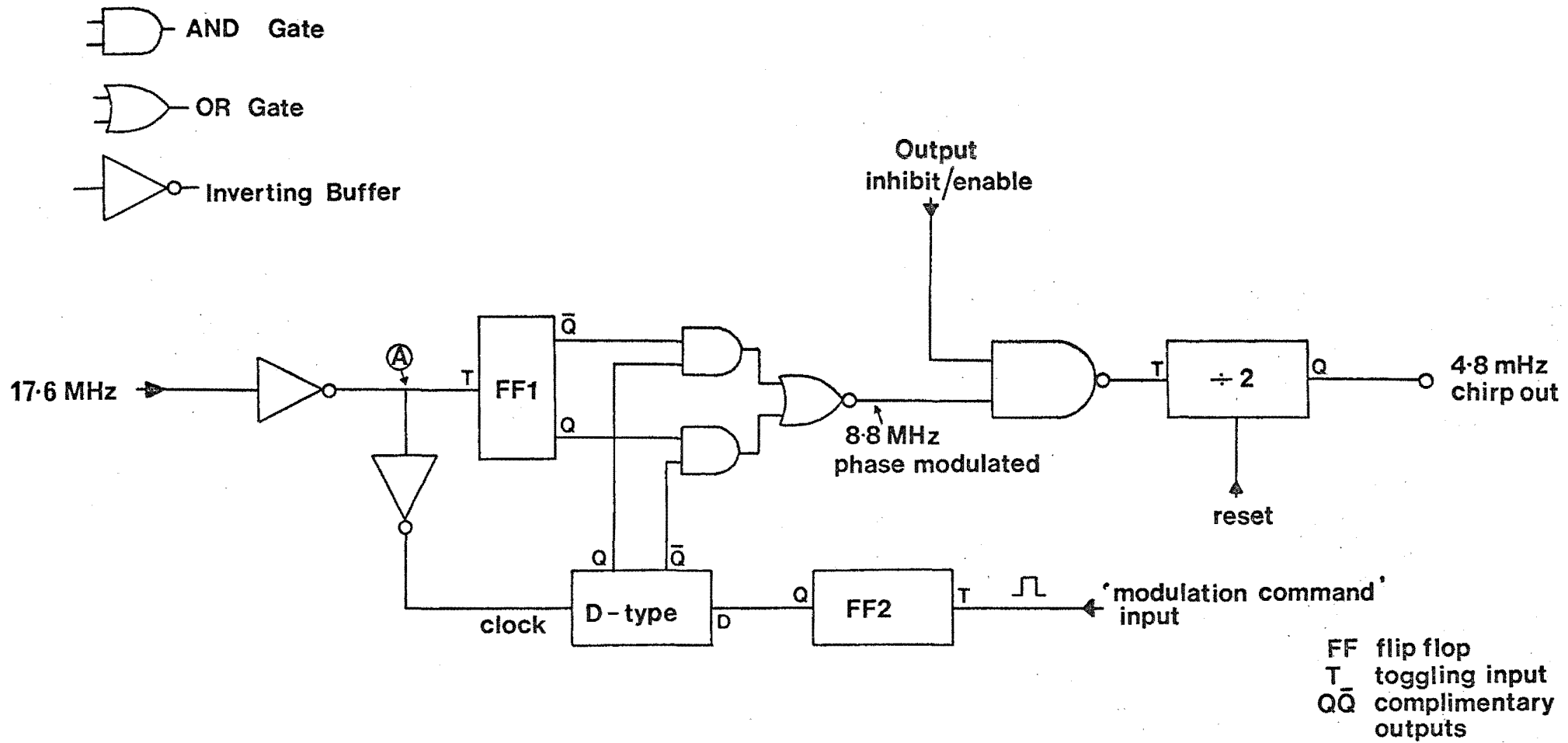
Fig. 5.10: Discrete phase modulator circuit.

88

its state immediately a modulation command is received, and this new state will be clocked into the D-type flip-flop when its clock signal rises, i.e. when the signal at point 'A' falls.

The selected signal then passes through a gate which inhibits the signal unless it is in the range corresponding to 2.3 to 2.5 MHz (the inhibit/enable command is produced in the control section of the chirp generator). Finally, the signal is divided by two. The output is thus a chirp pulse centred about 4.8 MHz, containing phase jumps of $\pi/2$. The further division to a 2.4 MHz chirp is left until the signal is within the transmitter. The $\div 2$ flip-flop at the discrete phase modulator output is reset at the end of each pulse, to ensure that successive chirps all have the same phase.

5.7.3 Modulation Command Controller Circuitry

A simplified schematic of this section, which is the essence of the chirp generator, is presented in Fig. 5.11. It operates as follows. The outputs of the full adder (Σ_{11} to Σ_1) always contain a binary word which is the arithmetic sum of the two binary words (A_{11}, A_{10}, ..., A_1) and (B_{11}, B_{10}, ..., B_1) at its inputs. The word (A_{11}, A_{10}, ..., A_1) effectively always contains the value $2n+1$, since A_{11} to A_2 are connected to the outputs of the n register, and A_1 is held in a '1' state. The word (B_{11}, B_{10}, ..., B_0) always contains the value of n^2, since it is connected to the outputs of the n^2 register. Thus, the word at the output of the adder, and hence at the data inputs to the D-type flip-flops comprising the n^2 register, always contains the value of n^2+2n+1, or $(n+1)^2$.

Count 1

Output
to Discrete
Phase
Modulator

NOR

Ⓠ

Ⓟ

X-OR

reset

to
B_{11}

Q_2

Q_1

to
B_2

Register Y   II bit D-type latch   contains n^2

clk

Count 2

D_{11}

D_2

D_1

Σ_{11}

Σ_2

Σ_1

II bit full adder

A_{11} B_{11}

A_2 B_2

A_1 B_1

hold high

Q_{10}

Q_1

Register X   IO bit binary counter Contains n count

Count 3
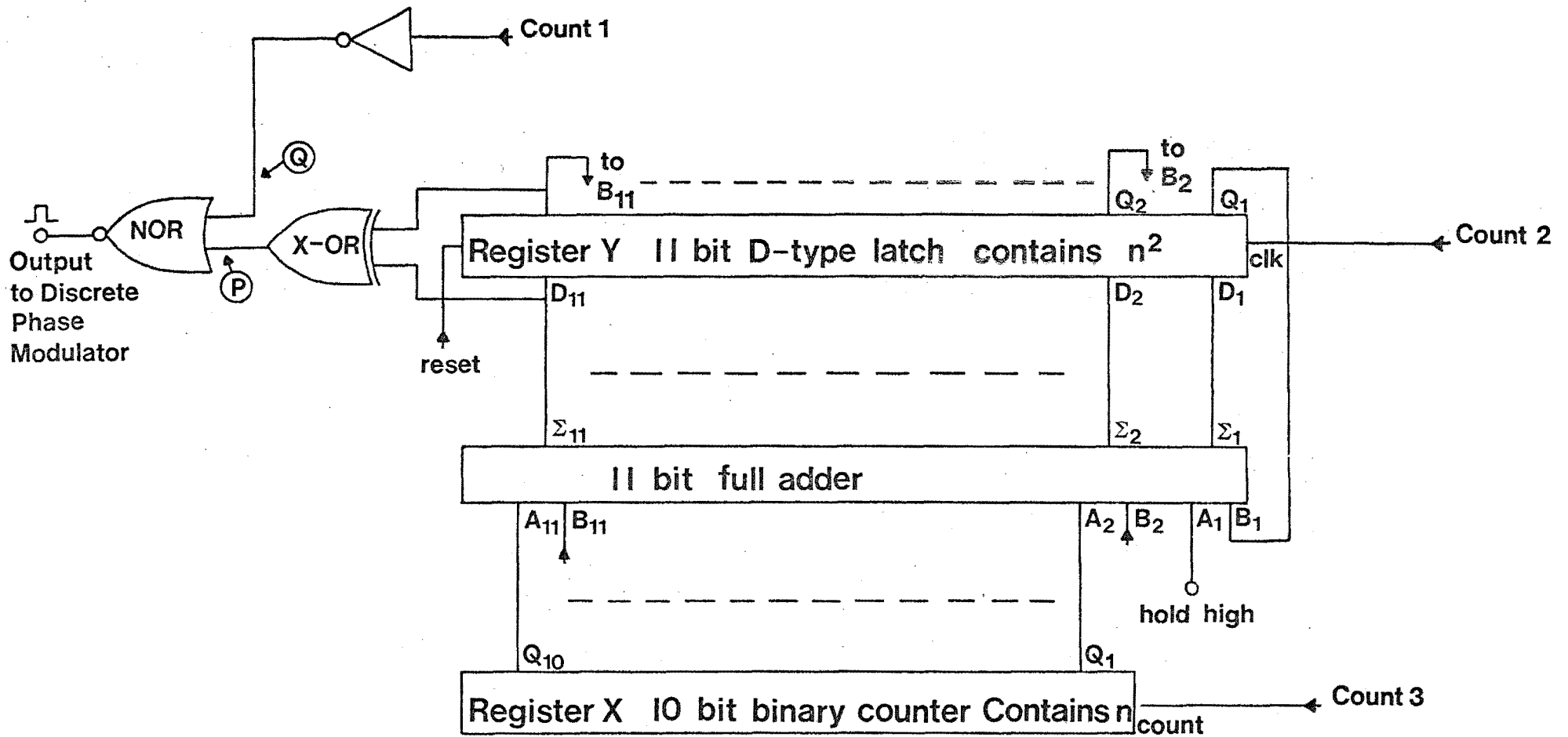
Fig. 5.11: Simplified modulation command controller circuit.

Now consider the Exclusive-OR gate. One of its inputs is connected to the 11th bit of n^2, the other to the 11th bit of $(n+1)^2$. Only when these two bits have the same value (a change of two or zero in the value of entier $[n^2/1024]$) will the output of the gate (point 'P') be low, and this can be taken as the signal for a modulation command to occur for this value of n.

The lines marked 'count 1', 'count 2', and 'count 3' are pulsed sequentially once each during each sample period. The modulation process thus enacts the following sequence:

1. The line 'count 1' is pulsed, causing a pulse to appear at point 'R' only if the level at point 'P' is low. This is the instant that a modulation command is sent to the discrete phase modulator.

2. The 'count 2' line is pulsed, causing the value of $(n+1)^2$ present at the data inputs to the Y register to be transferred to its outputs.

3. The 'count 3' line is pulsed, incrementing the value of n in register X.

4. There is a pause to allow any ripples to proceed through the X register, and to allow time for propagation delays to pass through the adder.

At the end of each output pulse (when register X reaches a value of n = 1024) a reset signal is applied to clear register Y in preparation for the next sweep. Register X will not need resetting, since it will have just cycled around to already contain zero.

5.7.4 Control Circuitry

A number of different control functions are performed by this section; each will be described with reference to the circuit diagram which appears in Fig. 5.12.

(a) Sequential Pulse Generator. The four outputs from this circuit are pulsed sequentially, in a cyclic manner, whenever clock pulses are applied to its input. This function is achieved utilizing two four bit shift registers. The output waveforms are shown in Fig. 5.13. These are used as the 'count 1', 'count 2', 'count 3' and 'pause' commands to the modulation command controller. The sequential pulse generator is clocked at 9.6 MHz; one complete cycle of the output sequence thus occurs in each sample period.

(b) 'Ready' wait state. As previously mentioned, the modulation command controller is operated with the chirp generator output inhibited until n reaches 683.   At this point, the sequential pulse generator is disabled, and the chirp generator waits for a trigger signal. The circuitry associated with this function operates as follows. The outputs of the X register are partially decoded by the 8-input gate, 7430, the output of which falls when 683, or binary 1010101011 is reached, triggering a monostable multivibrator, MONO 1. The output of the monostable resets an R-S flip-flop, FF1, which in turn prevents any further 9.6 MHz pulses from reaching the sequential pulse generator. The output from MONO 1 also clears the $\div 2$ flip-flop at the output of the discrete phase modulator, ensuring that all chirp pulses have the same phase.

(c) 'Chirp start' control. When a start pulse is gener-ated by the trigger logic, FF1 is set, allowing modulation to

count 1

count 2

count 3

pause

Q_A Q_B Q_C Q_D

74195
4 bit shift register

H

serial/load

clock

J $\overline{K}$

Q_A Q_B Q_C Q_D

74195

serial/load

clock

J $\overline{K}$ A B C D

L L L H H H

DATA LOAD
INPUTS

L = Hold low
H = Hold high

1·6 MHz
sync input

sequential pulse generator

9·6 MHz
input

S

X Register Outputs Q_1 Q_2 Q_4 Q_6 Q_8 Q_{10}

7430

trigger

clear ÷2
in DPM
output

Q FF 1 reset

set

⊔ Start pulse

Q MONO 1

Synchronising
logic

Computer trigger

External trigger

DPM Output
inhibit/enable

reset Y register

trigger

$\overline{Q}$ FF 2 Q reset Q MONO 2

set

MONO = monostable
multivibrator
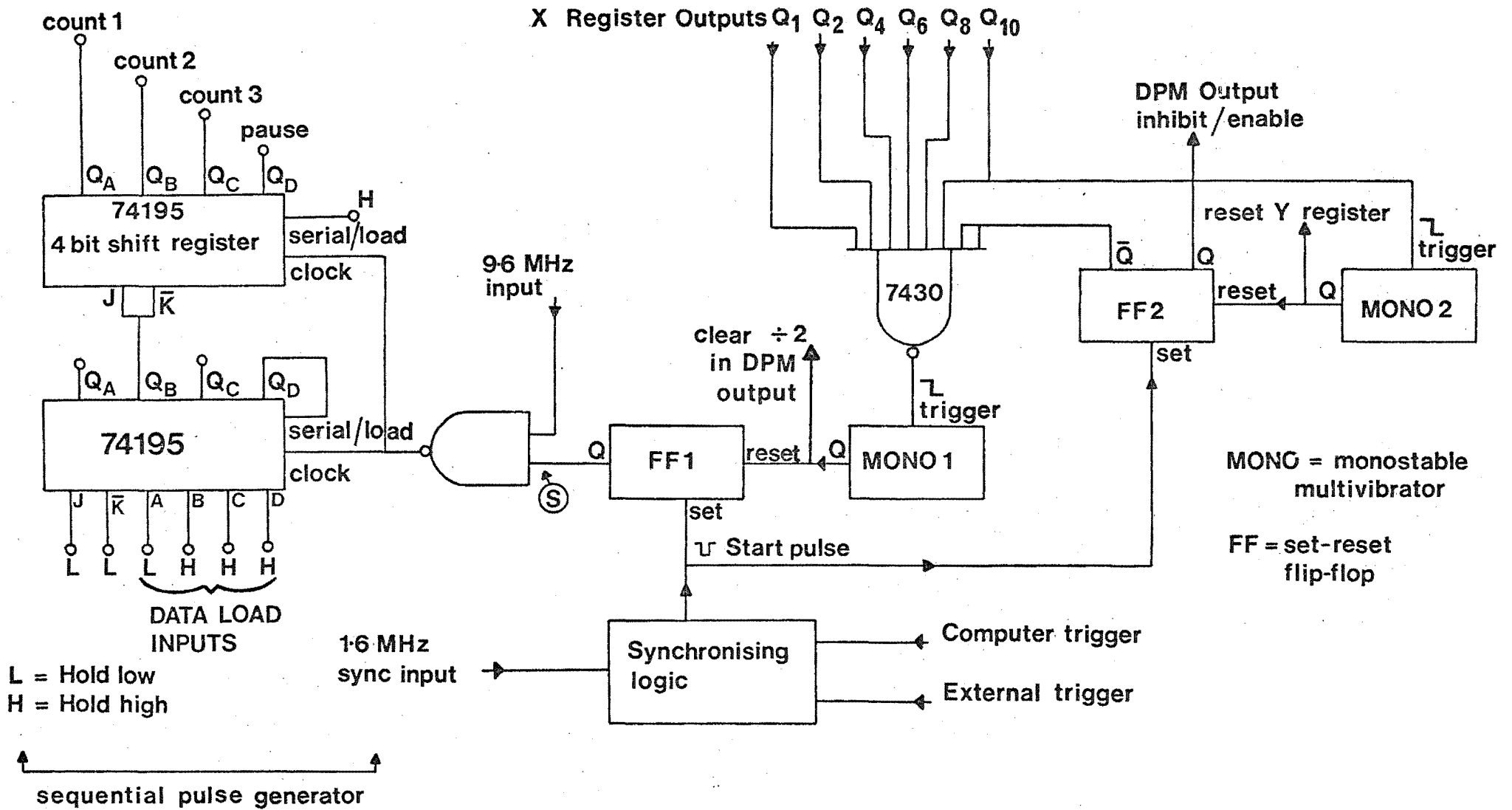
FF = set-reset
flip-flop

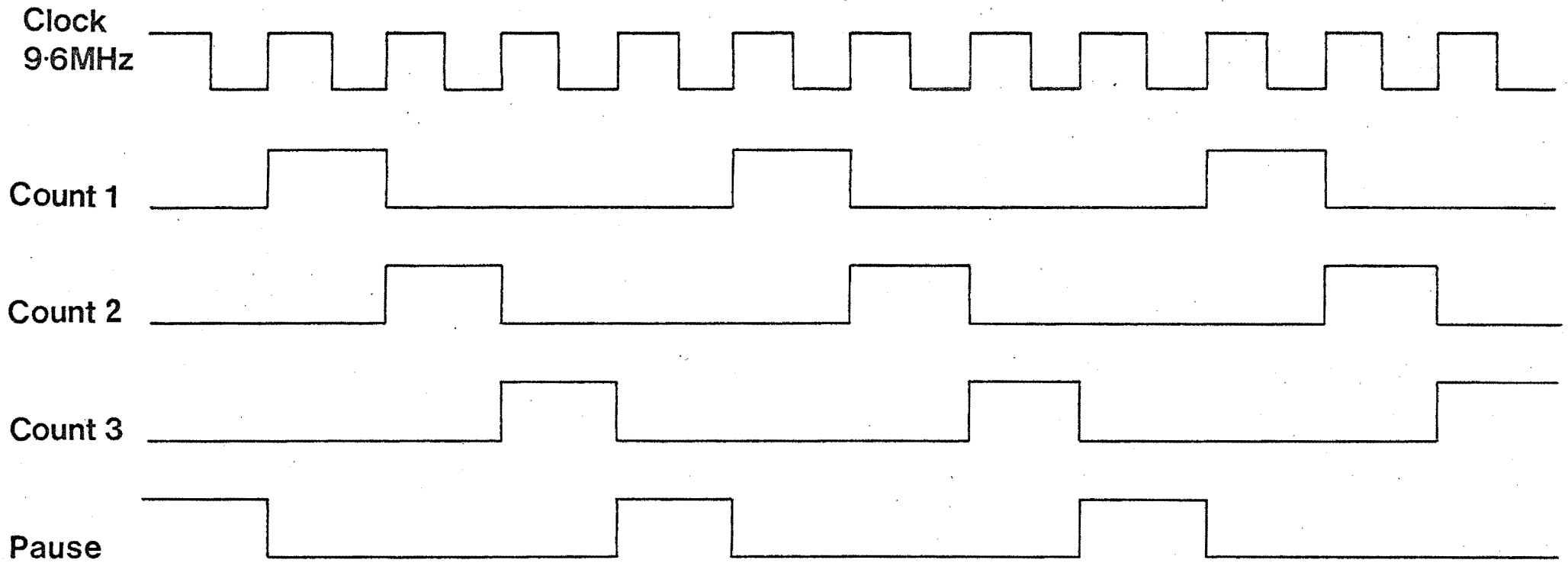Fig. 5.12: Control circuitry.

93

Fig. 5.13: Waveforms at the sequential pulse generator outputs.

continue. FF2 is also set; this provides two functions:

1. It disables the 7430, in order that higher values of n having bits 1, 2, 4, 8, and 10 set do not trigger MONO 1.

2. It enables the signal output from the chirp generator.

(d) 'End of pulse' control. The end of the chirp pulse is detected by MONO 2, which senses the transition from n = 1023 to n = 0 (i.e. when Q_{10} of register X falls). MONO 2 is used to clear register Y in preparation for the next modulation sequence, and also to reset FF2, inhibiting the signal output, and enabling the 7430 gate again.

(e) Trigger circuitry. It is desirable to be able to trigger the chirp generator either from the computer, as would be necessary during normal operation, or from some other signal source; this is essential for setting up and testing purposes. Further, in order to keep the phase of successive chirp pulses constant, it is necessary to synchronise the trigger command with the highest common factor of both input frequencies, i.e. 1.6 MHz. This function is accomplished by three gates and two flip-flops comprising the trigger synchronising logic section.

5.7.5 Timing Considerations

Most of the logic operations which occur in the chirp generator operate at a speed which is slow compared to the rise times of the logic, or the clock frequencies used. There are, however, a few instances where 'race conditions' might occur. These are:

1. The logic level at point 'P' in Fig. 5.11 (the signal for 'modulation' or 'no modulation') must be stable before the level at point Q falls due to the 'count 1' pulse.

2. 'End of pulse' reset. Similarly, when Q_{10} of register X falls (n = 1024), register Y must be reset before 'count 1' arrives.

3. Sequential pulse generator inhibit. When register X reaches n = 683 (on 'count 3') the point S (Fig. 5.12) must have reached its low level before the next rising edge of the 9.6 MHz signal.

These three cases were evaluated in detail, using published data for rise times, propagation delays, and ripple delays in all the circuit elements involved. Even assuming worst case delays for all elements, there was sufficient time in each of the three cases for the operations to be carried out correctly.

5.8 CONSTRUCTION

The chirp generator is housed in a 28 cm x 12 cm x 5 cm rack mounting chassis, this being the standard construction practice for most of the instrumentation at Birdling's Flat. The largest size printed circuit board which conveniently fits into such a chassis is 25 cm x 12 cm; the chirp generator utilizes 21 integrated circuits, and a 7 x 3 array of these fitted easily onto a printed circuit board of this size. The artwork for the board was laid out double sized, using standard double-sided printed circuit board techniques. The board itself was manufactured by a local commercial firm.

Assembly of the generator was straightforward, requiring only that the integrated circuits and other components be soldered onto the board, and power and signal wires installed.

A photograph of the completed unit appears as Fig. 5.14.

5.9   TESTING THE GENERATOR

Testing the discrete phase modulator was a straightforward process. A carrier frequency of 17.6 MHz was applied to the input, and a modulating frequency, f_m introduced at the 'modulation command input'. The expected frequency shift at the output is given by

$$\delta f = \frac{1}{2\pi} \frac{\Delta\phi}{\Delta t} = \frac{1}{2\pi} \cdot \frac{\pi}{4} \cdot f_m$$

$$\text{or} \quad \delta f = \frac{f_m}{8} . \quad\quad\quad (5.29)$$

A range of modulating frequencies sufficient to produce a maximum frequency shift of 0.3 MHz at the output was applied, and the output frequency observed for different modulating frequencies. A least-squares fit applied to the data showed a maximum deviation from linearity in equation (5.29) of 0.007%, which may be attributed to round-off error in the frequency counter used.

Testing the modulation command controller was a rather more complex procedure. After checking the obvious functions of the control and counting circuitry (e.g. that the sequential pulse generator halts exactly at n = 683, that the Y register contains n^2 at all times, etc.) it remained to confirm that the modulation commands all occurred at the correct values of n. To assist in this, a computer program was written which calculated
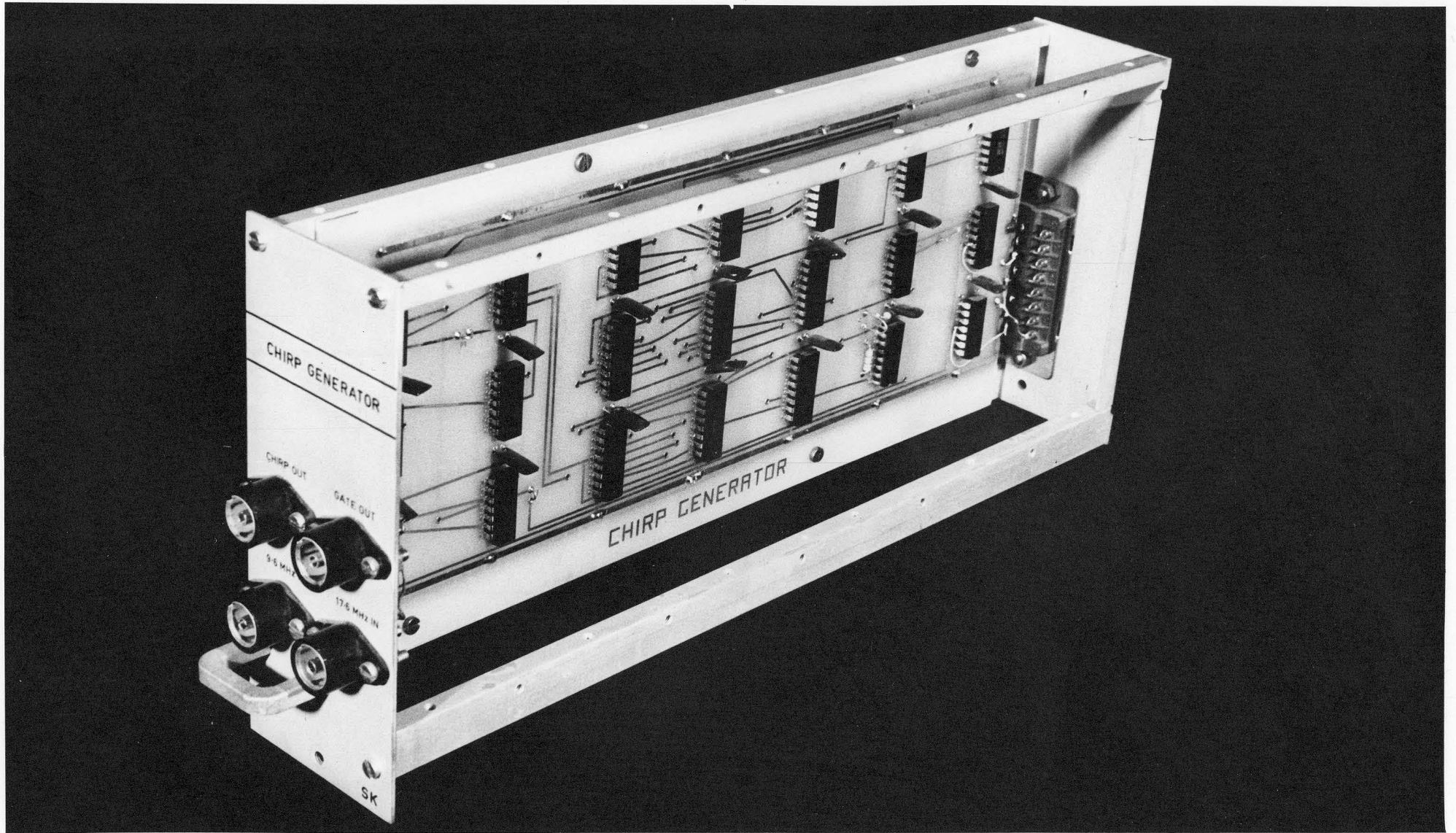
Fig. 5.14: The chirp generator.

the value of entier $[n^2/1024]$ - entier $[(n-1)^2/1024]$ for

$0 \leq n \leq 1023$. If this value was a 2 or a 0, two asterisks (**)

were printed on the line corresponding to that value of n. If

the difference was equal to 1, a single asterisk was printed.

Next, the clock input to the sequential pulse generator was

slowed down to 8 Hz, and the signal at the output of the

modulation command controller monitored by a chart recorder.

Each time a modulation command was issued, a pulse was drawn

on the chart. This sequence of pulses was then compared to the

sequence of computer generated asterisks. A portion of the

chart recorder output is re-drawn in Fig. 5.15, alongside the

corresponding computer output. A complete match between the

two sequences was obtained for all values of n.

The chirp generator was thus considered to be operating

correctly, though at this stage the actual chirp pulses had

not been checked for frequency content, or accuracy of frequency

sweep. However, two independent tests were later conducted when

the radar system was completed, which helped verify the operat-

ion of the chirp generator:

(a) The exciter stage of the transmitter approximated a

bandpass filter, centred on 2.4 MHz, with its gain falling off

sharply just inside the 2.3 to 2.5 MHz interval; when the

chirp pulse was passed through this stage, the output amplitude

was constant over most of the pulse length, tapering off rapid-

ly at its extremities.

(b) The output of the chirp generator was shifted down to

zero frequency, and sampled by an analogue-to-digital converter.

A Fourier transform was then performed on the data, and the

amplitude spectrum calculated. This spectrum is reproduced

in Fig. 5.16. An evaluation and discussion of this spectrum

100

Computer Output · Chart Recorder Output

n

n	
907	**
908	**
909	*
910	**
911	**
912	**
913	**
914	*
915	**
916	**
917	**
918	*
919	**
920	**
921	**
922	**
923	*
924	**
925	**
926	**
927	**
928	*
929	**

Fig. 5.15 Output from Modulation Command Controller

test.
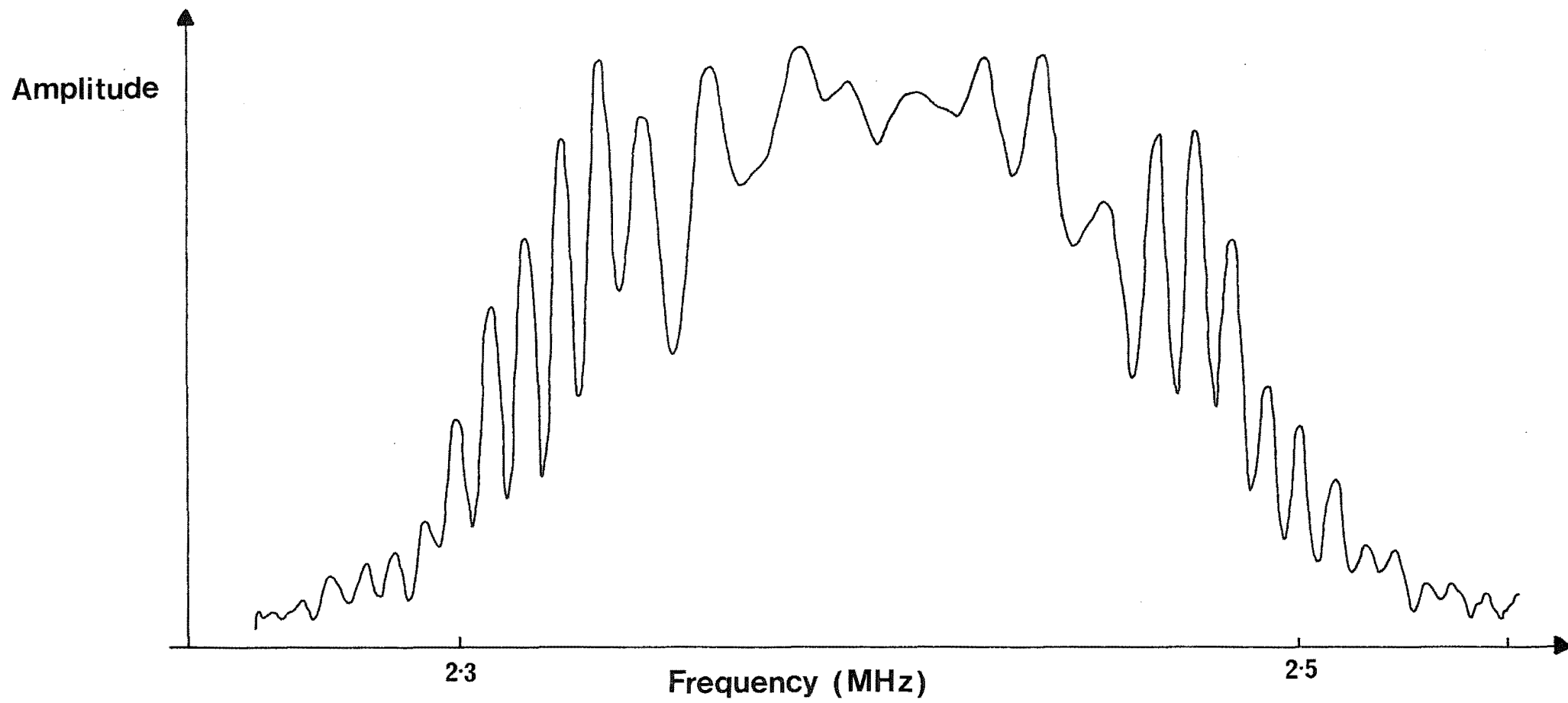
Fig. 5.16: Amplitude spectrum of chirp generator output.

is contained in chapter 10, however, a cursory inspection of the graph does indicate that the output of the chirp generator spans the required frequency interval.

5.10 SUMMARY

The scope of this chapter is in fact considerable. The mathematics of discrete phase modulation are first presented, followed by an indication of how the method may be applied in practice. An examination of the frequency content of a discrete phase modulated signal leads to the formulation of certain constraints which are reflected in an appropriate choice of signal parameters for the proposed generator. Next, the methods by which the technique is implemented electronically are introduced, followed by a detailed description of the actual circuitry used in the chirp generator. Finally, notes on the construction and testing of the device are presented.

CHAPTER 6

TRANSMITTER

The transmitter presently used for ionospheric observation
on 2.4 MHz is one of a pair built especially for the Birdling's
Flat field station by the Canterbury College Industrial
Development Division (CCIDD), in 1961. It is located in a
caravan approximately 0.5 km from the main building at the site.
The final stage of the transmitter employs four tetrodes oper-
ating at anode voltages of about 10 kv; peak power outputs of
up to 100 kW can be achieved with this arrangement. Pulse
widths in the range 20 to 50 μsec are used for most ionospheric
sounding experiments.

Two characteristics of a linear FM pulse must be consider-
ed if this transmitter is to be utilized in the pulse compress-
ion radar system. Of primary significance is the fact that the
chirp signal is approximately four times as long as the
presently used sounding pulses. The detrimental effects that
an increased pulse width may have on the transmitter output
tubes has been described in Chapter 3; in fact this considerat-
ion is responsible for creating an upper limit on the pulse
width of 150 μsec. A second aspect of the transmitter which
may be affected by larger pulse widths concerns power supply
regulation. Since the transmitter is designed to operate with
low duty factors, the output stage, when it is being pulsed,
draws considerably higher current than can be continuously
delivered by its power supply. This short burst of high current
is of course provided by the power supply reservoir capacitors.
It must therefore be ensured that voltage sag due to the

discharge of these capacitors does not occur across a 150 μsec pulse. Consultation of the original transmitter designs showed that the power supply had been considerably over-designed for the intended application, and should hold its voltage adequately over a 150 μsec transmission. In fact, in an experiment performed to test this factor, an amplitude sag at the transmitter antenna terminals of only 3% was measured across a 150 μsec pulse. The assumption was therefore made that the increased pulsewidth could be satisfactorily handled by the transmitter.

The second feature of the linear FM pulse which is of relevance to the transmitter is its large bandwidth. The exciter and driver stages of the transmitter were designed with fairly broadly tuned circuitry, having a -3 dB bandwidth of about 10% (roughly of the same order as that of the chirp signal). Hence the chirp pulse, as it appears at the output of the driver stage, is of maximum amplitude at its centre, tapering off by about 3 dB towards its extremities. The final stage of the transmitter operates in class C. This is a considerable advantage in the present context, since the power output of the stage is hence reasonably independent of its driving power, provided this driving power is above a certain threshold. Thus, if the amplitude at the extremities of the driving pulse is above this threshold, the final stage of the transmitter will emit a pulse of essentially constant amplitude. Introducing a chirp pulse into the transmitter showed that this criterion was not adequately met; the amplitude at the edges of the pulse appearing at the driver output was marginally below the required threshold. It was found, however, that this

problem could be rectified by an adjustment to the coupling transformer between the exciter and driver stages. With this alteration, the transmitter output amplitude was constant, to within 0.5 dB throughout the duration of the chirp pulse.

The transmitter RF stages were thus clearly capable of fulfilling the special requirements imposed by the linear FM pulse. The transmitter triggering and gating requirements differ for the 'normal' and 'pulse compression' modes of operation, and in fact the latter mode, which requires that the transmitter gates be synchronised with the edges of the chirp pulse, could not be realised with the existing circuitry. Since it is desirable that the radar system be conveniently changed from the 'normal' to 'pulse compression' modes, a new transmitter gating control unit was designed which included this capability.

In the 'normal' mode, this unit, on receipt of a trigger signal, supplies gating pulses to the exciter, driver, and final stages of the transmitter, the width of these gating pulses being determined by a monostable multivibrator inside the transmitter gating control unit. In the 'compression' mode, the unit senses the leading and trailing edges of the chirp pulse at the transmitter input, and opens the gates for the appropriate interval. The full circuitry of the transmitter gating control is described in the appendix.

With the addition of this new gating control, and with the small modification described previously, the 2.4 MHz transmitter was considered suitable for use in the pulse compression radar system. The transmitting antennas currently used by this

transmitter were, however, severely bandwidth limited; the following chapter will describe the design and construction of a suitable broadband transmitting array.

CHAPTER 7

TRANSMITTING ARRAY

7.1 THEORETICAL DEVELOPMENT

The 2.4 MHz transmitting array in use at the commencement
of this project consisted of eight half-wave folded dipoles,
arranged in the configuration shown in Fig. 7.1. The impedance
of the dipoles was matched to the transmitter driving impedance
using quarter-wave transmission line transformers (Kraus, 1950,
p.437). Whereas an arrangement of this kind can provide a good
impedance match at a single frequency, it exhibits poor broad-
band characteristics. This is partly due to the change in the
dipole impedance with frequency, but principally because of the
bandwidth limitations of the quarter-wave transformers.

It was thus apparent that a separate broadband transmitting
array, covering the frequency range from 2.3 to 2.5 MHz was
required for the pulse-compression radar system. An examination
of various broadband antenna configurations indicated that the
bandwidth requirement of approximately 10% could probably be met
with a 'thick', or cylindrical, half-wave dipole, provided care
was taken to match and compensate it properly.

Before a detailed treatment of the thick half-wave dipole
is considered, the manner in which bandwidth limitations of an antenna
are manifest must be clearly understood. Consider an antenna,
the impedance of which is a pure resistance of magnitude R, at
some frequency f_0. Suppose that this antenna is fed by a
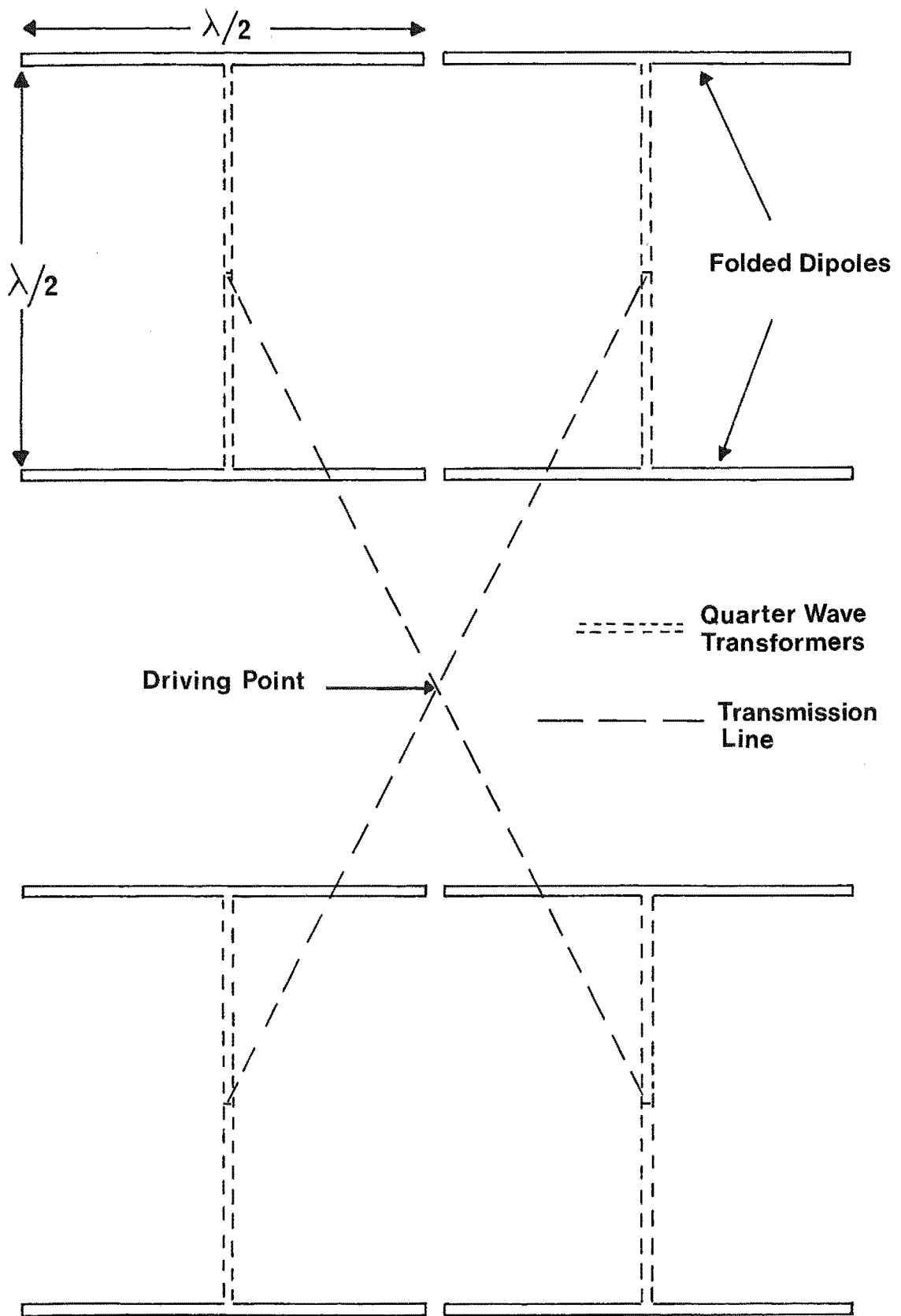length of transmission line of characteristic impedance, Z_0,

Fig. 7.1: 2.4 MHz narrowband transmitting array.

also equal to R. If the end of this transmission line is connected to a transmitter of output impedance R, then the antenna will be optimally matched to the transmitter. All the power generated by the transmitter will be delivered by the transmission line into the antenna, and radiated. Now, if the antenna impedance were not a pure resistance, or if the resistance were not equal to R, a partial reflection of the signal in the transmission line would occur at the impedance discontinuity at the antenna terminals. The proportion of the signal amplitude that is reflected is given by the reflection coefficient, Γ, where

$$\Gamma = \frac{Z-Z_0}{Z+Z_0} \tag{7.1}$$

where Z is the impedance of the antenna

and Z_0 is the characteristic impedance of the transmission line.

Note that in general both Γ and Z are complex, being of the form R+jX, where R is the antenna resistance and X is its reactance.

The proportion of the power reflected will be Γ^2, and this represents the percentage power lost from the antenna due to the mismatch. The reflected wave also causes standing waves to appear on the transmission line, the magnitude of which are defined by the 'standing wave ratio', given by

$$SWR = \frac{1+|\Gamma|}{1-|\Gamma|} \tag{7.2}$$

The SWR is thus a good index of how well the antenna is matched to the transmitter, and any matching scheme devised usually attempts to minimise this quantity.

The variation with frequency of the impedance of a typical half-wave dipole resonant (i.e. a pure resistance) at 2.4 MHz is shown graphically in Fig. 7.2. Suppose this antenna were optimally matched to a transmitter at 2.4 MHz. If the driving frequency deivated from 2.4 MHz, an SWR would become present on the feeder line, and since the reactive part of the antenna impedance changes more rapidly with frequency than the resistive part, it will be the major contributor to this SWR. The variation of reactance with frequency of any antenna considered for broad-band use must therefore be minimised.

A typical 'thick' half-wave dipole is depicted in Fig. 7.3. For an antenna of this type, the major factor affecting the variation of reactance with frequency is the ratio of diameter to length of the antenna (Kraus, 1950, p.220). This ratio is normally defined as

$$\Omega = 2 \, \ell n \, \frac{2h}{a} \tag{7.3}$$

where 2h is the dipole length

a is the radius of the dipole.

The larger the value of Ω, the smaller is the variation of reactance with frequency. Unfortunately, large values of Ω are difficult to obtain in practice, due to the large mass of copper present in a wire of any appreciable diameter. However, a cylindrical dipole of a given thickness may be approximated by a folded dipole comprised of conducting elements of much smaller diameter. The configuration of a two-wire folded dipole is shown in Fig. 7.4.
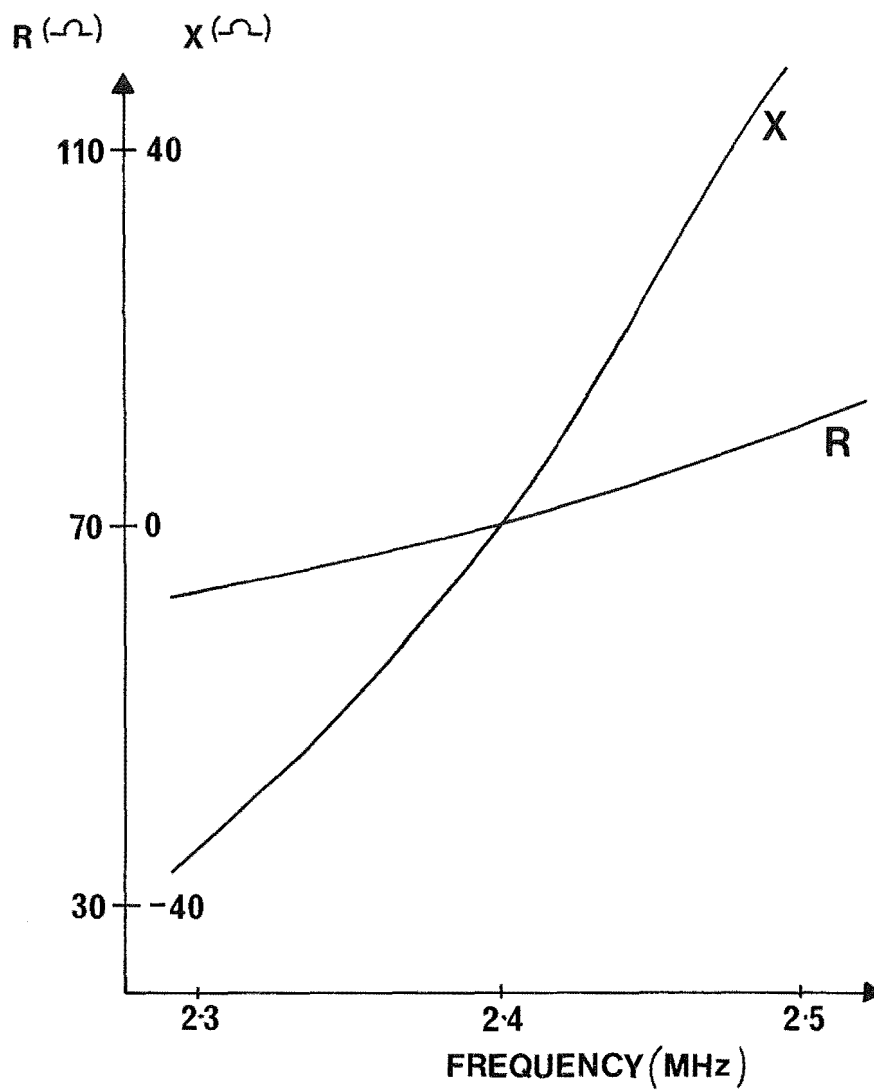
Fig. 7.2: Resistance (R) and reactance (X) of a
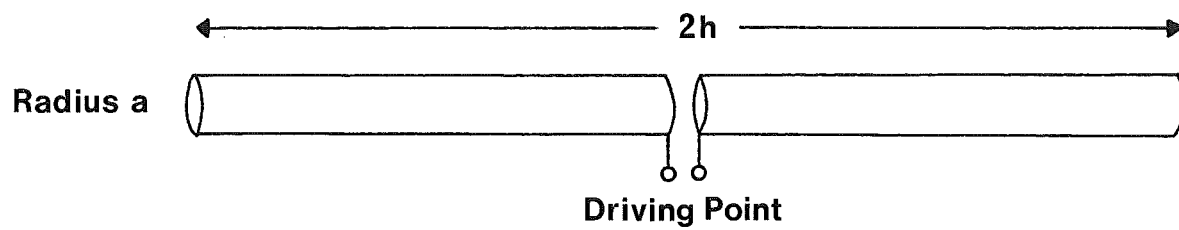typical half-wave dipole near resonance.
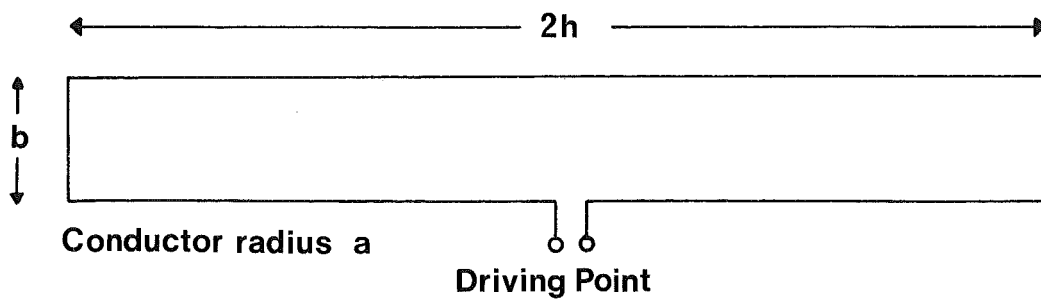
Fig. 7.3: A cylindrical half-wave dipole.

Fig. 7.4: A two-wire folded dipole.

A folded dipole with a conductor separation of b, constructed using wire of radius a can be shown (Kraus, 1950) to have similar bandwidth properties to a cylindrical dipole of radius a_e, where a_e is given by

$$a_e = \sqrt{ab} \qquad (7.4)$$

a_e is known as the 'effective radius' of the folded dipole.

The feasibility of using half-wave folded dipoles as the elements in the proposed transmitting array was investigated by evaluating the theoretical impedances of such a dipole over the desired frequency interval, and attempting to predict the maximum SWR that would be present on the array feeder line. It must be stressed that theoretical antenna impedances often bear little relation to antenna impedances measured in the field; invariably, effects such as the presence of a conducting ground under the antenna, the state of the weather, and other more subtle factors affect the actual impedance of antennas considerably. However, investigation of how a theoretical antenna behaves can give an indication of whether or not a proposed configuration will be feasible.

The theoretical impedance of a folded dipole is usually obtained from the theoretical impedance of a cylindrical dipole of an equivalent effective radius, according to the relation (King and Harrison, 1969)

$$Y_d = \frac{1}{4Z_e} + \frac{1}{j240 \, \ln(b/a)\tan k_0(h+b/2)} \qquad (7.5)$$

where Y_d is the admittance of the folded dipole

Z_e is the impedance of the equivalent cylindrical dipole

a, b and h are defined in Fig. 7.4

k_0 is the wave number of the antenna excitation.
The largest value of Ω which gives (by equations (7.3) and
(7.4)) a sensible separation to diameter ratio for the wires in
a folded dipole is about Ω = 15. This would give, for example,
an element separation of 1.3m for 1.6mm diameter antenna wire.

The theoretical impedances of a folded dipole resonant at
2.4 MHz were calculated for various frequencies, using equation
(7.5). The values of Z_e were obtained from published data for
a cylindrical antenna with Ω = 15. The folded dipole impedances
so obtained are given in Table 7.1.

Table 7.1   Terminal impedances for a theoretical folded dipole resonant
at 2.4 MHz.

Frequency (MHz)	Dipole impedance, Z_d (ohms)
2.3	252 - j215
2.4	286 + j0
2.5	336 + j214

A number of different feeder configurations were consider-
ed in an attempt to find the best method of matching this
dipole to the transmitter, the object being, as stated earlier,
to keep the SWR as low as possible at all frequencies in the
band. Eventually, a scheme first suggested by Rumsey (1950)
was adopted. This method, rather than providing a perfect
match at the band centre, and attempting to minimise the mis-
match at the edges of the band, deliberately mismatches the
antenna at the centre frequency by a controlled amount, and
attempts to keep the magnitude of the mismatch constant over
the whole band. The scheme requires that:

(a) The reactive component of the dipole impedance is zero at the centre frequency, increasing or decreasing reasonably smoothly across the band.

(b) The resistive component has a local minimum or maximum at the centre frequency.

The proposed matching and compensating scheme can best be illustrated by considering a fictitious antenna, the impedance of which conforms to these requirements. The impedance of such an antenna is shown graphically in Fig. 7.5.

Suppose it is desired to match this antenna to a transmitter having a driving impedance of 1 KΩ. The first step is to optimally match the antenna resistance at the band edges to the transmitter impedance. This may be achieved using a quarter-wave transmission line transformer, which provides an impedance transformation according to the relation

$$Z_{in} = \frac{Z_0^{\ 2}}{Z_{load}} \tag{7.6}$$

where Z_0 is the characteristic impedance of the transmission line

Z_{load} is the impedance connected to one end of the transformer

Z_{in} is the impedance appearing at the other end.

For correct matching in the case under consideration, then,

$$Z_{load} = 500\Omega$$

$$Z_{in} = 1K\Omega.$$

The resistive component of the dipole impedance will thus be matched to the transmitter at the edges of the band, but mismatched at the centre. The converse is true for the dipole
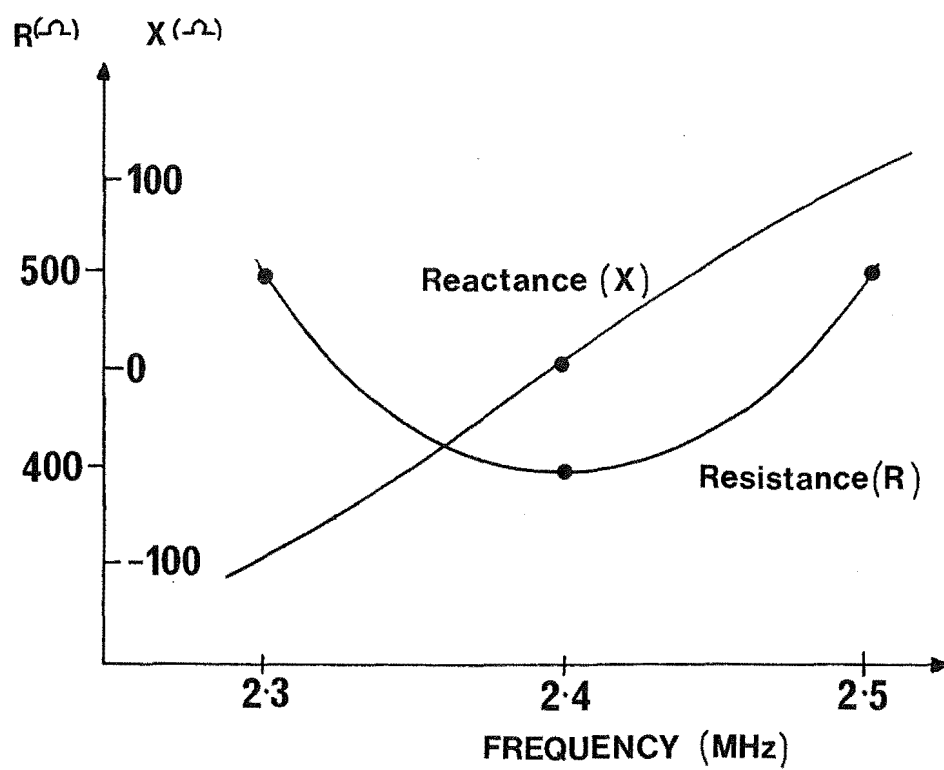
Fig. 7.5: Impedance of a fictitious antenna.

reactance, which will be matched at the centre frequency (where both the transmitter and dipole reactances are zero). The final step in the matching scheme is to provide enough cancellation of the dipole reactance so that the reactive mismatch at the band edges is of the same magnitude as the resistive mismatch at the centre. This 'reactive cancellation' may be provided by connecting a 'quarter-wave stub' in parallel with the input to the quarter wave transformer. A quarter-wave stub is a piece of transmission line, a quarter of a wavelength long (at 2.4 MHz, say) short circuited at one end. This configuration has essentially infinite impedance at 2.4 MHz, and is a pure reactance at other frequencies.

Hence, if the characteristic impedances of the quarter-wave transformer and stub are carefully chosen, a reasonably constant SWR over the band may be achieved. If this matching scheme is to be used to match the theoretical folded dipole under consideration, its impedances (given in Table 7.1) must first be made to meet conditions (a) and (b) given earlier.

Condition (a) is already met (the dipole reactance is zero at 2.4 MHz). Condition (b) requires that $\frac{dR_d}{df} = 0$ at $f = 2.4$ MHz, where R_d is the resistive part of the dipole impedance. Rumsey (1950) states that this condition can be realised by inserting a piece of transmission line of a certain length, with a characteristic impedance equal to the dipole's resistance at resonance, between the antenna and matching network. This statement is verified below.

The impedance appearing at the input to a piece of transmission line is given by the general transmission line transformer equation,

$$Z_{in} = Z_0 \cdot \frac{Z_L \cos \beta\ell + jZ_0 \sin \beta\ell}{Z_0 \cos \beta\ell + jZ_L \sin \beta\ell} \qquad (7.7)$$

where Z_0 is the characteristic impedance of the line,

Z_{in} is the impedance appearing at the input to the transmission line

Z_L is the 'load impedance', i.e. the impedance connected to the other end of the line

$\beta = \frac{2\pi}{\lambda}$, where λ is wavelength of the signal in the line

ℓ is the length of the line.

Fig. 7.6 shows this arrangement diagrammatically. Note that Z_{in} and Z_L are in general both complex impedances.

Replacing Z_{in} by $R_{in} + jX_{in}$, and Z_L by $R_d + jX_d$ (the dipole impedance) gives, after considerable manipulation,

$$R_{in} = \frac{Z_0^2 R_d}{Z_0^2 \cos^2 \beta\ell - 2Z_0 X_d \cos\beta\ell \sin\beta\ell + (X_d^2 + R_d^2) \sin^2\beta\ell} \qquad (7.8)$$

The length of line which will cause R_{in} to be a maximum or minimum at 2.4 MHz may be found by differentiating this expression with respect to frequency, equating the differential to zero, and making the substitutions $X_d = 0$ and $Z_0 = R_d$. This leads to the condition

$$R_d' + 2X_d' \sin\beta\ell \cos\beta\ell - 2R_d' \sin^2\beta\ell = 0 \qquad (7.9)$$
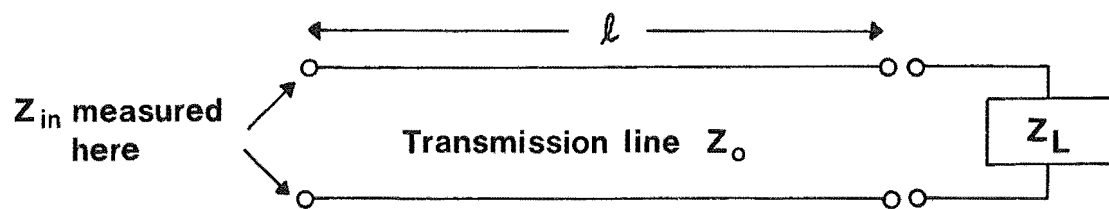
where $X_d' = \frac{dX_d}{df}$ at $f = 2.4$ MHz,

Fig. 7.6: A transmission line transformer.

and $R_d' = \dfrac{dR_d}{df}$ at $f = 2.4$ MHz.

R_d' and X_d' may be obtained graphically by plotting the dipole impedance about 2.4 MHz.

Equation (7.9) may be solved numerically to obtain the required value of ℓ. For the folded dipole under consideration, this becomes $\ell = 0.234\lambda$, where λ is the wavelength in the line of a 2.4 MHz signal. The impedances appearing at the input to this piece of transmission line should fulfil conditions (a) and (b), given earlier, and the proposed matching scheme may thus be applied at this point. These impedances are found using equation (7.7), and are presented in Table 7.2.

Table 7.2   Impedances appearing at input to transmission line transformer.

Frequency (MHz)	Impedance at transformer input, Z_t (ohms)
2.3	159 + j115
2.4	286 + j0
2.5	176 - j115

Inspection of these values shows that the transmission line transformer has caused the resistance appearing at its input to be a maximum, rather than a minimum, at 2.4 MHz.

Rumsey developed a set of equations to evaluate the optimum characteristic impedances of the quarter-wave transformer and stub to be used in the matching network. The data required for their application are:

(a) the impedance to which a match is desired (usually the transmitter driving impedance)

(b) the impedances at the band edges and centre at the point where the matching network is to be applied.

Substituting the impedances Z_t (given in Table 7.2) into these equations showed that a quarter-wave transformer of 508Ω characteristic impedance, and a stub of impedance 217Ω would provide optimum matching of the theoretical folded dipole to 1400Ω. (The reasons for choosing this last figure will become apparent later). Rumsey's equations also predicted that an SWR of approximately 1.3 would be present on the antenna feeder. Since this SWR is equivalent to a power loss from the antenna of only 2%, it was clear that a folded dipole, together with the matching network described here should have a sufficient bandwidth to be used with the pulse compression radar system. Fig. 7.7 shows a sketch of the proposed antenna and feeder system.

7.2 PRACTICAL DETAILS

Whereas the preceding development does include a specific design for an antenna and matching network, it must be recognised that theoretical antenna impedances often differ considerably from those measured in practice. Consequently, before commitment to any antenna design takes place, a dipole such as that proposed in the previous section must be erected, and its impedance measured. These measured impedances should then be used in the design of the matching network.

As is often the case, practical considerations influenced the antenna construction. For example, a set of masts existed which had originally been erected for a 1.75 MHz transmitting array, now obsolete. They were arranged to support eight half-wave dipoles in an identical layout to that shown in Fig. 7.1. The dimensions of the array were such as to give an antenna separation of 0.69 wavelengths at 2.4 MHz.
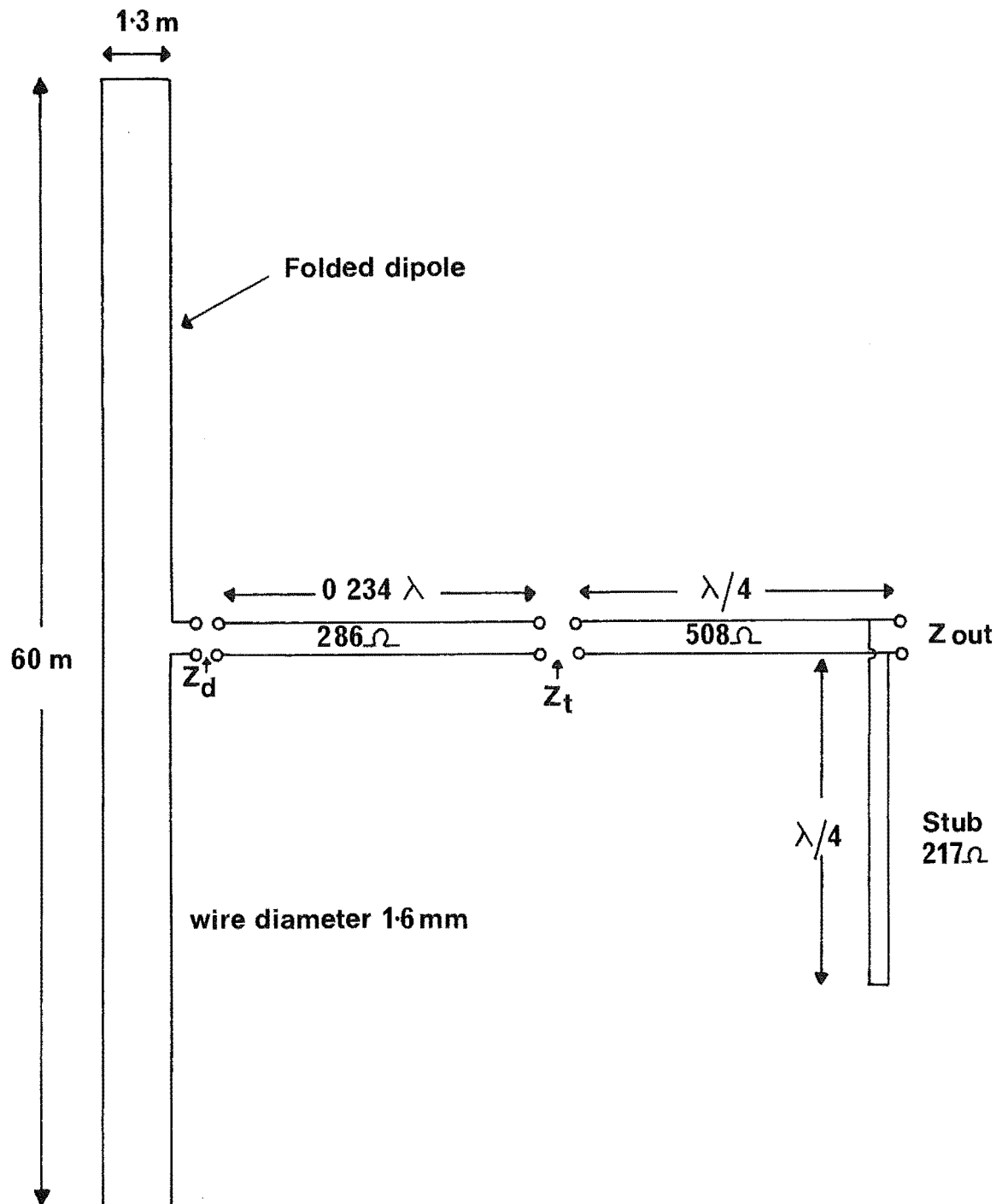
Fig. 7.7: Configuration of optimum matching
network for theoretical folded dipole.

The use of these masts for the 2.4 MHz broadband trans-
mitting array was rather desirable, but would only be permiss-
ible if the somewhat unusual antenna separation of 0.69λ did
not create a poor array field pattern. Accordingly, a computer
program was obtained (Lynn, 1975) which could predict the array
field pattern for various configurations of antennas. The
pattern for four dipoles in a broadside array at a spacing of
0.69λ is shown graphically in Fig. 7.8. For comparison, the
equivalent pattern for 0.5λ element spacing is included on the
same graph. (This is the configuration of the 2.4 MHz narrow-
band array currently in use.) The field pattern for the 0.69λ
element separation could be considered superior to that of the
array presently in use , as the main lobe is somewhat narrower,
and the sidelobes are of approximately equivalent amplitude.
The layout of the existing set of masts was thus considered
suitable for the broadband transmitting array.

The dimensions of a folded dipole that would be most
suitable for the intended application were then determined
experimentally. The following practical considerations
influenced the work to some extent.

(a) Whereas in theory the gauge of wire in the antennas is
a variable, it was desirable to use 1.6 mm diameter hard drawn
copper wire. This was a purely economic factor; the Physics
Department had access to considerable quantities of wire of
this specification. It was, however, acknowledged that if this
constraint compromised the performance of the array to any
reasonable extent, it would be abandoned.

(b) Certain complications are avoided if open-wire trans-
mission line is used for the antenna feeders. Using 1.6 mm
wire, characteristic impedances from about 325Ω to 825Ω may be
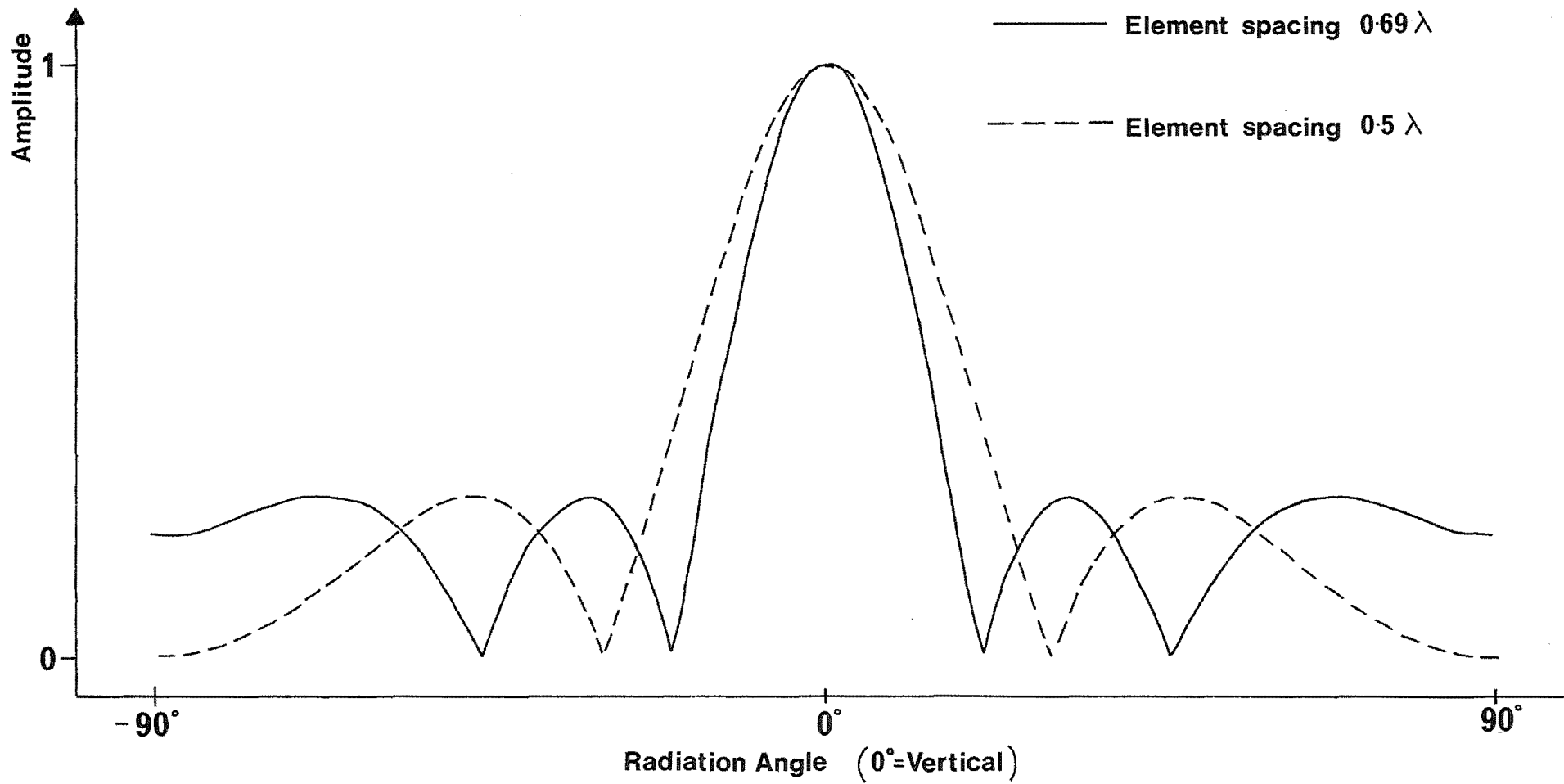
Fig. 7.8: Array field patterns for 4-element broadside arrays of different element separations.

conveniently realised (this corresponds to a wire separation of 12 mm to 1 m). Hence if the matching network described in the previous section is to be utilized, the resonant resistance of the dipole must be within this range.

The experimental procedure was as follows. A dipole was erected between two masts and its impedance measured using a radio-frequency impedance bridge at frequencies ranging from 2.3 to 2.5 MHz. Usually, the length of the dipole was adjusted until the dipole resonated at 2.4 MHz. The measured impedances were then substituted into equation (7.9) and also Rumsey's equations to determine:

(a) the length of transmission line required to make the dipole resistance have a stationary value at 2.4 MHz.

(b) the optimum characteristic impedances of the quarter-wave transformer and stub

(c) the approximate SWR over the band that would result from that configuration.
These calculations were made purely to determine the suitability of each dipole configuration.

Initial experiments showed that, presumably due to the presence of reflections from the ground (the masts held the antenna at only 0.1 wavelength above the surface of the earth), the resonant resistance of the folded dipole was only 245Ω. This falls outside the range of characteristic impedances which may be obtained for open wire transmission line.

A three-wire folded dipole (King and Harrison, 1969) was then erected, as this configuration has in theory a considerably higher resonant resistance. Measurements on such a dipole gave a driving point resistance at resonance of 565Ω, an impedance which may readily be realised using open-wire transmission line.

Various other configurations of folded dipoles were experimented with, including four-wire dipoles, a three-wire dipole with elements of different radii, and dipoles of different element separation. However, the optimum configuration was a simple three wire folded dipole with all elements of the same radius. A sketch of this antenna appears in Fig. 7.9. The measured impedances at various frequencies are given in Table 7.3.

Table 7.3   Measured impedances at the driving point of a three-wire folded dipole.

Frequency (MHz)	Impedance (ohms)
2.3	555 - j375
2.4	565 + j0
2.5	578 + j350

Rumsey's equations predicted an SWR after matching of approximately 1.28, indicating that the proposed antenna had sufficient bandwidth.

A consideration of prime importance when antennas are used as elements in an array is the mutual impedance between adjacent antennas. This mutual impedance is caused by radiation from one antenna creating parasitic currents in neighbouring antennas, thereby altering their impedances.
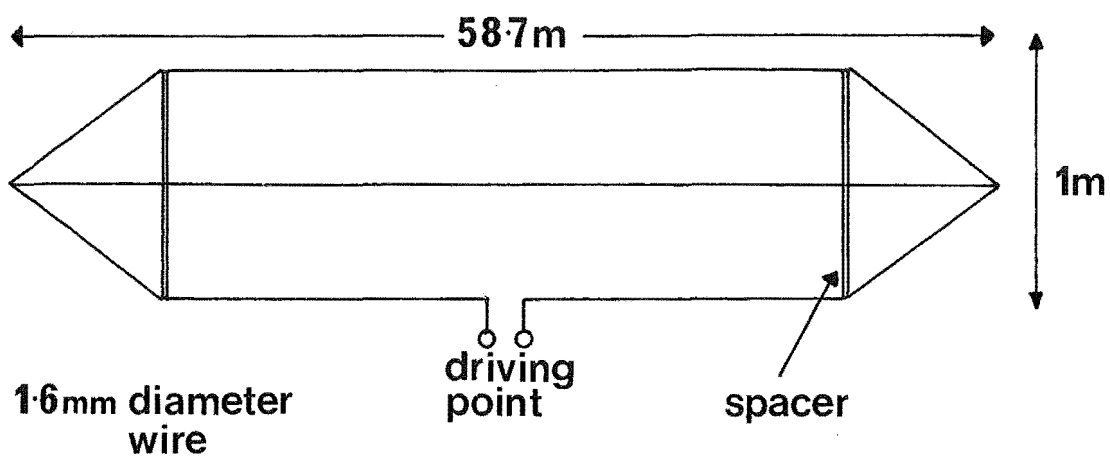
Fig. 7.9: Configuration of the proposed folded dipole.

Depending on the physical configuration involved, this effect may or may not be significant.

Consider two antennas located side-by-side. If the impedance of antenna number 1 alone (the 'self impedance') is Z_1, and the mutual impedance between the two is Z_{mutual}, then when both antennas radiate together, antenna 1 will have an effective terminal impedance given by

$$Z_{eff} = Z_1 + Z_{mutual} \qquad (7.10)$$

The mutual impedance between various pairs of elements in the proposed array was measured by a method reported by Altshuler (1960). This technique involves measuring the self impedance of one of the antennas (Z_{self}), and then the impedance of that antenna when both antennas are driven anti-symmetrically, i.e. 180° out of phase (Z_{anti}). Altschuler shows that the mutual impedance is given by

$$Z_{mutual} = Z_{self} - Z_{anti} \qquad (7.11)$$

Experiments showed that the effect of mutual impedance was only significant between immediately adjacent antennas in the array. The magnitude of the mutual resistance was about -20Ω over the band, while the mutual reactance varied from $-j60$ to $-j10$ ohms. The measured impedances of the dipoles were correc-ted by the appropriate amount, according to equation 7.10. Note that the resistance at resonance had been altered by the effect of mutual impedance to 545Ω, and that the length of the antenna had to be adjusted slightly to compensate for the effect of mutual reactance.

At this stage, a slight deviation from the matching procedure outlined in section 7.1 was introduced. It will be recalled that the purpose of the quarter wave stub in the matching network (see Fig. 7.7) is to partially cancel the reactance appearing at the input to the quarter-wave transformer. Now, the impedance of a piece of transmission line shorted at one end is always a pure reactance (assuming a loss-less line), the value of which is given by

$$X = Z_0 \tan \frac{2\pi\ell}{\lambda} \qquad (7.12)$$

where ℓ is the length of the line

λ is the wavelength in the line of the excitation

Z_0 is the characteristic impedance of the line.

Hence, for a piece of shorted transmission line which is a quarter of a wavelength long at a frequency f_0, the reactance at any frequency f is given by

$$X = Z_0 \tan \frac{\pi}{2} \cdot \frac{f}{f_0} \qquad (7.13)$$

At frequencies slightly below f_0, this is a pure inductance (X is positive), whereas above f_0 it is a capacitance. The reactance tends towards infinity as the frequency approaches f_0 from either direction.

Now consider a parallel tuned circuit of reasonably high Q, resonant at f_0. The reactance of such a circuit for frequencies near f_0 is given to a good approximation by

$$X = \frac{2\pi fL}{1-f^2/f_0^2} \qquad (7.14)$$

where L is the value of the inductance in the tuned circuit

f is the frequency.

Whereas equations (7.14) and (7.13) do not immediately appear to be similar, the values of these functions are remarkably close for frequencies near f_0. These two functions are plotted in Fig. 7.10, where susceptance, rather than reactance has been plotted due to the asymptotic behaviour of the functions near f_0. The value of the L-C ratio in the tuned circuit is the analogue of the characteristic impedance of the stub; in Fig. 7.10, these parameters have been chosen for optimum similarity between the curves.

It is thus demonstrated that the quarter-wave stub used in the antenna matching network may be replaced by a parallel tuned circuit; furthermore, this course of action is rather desirable for two reasons:

1. The possible variation in the L-C ratio of a tuned circuit is far larger than the variation available in the characteristic impedance of open-wire transmission line; this gives more freedom in the design of the matching network.

2. A tuned circuit is more likely to behave as theory predicts than is a piece of transmission line - this will allow a more accurate realisation of the matching network.

For these reasons it was considered that the necessary 'reactive cancellation' would best be achieved using a parallel tuned circuit.

The first step in the application of the matching scheme is to determine the length of the transmission line transformer that will cause the dipole resistance to have a stationary value at 2.4 MHz. This transmission line, it will be recalled, must

Susceptance, B
(mmhos)

0·15

$$B = 1 \Big/ z_0 \tan \frac{\pi}{2} \frac{f}{f_0}$$

$$B = 1 \Big/ \frac{2\pi f L}{1 - f^2/f_0^2}$$
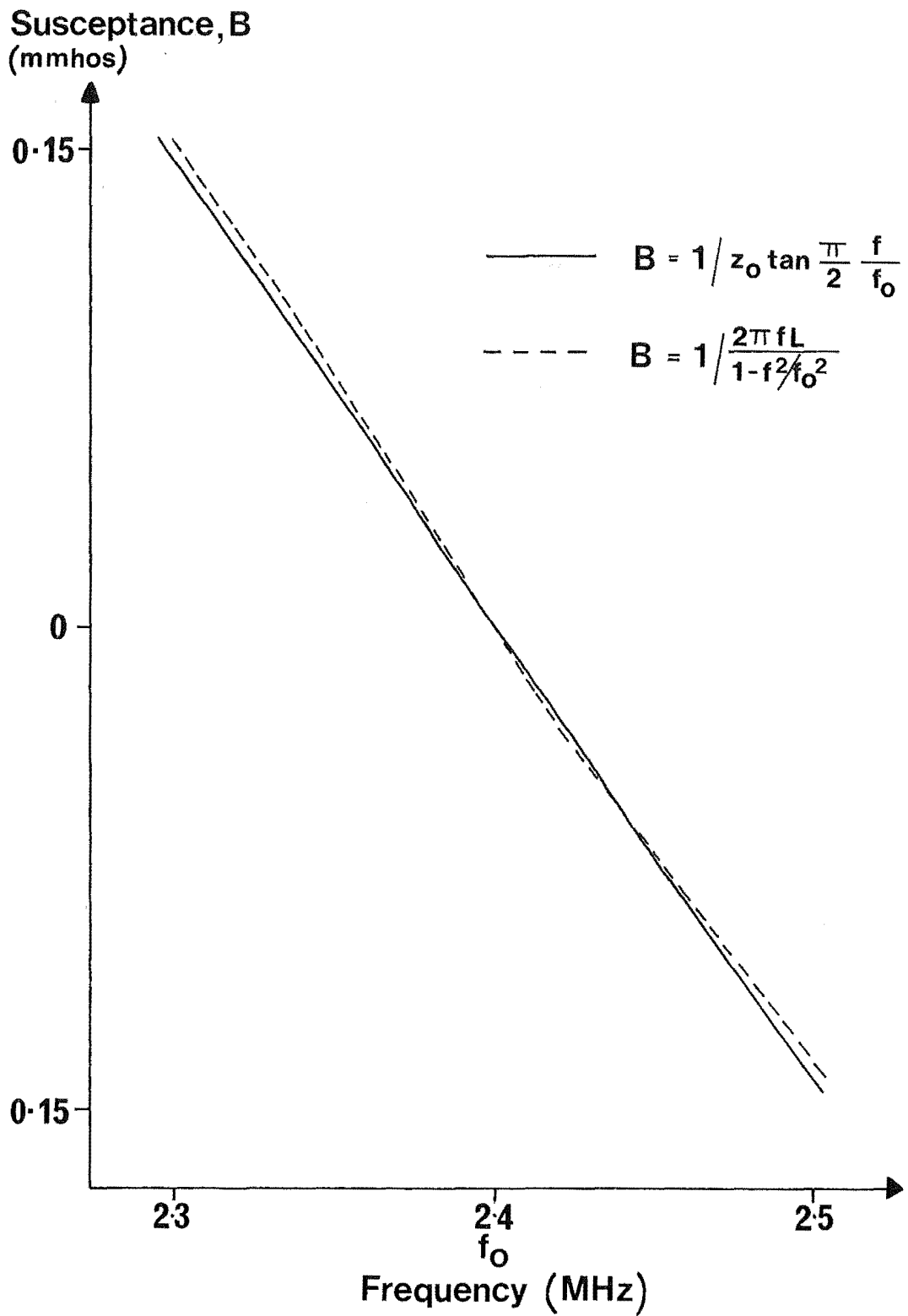
0

0·15

2·3

2·4
f_0

2·5

Frequency (MHz)

Fig. 7.10: Similarity of susceptance functions for transmission line stub and parallel tuned circuit.

have a characteristic impedance equal to the resonant resistance of the dipole (545Ω in this case). The required length was found, using equation (7.9) to be 0.24 wavelengths at 2.4 MHz. The impedances appearing at the input to this transformer were then optimally matched to 1400Ω, using a quarter wave transformer and a parallel tuned circuit; the parameters of the matching elements were found as follows.

An interactive computer program was developed which could calculate the mismatch present at the input to the matching network as a function of frequency for any combination of matching element parameters. The characteristic impedance of the quarter wave transformer, and the values of the tuned circuit elements could be varied in an on-line mode via a screen terminal during program execution, and the mismatch at 11 points in the band for any such configuration could be seen immediately. In this manner, by a pseudo-iterative process (using human interaction as part of the loop) it was easy to get the best combination of parameters for optimum matching across the band. The values of the tuned circuit elements were such that these could be realised with a spaced-winding air-cored coil, and readily available high voltage capacitors. The optimum characteristic impedance of the quarter-wave transformers was found to be 810Ω, corresponding to a conductor separation of 70 cm.

The most feasible method of driving the eight dipoles identically was to arrange them in four pairs, in a similar manner to the 2.4 MHz narrowband array, pictured in Fig. 7.1. The ends of the quarter-wave transformers from the two antennae in each pair were connected in parallel, and a single tuned circuit provided reactive cancellation for both elements in

the pair. The driving point of each pair (now optimally matched to 700Ω) was fed from the centre of the array with a length of 700Ω transmission line. Fig. 7.11 shows the physical layout of one pair of dipoles. The 'dog-legs' in the transmission lines exist solely to provide sufficient path length for the 545Ω length of line, and the quarter-wave transformer.

The 700Ω transmission lines from each dipole pair were all connected in parallel at the array centre, giving an array driving impedance of 175Ω. The centre of the array is located approximately 300 meters from the transmitter; some means is therefore required to carry the transmitter signal over this distance. A straightforward method would be to employ a transmission line having a characteristic impedance of 175Ω. This impedance is, however, difficult to achieve with open-wire transmission line, since even using four-wire line, the required conductor separation is 16 mm, which is impractical to maintain over large distances. Another possible method, particularly if the transmitter driving impedance were to differ markedly from 175Ω, would be to use a tapered transmission line; this can provide good matching over large bandwidths (Burrows, 1938; Wheeler, 1939; Collin, 1956). This technique does have the disadvantage that the conductor separation must vary continuously over the length of the line, and must be accurately maintained.

Eventually, a compromise was achieved which provided adequate matching for frequencies in the range 2.3 to 2.5 MHz. A 'quasi-tapered' line was employed; a short section of 190Ω four-wire transmission line was constructed at the array end of the line, the remainder of the feeder being comprised of 225Ω

dipole

**0·24 wavelength
545Ω line**

**quarter wave
transformer**

**lumped
constant
network**
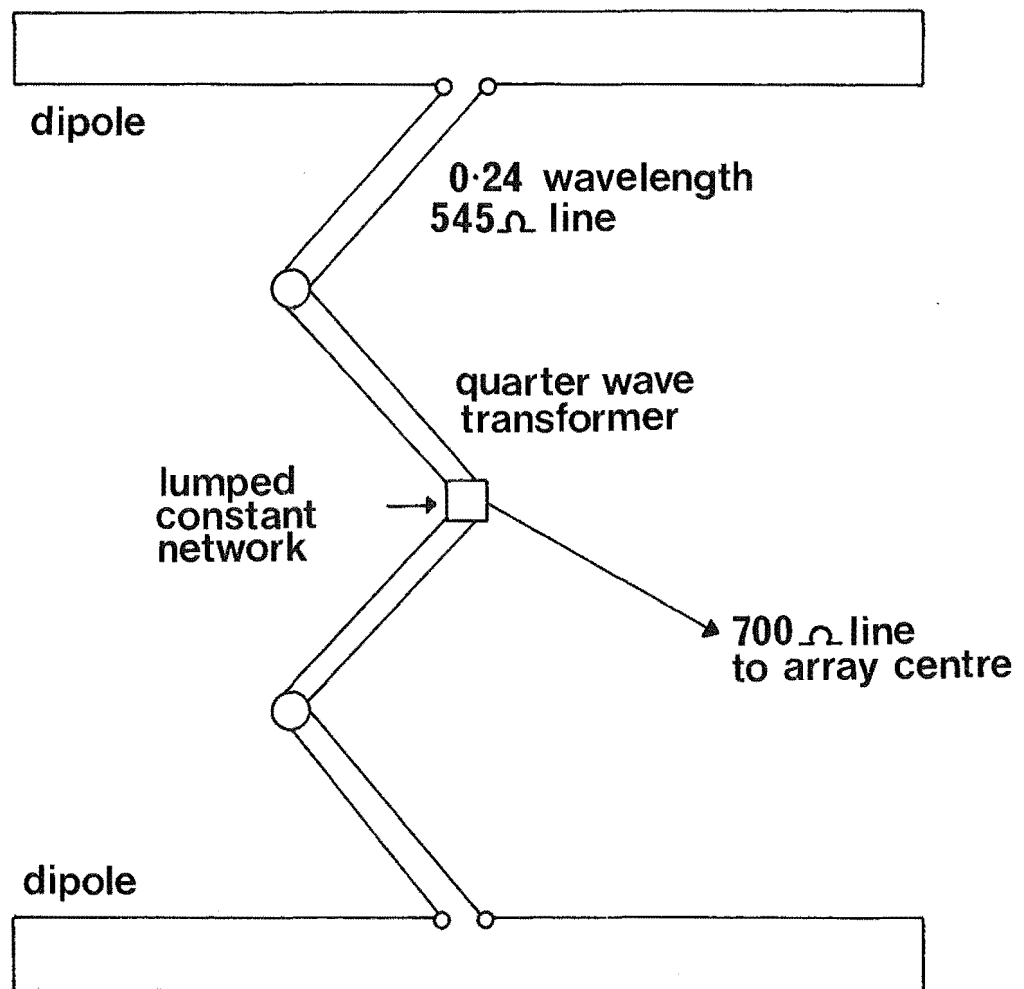
**700 Ω line
to array centre**

dipole

Fig. 7.11: Feeder arrangement for each pair of dipoles.

four-wire line. The transmitter driving impedance was variable to some extent, and this was adjusted to provide the optimum match.

The justification for using this configuration stems entirely from its performance. Bridge measurements were made of the impedance at the transmitter end of the feeder line, and the reflection coefficient at that point calculated for different frequencies in the band. The results of this procedure are reproduced in Fig. 7.12. The reflection coefficient has a maximum value of 0.21, which is equivalent to a power loss from the array of only 5%. This in itself is a direct indication that the feeder and matching network was performing adequately.

Further confirmation of the effectiveness of the array was derived from a qualitative test, in which the broadband and narrowband arrays were alternately connected to the transmitter, whilst the amplitude of the ionospheric return from a pulsed 2.4 MHz transmission was monitored. A small but discernable increase in amplitude was noted when the transmitter was switched to the broadband array.
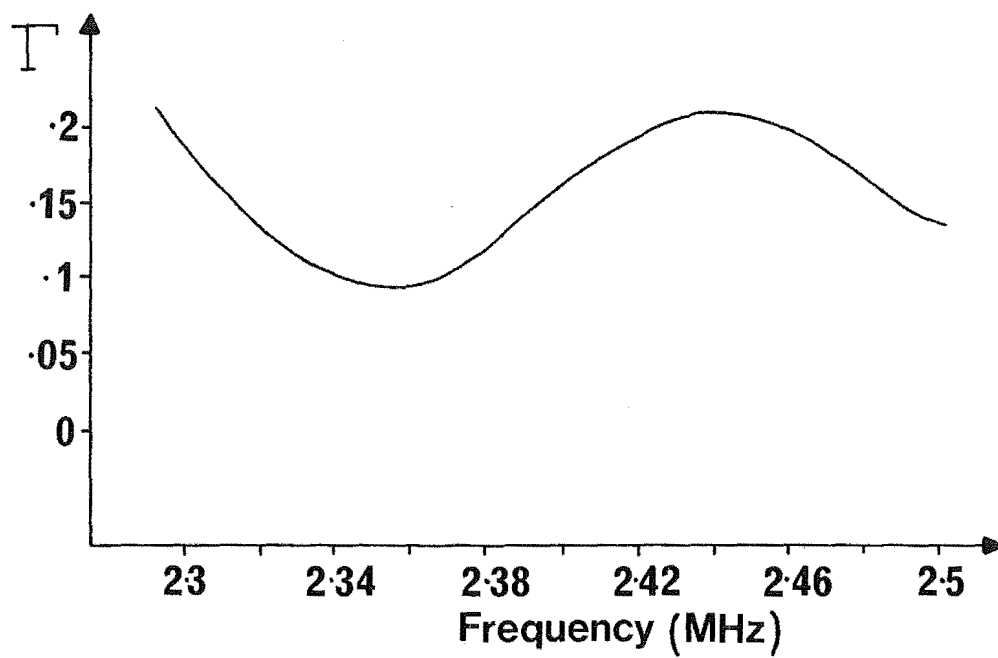
Fig. 7.12: Magnitude of reflection coefficient
at transmitter terminals.

CHAPTER 8

BROADBAND RECEIVER

8.1 PERFORMANCE REQUIREMENTS AND CONFIGURATION

The conceptual design of the receiver described in this chapter was relatively straightforward, in that a considerable proportion of this task was directed by the special requirements of the pulse compression system. The methods by which the various receiver parameters were evaluated are given below.

(a) Input. The antenna input to the receiver should be unbalanced, with an impedance of 75 ohms, to ensure optimum matching to the antenna feeder.

(b) Bandwidth. The complete receiver system must, of course, have a bandwidth of 200 kHz, centred on 2.4 MHz. The response of the receiver should taper off as sharply as practical outside this band, for maximum rejection of unwanted signals.

(c) Output. The receiver is to be connected to an analogue-to-digital converter having an input range of ±5 volts; maximum receiver output must hence be of this amplitude.

(d) Gain. Ionospheric returns at Birdling's Flat produce typical maximum amplitudes in the receiving antennas of 0.8 mV RMS. If full receiver output (10 volts peak-to-peak) is to be obtained from this input level, a gain of approximately 73 dB is required. Also, some means of varying the receiver gain is desirable.

The actual configuration of the receiver circuitry was partly dictated by the signal processing method. It will be recalled (Chapter 4) that the received signal requires mixing to

'baseband' before processing. Fig. 4.2 shows a means by which this may be accomplished; circuitry which implements this function is included in the receiver.

A block diagram of the complete receiver system is shown in Fig. 8.1. The RF amplifier was considered necessary to ensure a good signal-to-noise ratio at the inputs to the 1496 multipliers. The output of each mutliplier is at all times the product of the instantaneous voltages present on the RF amplifier and local oscillator outputs; it is in this stage that the baseband mixing takes place. Since the 1496 has a maximum output of 6 volts peak-to-peak, a video amplifier is required to produce an output from the receiver at an appropriate level for the analogue-to-digital converters. The bandwidth of the receiver is essentially controlled by the low pass filters. The RF amplifier is tuned as a band pass filter centred on 2.4 MHz; the tuning is broad compared with the effect of the low pass filters, but the stage does serve to prevent large out-of-band signals (e.g. broadcast stations) from saturating the multiplier inputs.

8.2 CIRCUIT DESCRIPTIONS

(a) RF amplifier. The unit selected to perform this function was the RCA CA3028 Integrated RF Amplifier. The operation of this device is described fully in an application note (Kiehn, 1974) and will not be detailed here. The differential mode of operation was chosen, this having the advantages of high input impedance, good gain control, and good limiting.

Antenna

RF Amplifier

Multiplier 1496

Low Pass Filter

Video Amplifier

Sine Channel Output

Local Oscillator

2·4 MHz sine

2·4 MHz cosine

Multiplier 1496

Low Pass Filter

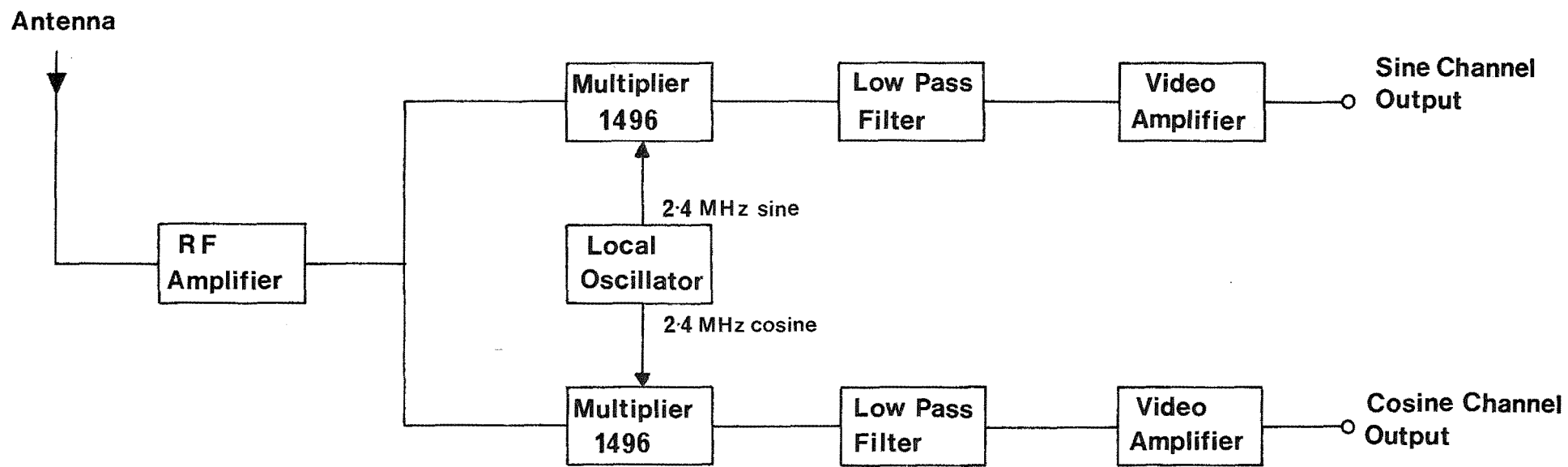Video Amplifier

Cosine Channel Output

Fig. 8.1: Receiver block diagram.

The circuit of the RF amplifier is shown in Fig. 8.2. The 'split capacitance' in the input tuned circuit effects an impedance transformation from 75 ohms to the input impedance of the CA3028. Both the input and output tuned circuits are designed with a -3 dB bandwidth of 200 kHz. Gain control is achieved by varying the bias on the constant-current source which supplies the emitters of a 'differential pair' in the CA3028. The maximum gain of the stage is predicted to be 50 dB; the gain can thus be set to any value between zero and this figure.

(b) Multipliers and low pass filters. The multiplier circuit was designed following guidelines given in an application note for the 1496 (Motorola, 1971). The 1496 is operated with the upper quad differential amplifier (carrier input) in the saturated mode; this has the advantage of making the output signal insensitive to changes in carrier amplitude. The carrier signal is introduced into the multiplier in a balanced form in an attempt to minimise stray 2.4 MHz radiation inside the receiver. The gain of the stage is controlled by a resistor between pins 2 and 3 of the 1496. The value of this resistor was adjusted when the receiver was completed to set the overall receiver gain to 73 dB. Balanced outputs are taken from the multiplier in order to minimise the effects of DC drift, which could otherwise be severe at the output of the video amplifier.

A passive L-C circuit is used for the low pass filter. This has the advantages over an active filter of zero DC drift, and, if components are carefully chosen, a sharp 'rolloff' in the stopband. A constant-k pi section configuration is utilized with a cut-off frequency of 100 kHz.
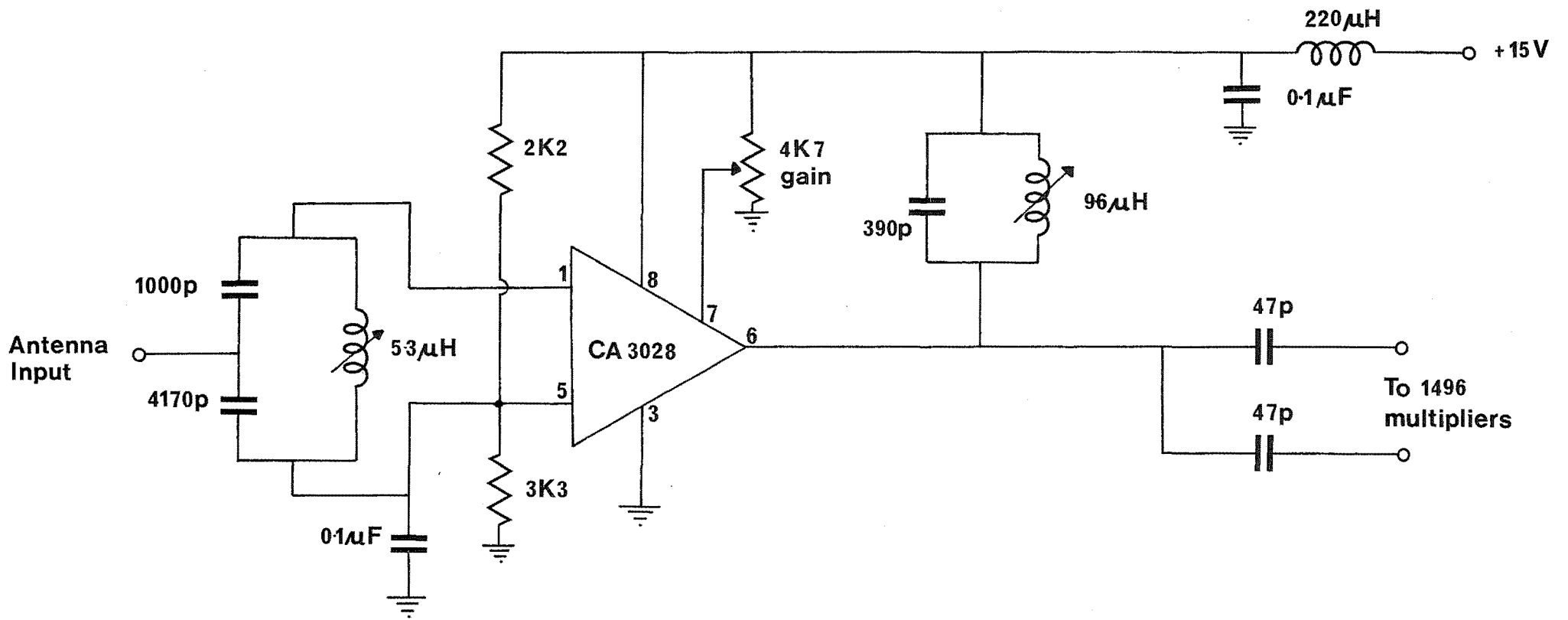
Fig. 8.2: RF amplifier circuit.

A circuit diagram of the multiplier and low pass filter is presented in Fig. 8.3. This circuitry is, of course, duplicated, the local oscillator inputs to each channel differing in phase by 90°.

(c) Video stage. The video amplifier must function in a differential input configuration, subject to the following constraints:

1. It must be capable of producing a full 10 volt peak-to-peak output signal at 100 kHz without slew rate limiting.

2. Long term drift on the output should not exceed the equivalent of 1 bit of the analogue-to-digital converter (i.e. 10 mV).

3. Provision for offset adjustment must be available to counteract any imbalance in the 1496 outputs.

Whereas these are not severe requirements in themselves, a high quality operational amplifier is necessary to fulfil conditions 1 and 2 simultaneously, especially if the stage is to provide any appreciable gain. A unit manufactured by RCA, the CA3140, had just been released in New Zealand which, according to its specifications, would be adequate for the application. This op-amp is used in a standard differential amplifier configuration, with a gain of 10 (see Fig. 8.4). The output is adjusted to zero volts with the oscillator running, and the antenna input terminated.

(d) Local oscillator. Two balanced square wave signals at 2.4 MHz, differing in phase by 90° are derived from the master 9.6 MHz source. The circuitry is implemented using TTL dividers in the configuration shown in Fig. 8.5. The output amplitudes are adjusted so that the carrier inputs of the multipliers are just saturated, care being taken to ensure that each output is properly balanced.
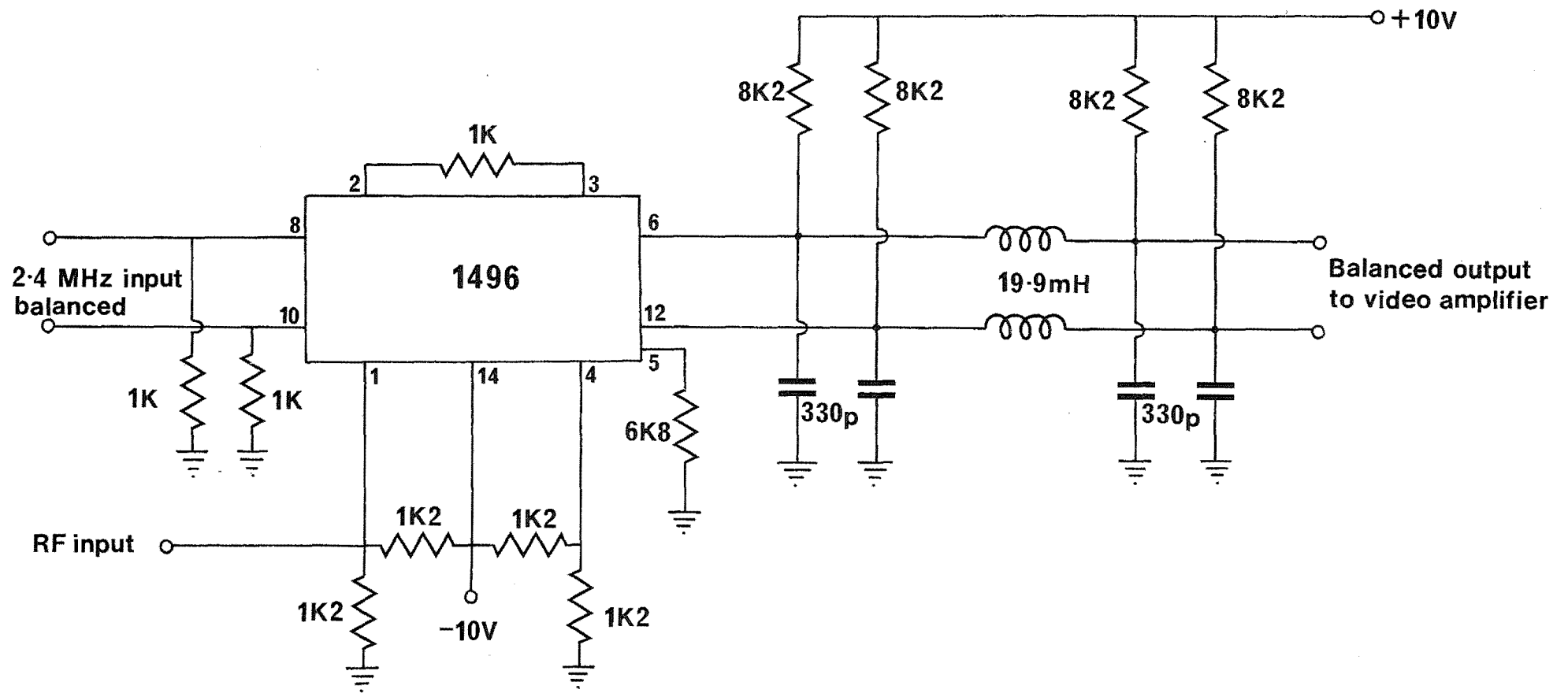
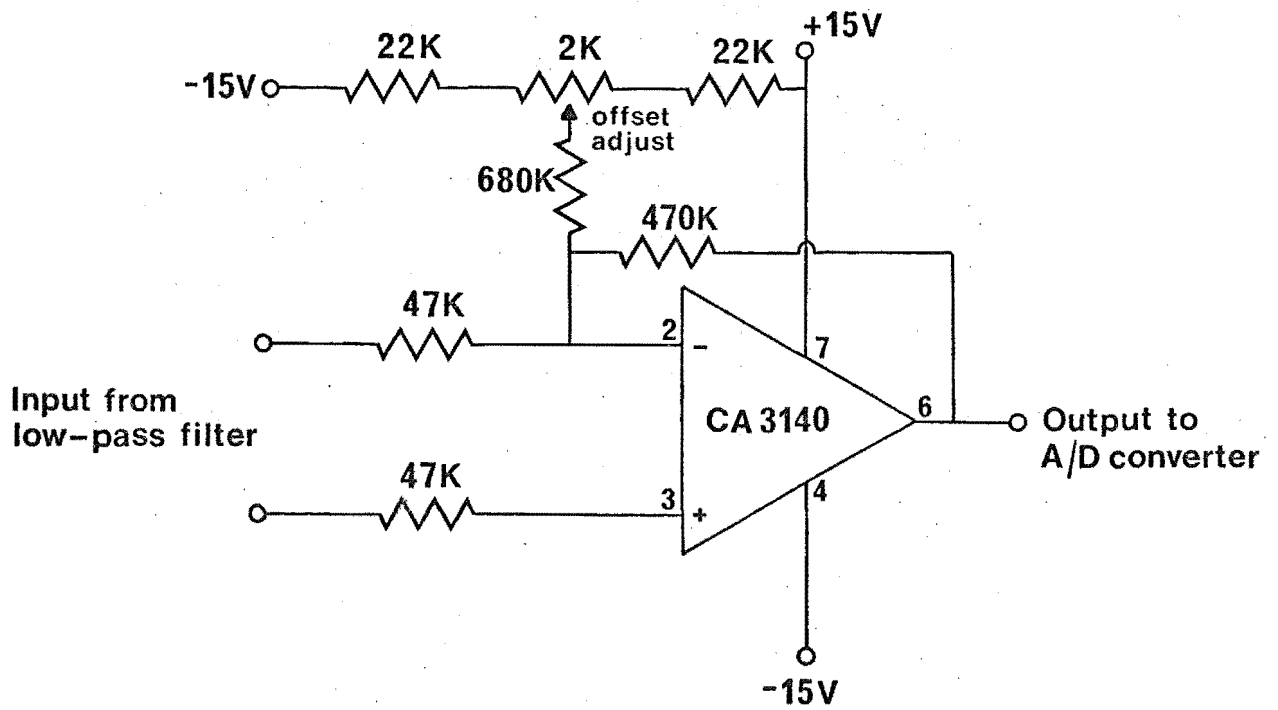Fig. 8.3: Multiplier and low pass filter circuit.

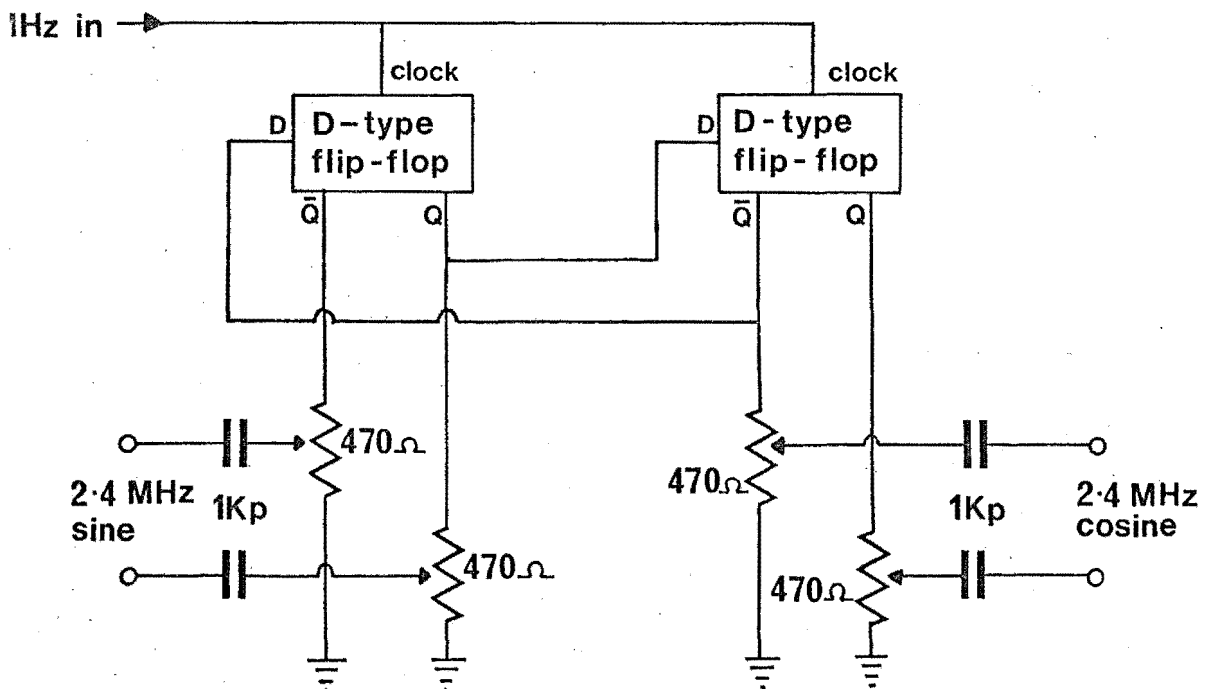Fig. 8.4: Video amplifier circuit.

Fig. 8.5: Local oscillator configuration.

8.3 CONSTRUCTION

    With the exception of the local oscillator section, all the
receiver components are mounted on a single printed circuit
board, which is installed in a standard modular chassis. The
local oscillator resides in a sealed copper box, to prevent 2.4
MHz signals at TTL levels from being radiated to the receiver
input.

8.4 BENCH TESTS

    Though both the input and output circuits of the RF
amplifier are designed for -3 dB attenuation at the band edges,
it is possible, by carefully 'stagger tuning' the circuits, to
obtain a response for the whole amplifier which is reasonably
flat over most of the passband, with attenuation at the band
edges negligibly greater than 3 dB. Fig. 8.6 is a graph of the
frequency response of the RF amplifier after optimum tuning.
The gain of the amplifier was somewhat lower than that calcul-
ated, the measured figure being 46 dB, with the gain control at
its maximum.

    Fig. 8.7 shows the response curve of the low pass filters.
The slight rise in amplitude rowards 100 kHz combines well with
the falling 'shoulders' of the RF amplifier response to give an
extremely flat passband for the whole receiver.

    The video amplifier was tested to ensure that its output
could be satisfactorily zeroed (under no-signal conditions) and
that it had sufficient slew rate to pass high amplitude, high
frequency signals without distortion. Signals at 120 kHz, with
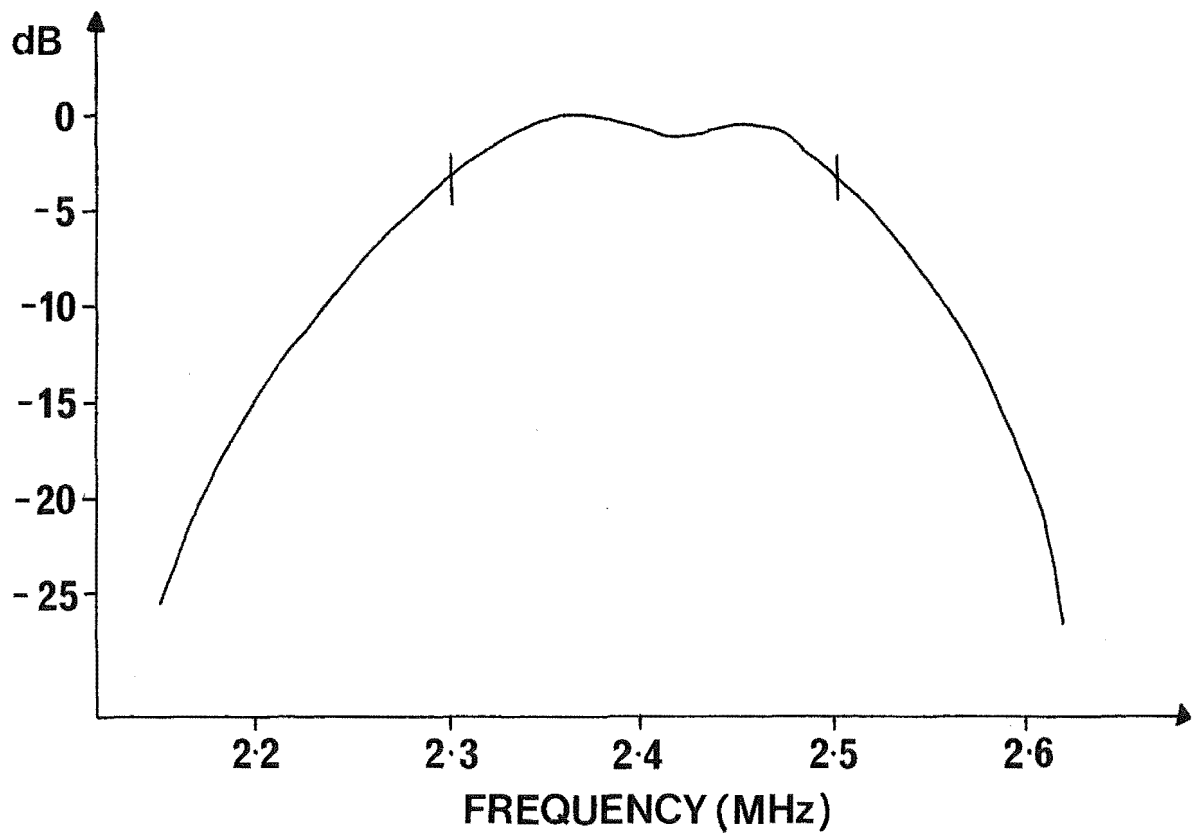amplitudes of up to 12 volts peak-to-peak were handled by this
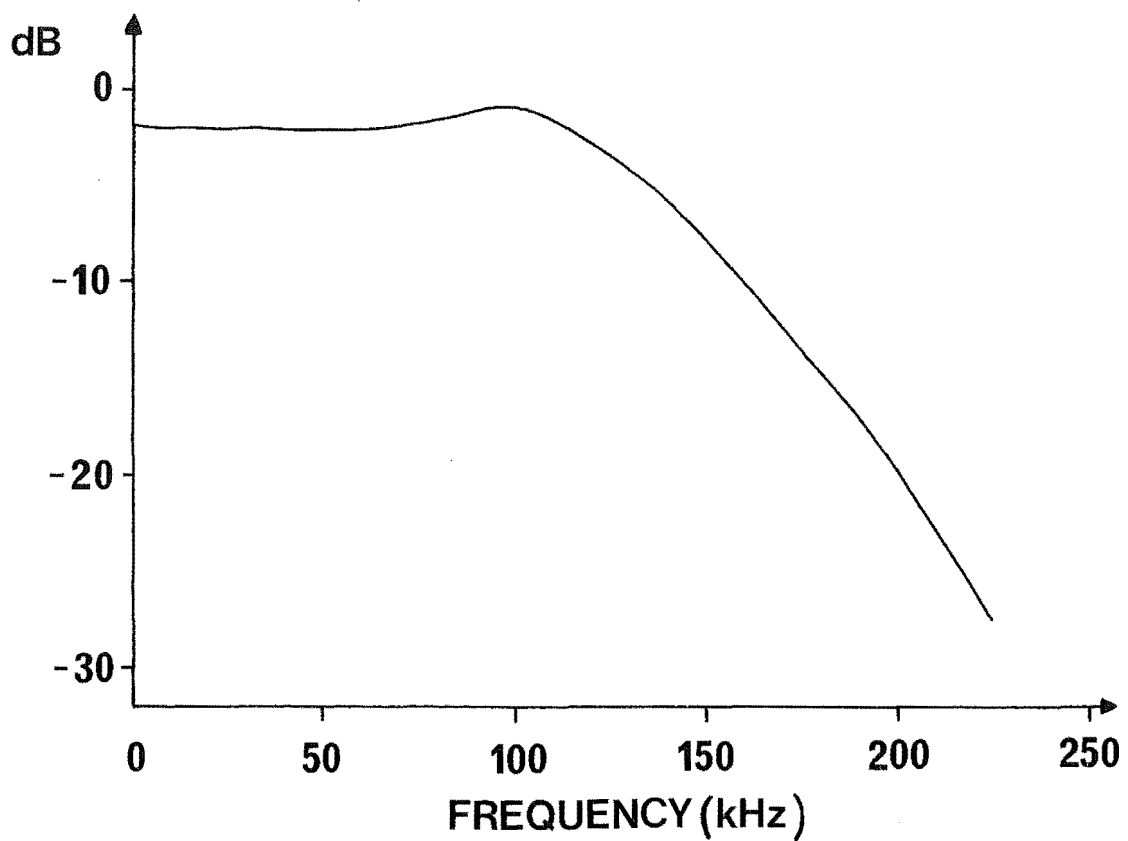
Fig. 8.6: RF amplifier frequency response.

Fig 8.7: Low pass filter characteristic.

amplifier without visible distortion, and hence it was consider-
ed satisfactory.

The gains of the 1496's were then adjusted so that the
overall receiver gain was 73 dB, with the RF gain set to
approximately 80% of its maximum. The gain could then be
finally set by the RF gain control when in the field.

The smallest input signal that could be resolved from the
receiver noise had an amplitude of 1.5 µV RMS; this value
results in a useful dynamic range of 55 dB for the receiver.

The final measurement made on the receiver before its
installation at Birdling's Flat concerned channel similarity.
Since the outputs of the receiver represent the sine and
cosine functions of the received signal, it is vital that the
information is not degraded by variations in amplitude or phase
between the two channels.

Measurement of differential amplitude was a straight-
forward process, which involved introducing sinewaves of various
frequencies and amplitudes into the receiver input, and compar-
ing the levels of the two outputs. The maximum difference over
the full receiver bandwidth, and over a range of amplitudes,
was 0.17 dB.

Measurement of phase difference was rather more complex,
and involved a careful setting up of the two outputs on a dual
trace oscilloscope. For phase differences in the vicinity of
90°, this measurement technique had an accuracy of about $\pm 2^{\circ}$.
Channel phase differences were measured over a range of
frequencies and amplitudes, the maximum deviation from 90° being
$3^{\circ} \pm 2^{\circ}$.

It was considered that these channel dissimilarities in both amplitude and phase would not have a significant effect on system performance.

8.5 FIELD TESTS

Final setting of the overall gain was the only aspect of the receiver which was dependent upon conditions in the field. Initial gain calculations had been made assuming a particular signal level in the antenna; these had to be ratified by operating the receiver in an actual ionospheric sounding experiment. The amplitude of the ionospheric returns obtained by operating the transmitter in the pulse compression mode was such that E-region echoes would produce full receiver output when the receiver gain control was at about 75% of its maximum. This is a desirable situation, in that the gain can be raised somewhat should one wish to investigate low-amplitude D-region reflections, or lowered if more 'headroom' is required. The gains of both the multiplier and the video stage were thus kept at their existing levels.

Once installed, the receiver was checked frequently over a period of six months for DC drift on its output. The output voltage present with the antenna input terminated was never more than ±7 mV in either channel; since this is less than the equivalent of 1 bit of the analogue-to-digital converter output, the receiver was considered to have adequate long-term stability.

8.6 RECEIVING ANTENNAS

The receiving antennas utilized in the pulse compression radar system consisted of two half-wave dipoles arranged in a broadside array. A full description of the antennas, feeders, and impedance matching elements may be found in Cooper (1978).

Impedance measurements were made at the receiver end of the feeder line to determine the bandwidth characteristics of this array; these indicated that standing wave ratios of less than 1.1 would be present at all frequencies in the band. Hence the receiving antennas clearly have an adequate bandwidth for use in the pulse compression system.

CHAPTER 9

SIGNAL PROCESSING SOFTWARE

9.1 INTRODUCTION

This chapter contains a description of the means by which the processing filter, treated mathematically in chapter 4, is implemented using the PDP8 computer. An outline of the hardware associated with the process is first given, followed by the method of evaluating the filter coefficients (or 'multiplication factor'). The structure of the program which actually performs the 'de-chirping' function is also presented.

At this stage a decision must be made concerning the number of sample points to be used in the filtering process. (This is the quantity N, introduced in equation (4.15)). Two factors affect this choice: firstly, the FFT routine requires that N be some power of two, and secondly, the observable height range of the system is dependent solely on N (since there are N 'heights' in the output data, and sampling takes place at a fixed rate). If this rate is assumed to be 3.3 µsec (see section 9.2), the height range covered by N samples is given by

$$H = \frac{3.3 \text{ Nc}.10^{-6}}{2} \qquad (9.1)$$

where c is the speed of electromagnetic radiation. This reduces to

$$H(km) = \frac{N}{2} \qquad (9.2)$$

The region of interest in the ionosphere would be adequately covered by a height range of about 100 km; a choice of 256 for N is therefore the most appropriate.

9.2 COMPUTER INTERFACES

The chief means of communication with the PDP8 is via a DECWRITER II keyboard terminal. This is used during program execution to enter commands to the program, and to print output messages and prompts. The computer also supports two DECTAPE units, used primarily for program and file storage.

The input data to the PDP8 are obtained with a Datel G10B3C analogue-to-digital converter. This device, one of the fastest available at the time of its purchase, performs one 10-bit conversion in about 1 μsec. Since the receiver has two output channels requiring simultaneous sampling, each channel is connected to a track-and-hold circuit. At each sampling instant, both of these circuits are put into the 'hold' mode, and the analogue-to-digital (A-D) converter multiplexed between the two track-and-hold outputs, sampling first the real, then the imaginary channel. The time taken to multiplex the A-D converter, and to perform both conversions is 3.3 μsec, corresponding to a sampling rate of 300 kHz for each channel. Since the maximum signal frequency present is 100 kHz, sampling takes place at 1.5 times the nyquist rate. The 10-bit output of the A-D converter has a resolution of 1 part in 2^{10}; this corresponds to an effective dynamic range for the A-D converter of 60 dB.

Data output from the computer is of two types. The primary output is to 7 track magnetic tape. After each scan, 256

complex numbers are written to this tape, each number represen-
ting the amplitude and phase of the radar return from a
particular virtual height. Also, the magnitude of each of
these complex numbers is converted to analogue form, and dis-
played in an 'A-scan' format on a cathode-ray tube. This gives
an immediate visual check on system performance. This output
may also be plotted on an X-Y chart recorder if desired.

9.3 EVALUATION OF THE FILTER COEFFICIENTS

The 'multiplication factor' which performs the filtering
operation is a discrete function, $Y_c(n)$, the value of which is
obtained from the equation given in chapter 4:

$$Y_c(n) = \frac{W(n)}{E(n)} \qquad 0 \le n \le 255 \qquad (4.16)$$

where $W(n)$ is a weighting function

and $E(n)$ is the spectrum of the chirp signal.

A straightforward means of evaluating $E(n)$ would be to perform
an FFT on the sampled chirp function, $e(j)$, given by

$$e(j) = \exp 2\pi i \left\{ \frac{k[(j-N/2)t_s]^2}{2} \right\} \qquad 0 \le j \le 255 \qquad (4.15)$$

where k is the rate of frequency modulation

and t_s is the sampling interval.

This approach would result in a filter which is perfectly
matched to an input signal of the form given in equation (4.15),
that is, a signal which is an undistorted, perfectly linearly
swept pulse of constant amplitude. A chirp pulse introduced
into the receiver is, however, unlikely to be exactly of this

form after sampling; the receiver does not have an entirely
flat passband, and some distortion is likely to be introduced
in the receiver, track and holds, and the A-D converter.

A more accurate method of obtaining E(n) is therefore to
introduce a generated chirp pulse, suitably attenuated, into
the receiver, sample the output, and perform an FFT on the
numbers thus obtained. A filter derived from this particular
E(n) function would then be truly matched to the signal *that
actually appears at the output of the A-D converter during data
collection*. In fact, it is even irrelevant what specific form
e(j) takes, since any amplitude-independent distortions in the
receiver, and errors in the FM rate of the chirp are all incor-
porated into the multiplication factor, and hence do not intro-
duce any signal degradation. The only restriction is that the
spectral energy of the function e(j) should be reasonably evenly
distributed in the interval -100 kHz to +100 kHz.

A weighting function, centred about zero frequency, and
composed of real numbers, will have a Fourier transform which
is centred upon time t = 0. However, it is proposed to use
a weighting function for which the Fourier transform is centred
about t = 128 sampling intervals, that is, in the centre of the
time interval created by a 256 point inverse Fourier transform.
This new weighting function may be obtained by considering the
time-shifting theorem of discrete Fourier transforms:

$$h(j-k) \quad \overset{DFT}{\Longrightarrow} \quad H(n).\exp\{-2\pi i kn/N\} \qquad (4.19)$$

That is, a time function delayed by k sampling intervals has a
linear phase function added to its spectrum. For a 256 point
transform, and a time shift of 128 points, the function W(n)

must thus be multiplied by exp(-iπn). Fig. 9.1 shows this process diagrammatically.

This adjustment to the phase of the weighting function is necessary to ensure that a radar echo occurring in the centre of the input data appears after processing as a 'blip' in the centre of the output scan. Correct phase of the filter function will only be obtained if the chirp signal from which the filter is derived also occurs in the centre of the input data sequence.

The multiplication factor is found in practice by running a PDP8 program called SETUP, which operates as follows:

a) The output of the chirp generator is sampled. Initially the computer enters a loop which repeatedly triggers the chirp generator, and performs a set of 256 complex A-D conversions. A 'flag' is set while the A-D converter is operating, and this is displayed on an oscilloscope, together with the chirp generator output. The time at which the chirp generator is triggered may then be adjusted by means of an analogue delay until the chirp occurs in the exact centre of the input samples. When this has been achieved, a final set of samples is taken, and stored in the computer's core.

b) The function e(j) obtained in a) is transformed by the FFT routine to give the spectrum E(n). This is also held in core.

c) The weighting function is entered. The function (with its phase already adjusted) is actually calculated by the B6700 at Canterbury, and the values of the function for each n are entered manually into the PDP8 through the DECWRITER keyboard.

d) Complex division of this weighting function by E(n) is then performed for each value of n. The multiplication factor,

FREQUENCY DOMAIN
TIME DOMAIN

W(n)

w(j)

FFT

0

0   255 n

0   128   255 j

$\left| W(n) \exp(-in\pi) \right|$

w(j-128)

FFT

0

0   255 n
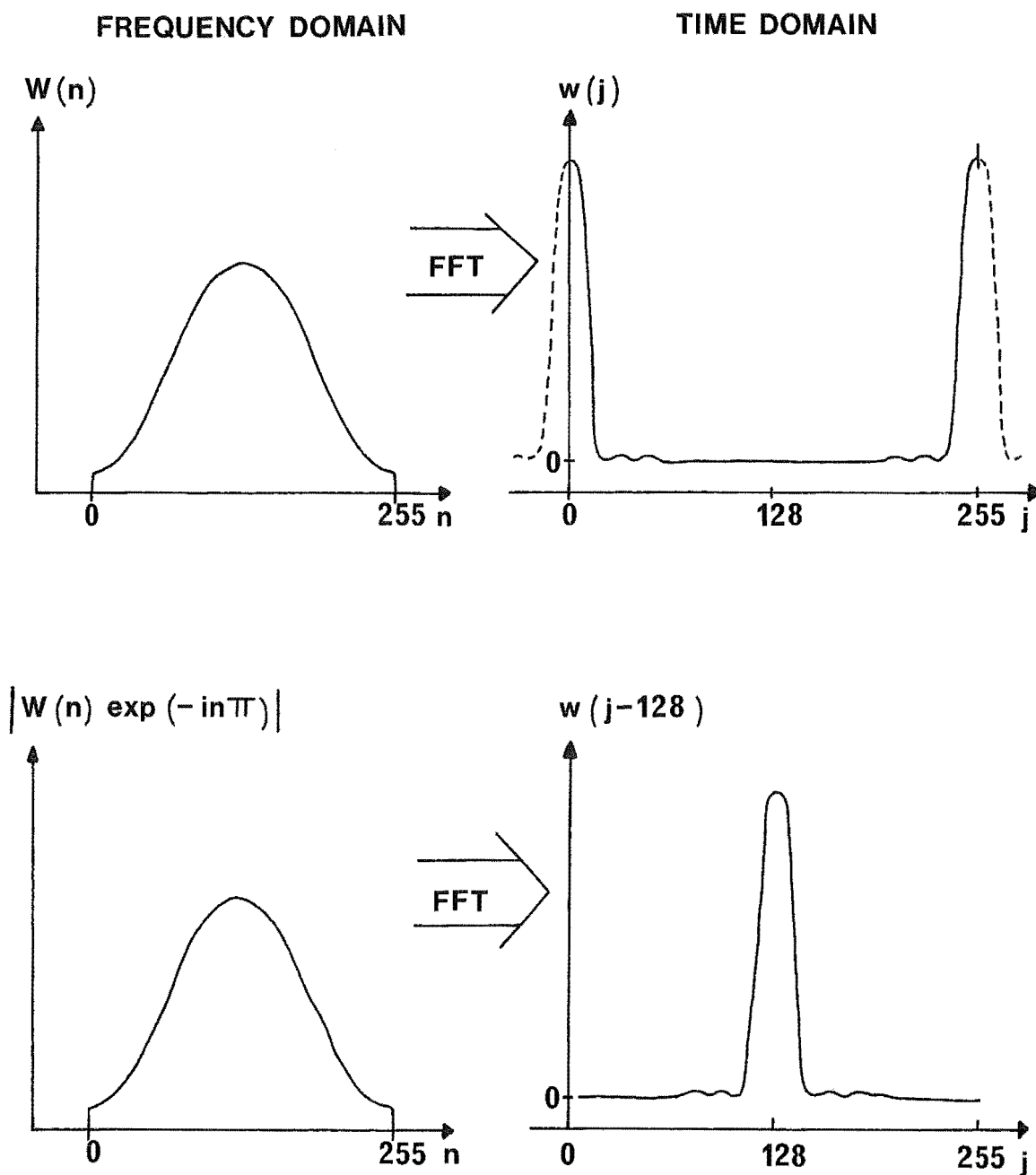
0   128   255 j

Fig. 9.1: Effect of a linear added phase on a weighting
function and its transform.

$Y_c(n)$, thus produced is given a title, and written as a file to DECTAPE, for storage.

e) The weighting function is then transformed by the FFT routine, and the moduli of the resulting complex numbers displayed graphically on a cathode-ray tube. This is an important step, since the Fourier transform of the weighting function has the same form as a processed radar echo from a point target (see section 4.2). This step thus gives the operator a frame of reference for his interpretation of ionospheric returns.

All arithmetic operations in SETUP (excluding the FFT) take place in a 'floating point' format, the mantissa of each variable occupying two 12-bit words, and the exponent one. This ensures that round-off errors in the arithmetic never become significant (since the data are essentially of 10-bit precision). The FFT routine uses fixed point arithmetic, but constantly scales its data during the transform to ensure maximum bit usage throughout (Rothman, 1968).

9.4 PROCESSING THE RADAR RETURNS

In essence, implementation of the signal processing method is a simple procedure , described by the sequence

Data from A-D converter $\xrightarrow{\text{FFT}}$ spectrum $\xrightarrow{\text{multiply by filter}}$ linear combination of weighting functions $\xrightarrow{\text{IFFT}}$ 'A-scan'

However, the fact that a computer of limited word size is utilized means that considerable effort must be expended to ensure that sufficient precision is maintained at all times. The FFT routine achieves this by examining the magnitude of the data after each stage in the transform algorithm. The data are scaled by a factor of two, either up, to maintain full bit

usage, or down, to prevent overflow. A tally is kept of these scaling operations, and when the routine is completed, this number is accessible as the 'scale factor' for the transform. The correct spectral coefficients may then be found from the relation

$$\text{true values} = \text{calculated values} \times 2^{(\text{scale factor})} \quad (9.3)$$

Scaling of numbers also occurs when data are converted from floating point to fixed point numbers; this conversion is necessary during processing, as the FFT routine and the final output require numbers in fixed point, single precision format. A floating point number cannot be 'fixed' unless its modulus is less than 2047, this being the largest number that can be expressed in 12-bit, 2's complement form. This is equivalent to requiring that the exponent (to base 2) of a floating point number is less than 12 before attempting to fix that number.

A detailed description of the signal processing sequence will now be given. The data from the A-D converter are loaded into the FFT data locations, and a transform performed. The scale factor for this transform is stored in a variable, SCALE1. Each of the 256 complex spectral weights is then converted to floating point format, and multiplied by the appropriate element of the multiplication factor. The exponents of the resulting numbers are all successively decremented until the largest of them equals 11; the number of these operations required is stored in a variable, FIX. The data are then fixed, and an inverse FFT performed, the scale factor for this transform being stored as SCALE2. The resulting function is once again converted to floating point format, and each exponent altered by a factor

named ADJUST, the magnitude of which is given by

$$ADJUST = SCALE1 + FIX + SCALE2 + FACTOR \qquad (9.4)$$

where FACTOR represents a quantity called the 'external scale factor'. This final adjustment to the exponents compensates for the scaling introduced in the FFT's and the fixing operations; this is essential to ensure that successive scans have meaningful relative amplitudes. (It is not possible to predict whether scaling will be required prior to fixing the data, nor what the scale factors for the transforms will be. These depend solely on the input data.)

The external scale factor is a number set by the operator prior to a data collecting run. It determines in effect the 'gain' of the processing filter, and is usually set such that input data having the maximum amplitude that can be represented by a 12-bit word results in a processed 'A-scan' of similar magnitude.

Finally, these adjusted floating point numbers are once again fixed. The 256 complex amplitudes are written to magnetic tape, and their moduli displayed on a cathode-ray tube. Should any of the floating point numbers be too large to fix, the external scale factor is decremented by 1, and a message to this effect printed on the DECWRITER. The exponents of the floating point numbers are then re-adjusted, and the fixing operation attempted again.

The process just described takes place under the control of a program named SKY. This program begins by requesting from the operator the name of the file containing the desired multiplication factor, which is then read into core from

DECTAPE. Following this, the values of the external scale factor, and the 'starting height' are entered from the keyboard. The starting height specifies the lowest height in each scan from which data are collected. These two values may be altered at any time during a run by appropriate keyboard input.

The program then begins to collect ionospheric data. The transmitter is pulsed, and after a delay given by

$$\tau = \frac{2 \, h_s}{c} \tag{9.5}$$

where h_s is the starting height

c is the speed of electromagnetic radiation

the A-D converter takes a set of 256 complex samples. These are processed according to the method described earlier in this section, and the sequence then repeats continuously until halted by the operator. The pulse repetition rate is limited by the time taken to process each scan, which is about 12 seconds. This time would be substantially reduced by the addition of a 'hardware multiplier' to the computer; such circuitry is, in fact, presently under construction.

At the completion of a run, the magnetic tape is retained and may be read into the B6700 for further reduction and data presentation.

CHAPTER 10

SYSTEM EVALUATION

10.1 HARDWARE

The electronic hardware comprising the complete pulse-
compression radar system falls logically into four discrete
areas:

1. Chirp Generator

2. Transmitter subsystem

3. Receiver subsystem

4. Track-and-holds and Analogue-to-digital converter.
With the exception of the last category, the evaluation and
testing of the system electronics has been described fully in
previous chapters; the major portion of this section will
therefore describe the operation and testing of the track-and-
holds and the A-D converter.

The A-D converter itself is a 10-bit, high speed device,
manufactured by Datel Systems Inc. This unit is, however,
only a small part of a complex, exceptionally versatile machine,
which was conceived to enable the A-D converter to be utilized
in various experiments having widely differing requirements.
Since the A-D converter is capable of sampling at a rate
exceeding that at which the computer can store the samples, it
has associated with it 1024 words of fast-access memory, in
which the samples are stored as they are generated. The com-
puter later reads these stored samples at a slower rate.

The machine incorporating the A-D converter was originally
designed to take pairs of samples at a minimum sampling interval

of 6.6 μsec. This, however, was unacceptably slow for the pulse compression system, being below the nyquist sampling rate for the maximum signal frequency of 100 kHz. The task of reducing this sampling interval was undertaken by the designer of the machine, Mr Alec Black, and considerable credit is due to him for his ingenuity and perseverance in attaining a final sampling interval of 3.3 μsec. Some idea of the magnitude of this task may be inferred from his description of the timing of the multiplexing function, quoted below (Black, 1978). It should also be borne in mind that during each 3.3 μsec sampling interval, 300 nsec must first be allowed for the track-and-holds to settle, and that two conversions, each requiring 1.1 μsec take place.

> "After each conversion, the multiplexer is switched to the next input channel, the analogue signals requiring 450 nsec to settle. During this period, the A-D data are strobed into a buffer, and the number-of-samples per height gate counter is incremented and tested. The analogue switches have a 'turn-on' propagation delay of 400 nsec. If this time were added to the above 450 nsec it would be impossible to complete the 2 samples in the required period. To overcome this, the multiplexer command is given while the previous conversion is still in progress; in this way, the actual instant of switching can be made to concur with the end of the conversion period."

Understandably, timing adjustments were critical, and fine tuning was often necessary at the start of each data collecting period.

The operation of the A-D converter and associated hardware was frequently checked by running a PDP8 program which took a set of samples every 20 msec, displaying each set as a trace on

a cathode-ray tube. The analogue input could also be displayed,
thus allowing direct visual comparison between the A-D converter
input and output.

The following procedure was developed as a means for
testing the chirp generator, the receiver, and the computer
interfaces simultaneously. The chirp generator was triggered,
and the output introduced, via an attenuator, into the receiver.
The receiver outputs were sampled by the A-D converter, and the
'sine' and 'cosine' chirp signals displayed on a cathode-ray
tube and plotted. An FFT was then performed using these signals
as real and imaginary data inputs, and the amplitude spectrum
also displayed and plotted. The plotter output from one such
experiment is reproduced in Figs 10.1 and 10.2.

It can be appreciated (qualitatively) by inspection of Fig.
10.1 that the signals from the two channels pass through zero
frequency at their centres, and that they differ in phase by
90°. It is also apparent that there is some bandwidth limitat-
ion in the system, since the amplitude of the pulses tapers off
noticeably towards their extremities. It was found that the
principal contribution to this high frequency attenuation
originated from the track-and-hold amplifiers being inherently
bandwidth limited.

It is also apparent that the spectral ripples observable
in Fig. 10.2 are rather large compared to those in the theoret-
ical chirp spectrum, shown in Fig. 2.2; it was assumed that this
phenomenon was also due to the attenuation of the higher
frequencies. This deviation from the theoretical spectrum of
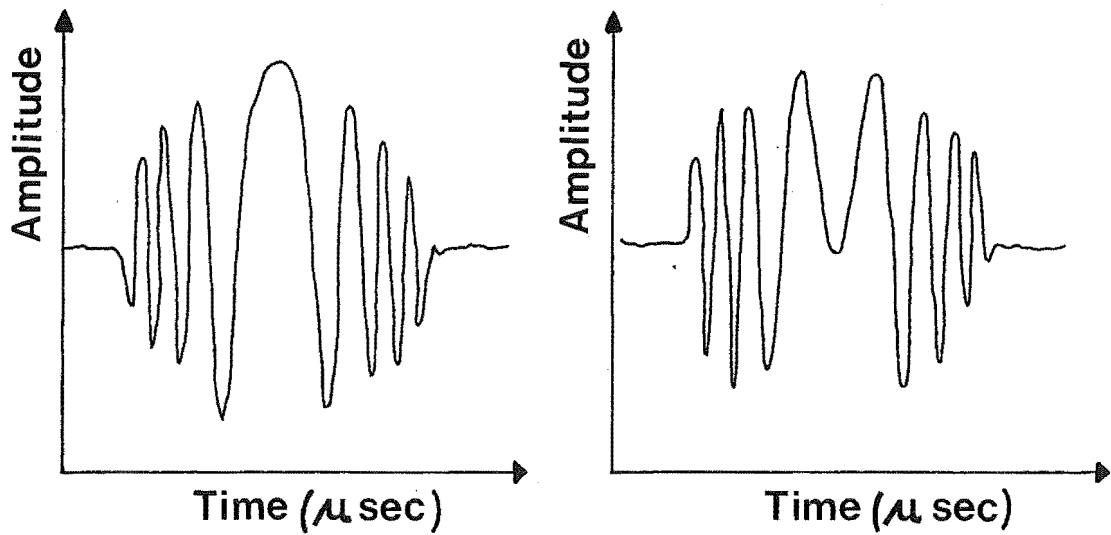a swept-frequency pulse is not, however, important, since the

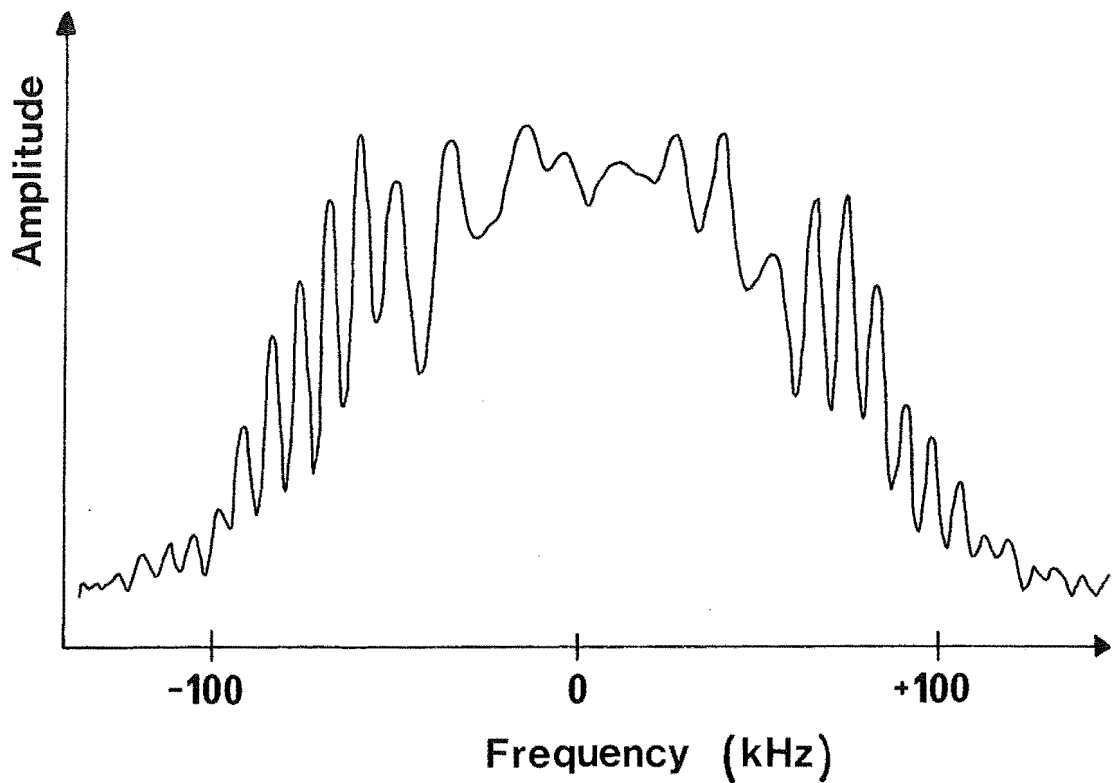Fig. 10.1: Cosine and sine chirp signals mixed to baseband.

Fig. 10.2: Amplitude spectrum of the swept-frequency pulse.

spectrum obtained in the experiment does fulfil the criterion given in section 9.3, namely that the major portion of the spectral energy is reasonably evenly distributed in the interval from -100 kHz to +100 kHz.

An indication is thus given that the system hardware is performing adequately. Providing that the PDP8 software is properly operational, then, effective pulse compression should be readily attainable.

10.2 SIGNAL PROCESSING

In order to evaluate the performance of the signal processing software, it is essential that a known, repeatable signal is introduced into the receiver input. Accordingly, the program SKY (described in Section 9.4) was run with the transmitter de-activated, and the output of the chirp generator connected to the receiver via an attenuator and a variable delay. This input signal thus simulated an undistorted radar echo from a point target. The filter function used in this experiment was obtained according to the method described in section 9.3, using an appropriate Hamming weighting function.

A typical output scan from the compression filter is reproduced in Fig. 10.3. The 'pulse widening factor' for the Hamming function is given, in Table 2.1, as 1.47; the expected resolution for the system thus becomes

$$\sigma = 1.47 \times 5 \ \mu sec$$

$$= 7.3 \ \mu sec.$$

Measurements of the plot shown in Fig. 10.3 indicate that the width of the output pulse at the -3 dB points is 6.9 μsec; this gives a positive indication that the predicted resolution
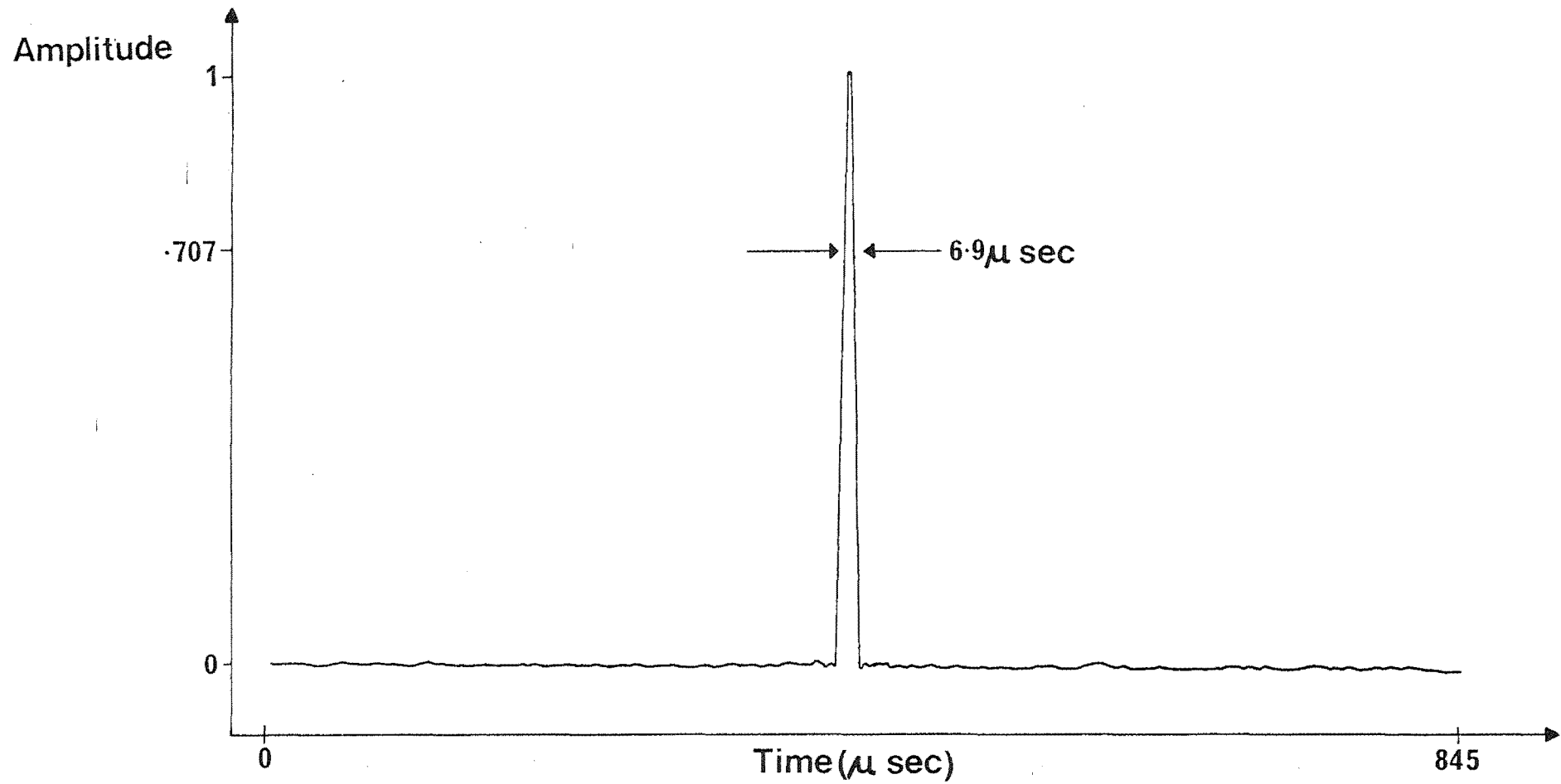
Fig. 10.3: Compression filter output produced by a single chirp pulse.

is obtainable in practice.

The sidelobes of the output pulse (just visible in Fig. 10.3) may be measured by re-plotting the graph with an expanded ordinate scale. This procedure gives a sidelobe level of -42 dB relative to the main pulse. Care should, however, be exercised in the interpretation of this figure, since the side-lobe amplitudes are low enough to be of the same order as the resolution of the digital-to-analogue converter used to produce the graph; strictly, the equivalent of half a bit of amplitude should be added to the sidelobes to obtain an accurate upper limit for the sidelobe levels. Using this procedure, it may be shown that the sidelobe levels are at least 40 dB lower than the main pulse. This figure still compares favourably with the theoretically predicted value of 42.8 dB (Table 2.1).

In section 2.4, it was demonstrated that, in addition to significantly increased resolution, one may expect an increase in signal amplitude to be effected by the compression process. The magnitude of this increase is equal to the square root of the compression ratio (from equation 2.26). It is of little value to consider the actual amplitude at the filter output when attempting to assess this kind of performance, since the 'gain' of this computational filter depends not only on the various scaling factors used in the calculation, but also on the amplitude of the reference signal from which the multiplic-ation factor is derived, and the magnitude of the weighting function employed. Measurement of the output pulse amplitude must therefore be made with respect to some independent level; the noise level present in the scan was used as this reference. The method employed is as follows.

A chirp pulse was sampled, and stored in the computer's memory. The amplitude of the pulse envelope was found, together with the amplitude of the noise appearing in the input before and after the pulse. This input scan was then processed by the compression filter. The amplitudes of the output pulse, and the noise level in the output scan, were then measured. The signal-to-noise ratio before and after processing could then be determined. Results from a typical experiment of this nature are presented in Table 10.1.

Table 10.1 Signal and noise levels before and after signal processing

(arbitrary amplitude units)

	Pulse Height	Noise Level	S/N Ratio
Before processing	638	26	27.8 dB
After processing	854	8	40.5 dB

Inspection of this table shows that the compression filter has effected an increase in the signal-to-noise ratio of 12.7 dB.

As mentioned earlier, the amplitude increase predicted by theory is equal to the square root of the compression ratio (in this case, 28). From this must be subtracted the mismatch loss introduced by the Hamming weighting function (see Table 2.1). Hence the expected increase in signal-to-noise ratio introduced by the compression process is given by

$$\text{Increase} = 20 \log\sqrt{28} - 1.34 \text{ dB}$$
$$= 13.13 \text{ dB}.$$

The 'amplitude enhancement' of the pulse compression radar system at Birdling's Flat is thus within 0.5 dB of the predicted value.

The dynamic range of the system was evaluated by reducing the amplitude of the input signal until the output pulse was just clearly discernible from the noise; the difference in amplitude between this signal and that which drove the receiver to full output gave an indication of the system dynamic range. Fig. 10.4 shows an output scan produced by an input 47 dB below peak signal level. By comparison, the dynamic range of the conventional radar system presently in use at Birdling's Flat is 55 dB. The dynamic range of the pulse compression system is expected to be about 1 dB less than this figure (the gain in signal amplitude in the compression process is offset by an increase in the noise bandwidth of the receiver). The relatively poor measured dynamic range of 47 dB for the pulse compression system can, however, be directly attributed to noise introduced by the A-D converter; this is discussed more fully later in this chapter.

The results of the tests outlined in this section were encouraging, indicating that the pulse compression system was in most respects operating near its design capabilities. The system was thus commissioned for ionospheric sounding tests.

10.3 PERFORMANCE WITH IONOSPHERIC RETURNS

In order to assess system performance using radar returns from this essentially variable target, a special version of the program SKY was written, which operated as follows. The system was initially put in the 'normal' (straight-pulse) mode, and a 30 μsec pulse transmitted. After a certain delay ('starting height') a set of samples was taken from the receiver output, and this scan stored in memory. The system
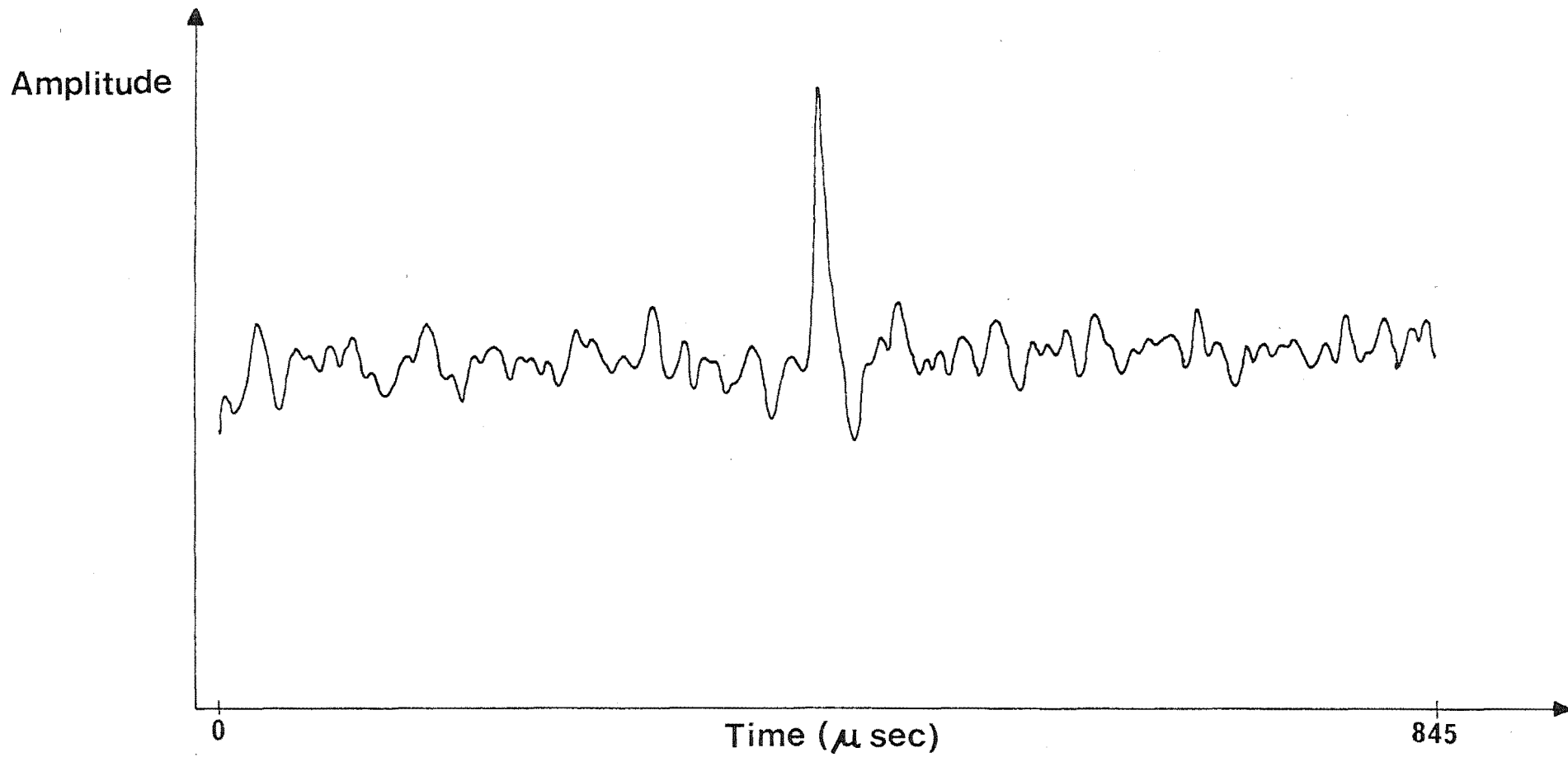
was then switched to the 'compression' mode, and a swept-frequency pulse transmitted. The receiver samples obtained from this sounding were then processed with the compression filter. The two scans thus obtained could be plotted and compared.

A number of these pairs of scans are reproduced in Figs 10.5 to 10.11. In each figure the upper trace represents the amplitude of the return from a 30 μsec 2.4 MHz pulse. The lower trace is the output from the compression filter after processing the return from a swept-frequency pulse transmitted 100 msec later. It can reasonably be assumed that the ionosphere remains nearly constant as a reflecting medium throughout this short interval.

Figs 10.5 to 10.8 show returns from the D- and E-regions of the ionosphere, taken near midday on 5th and 6th May, 1978. In Fig. 10.5, the pulse compression mode highlights the sharpness of the E-region reflection; from the 'normal' return this may be erroneously interpreted as a broader target. The scans shown in Fig. 10.6 include some partial reflections from the D-region. The higher resolving power of the 'compression' mode shows some fine structure which is effectively 'washed out' by the lower resolution of the 30 μsec pulse. Also, the pulse compression system seems capable of obtaining echoes from about 15 km lower than the 'straight' pulses. The 'normal' returns shown in Figs 10.7 and 10.8 show echoes from what appear to be broadly distributed targets. However, the pulse compression mode shows these targets to be rather finely structured composite reflecting regions.
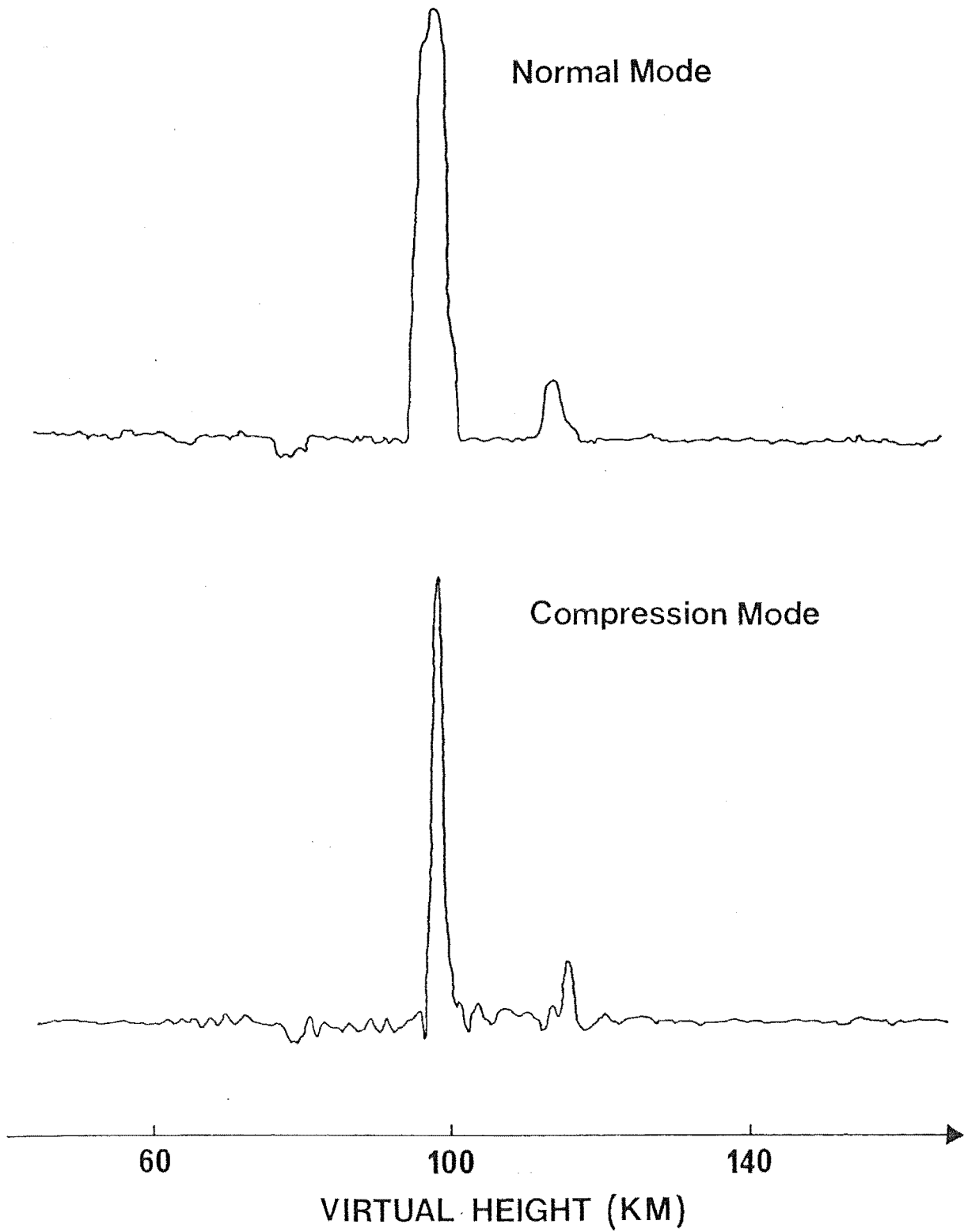
Normal Mode

Compression Mode

60   100   140

VIRTUAL HEIGHT (KM)

Fig. 10.5: Ionospheric returns, D- and E-regions.

Normal Mode

Compression Mode

VIRTUAL HEIGHT (KM)
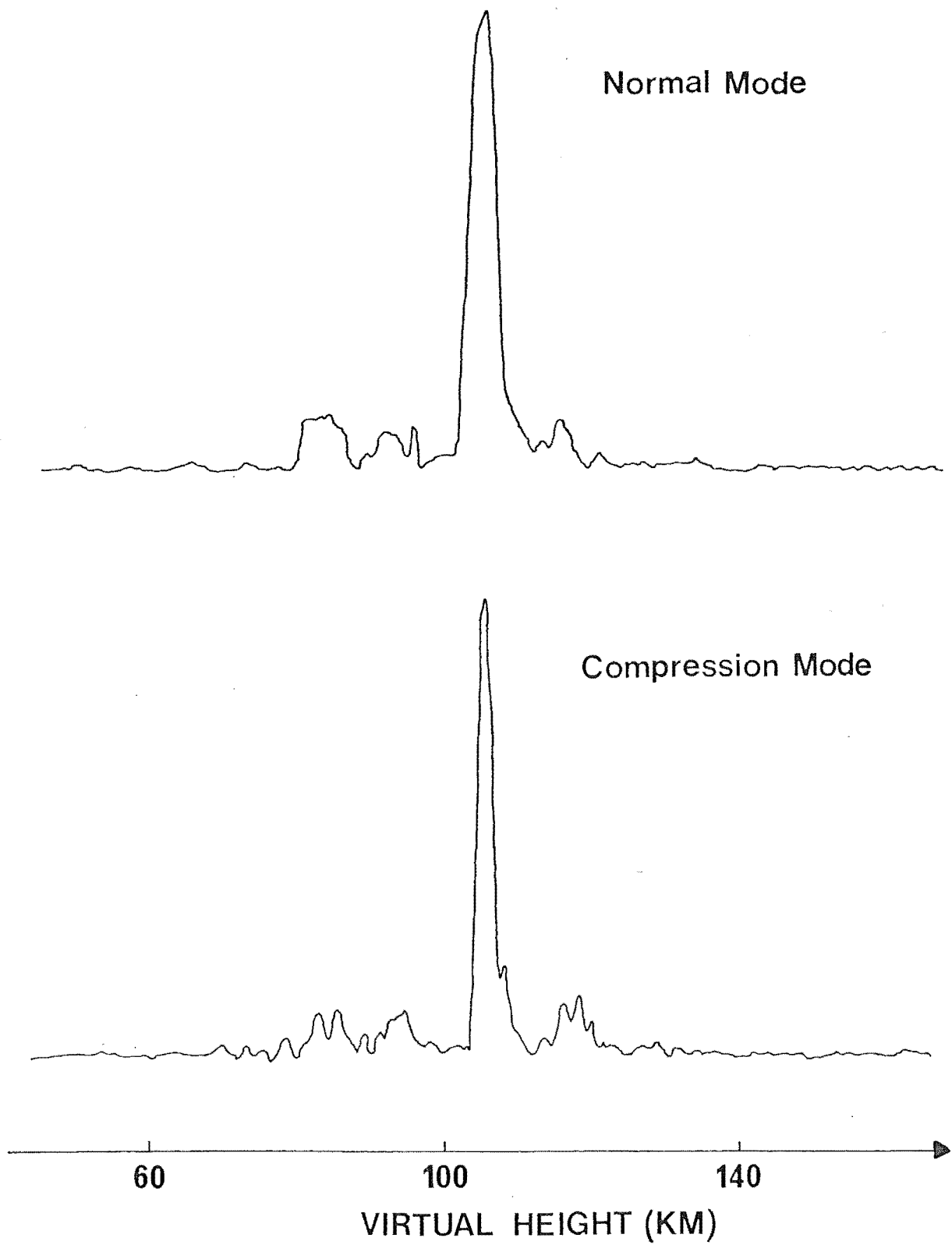
Fig. 10.6: Ionospheric returns, D- and E-regions.

Normal Mode

Compression Mode

60   100   140

VIRTUAL HEIGHT (KM)
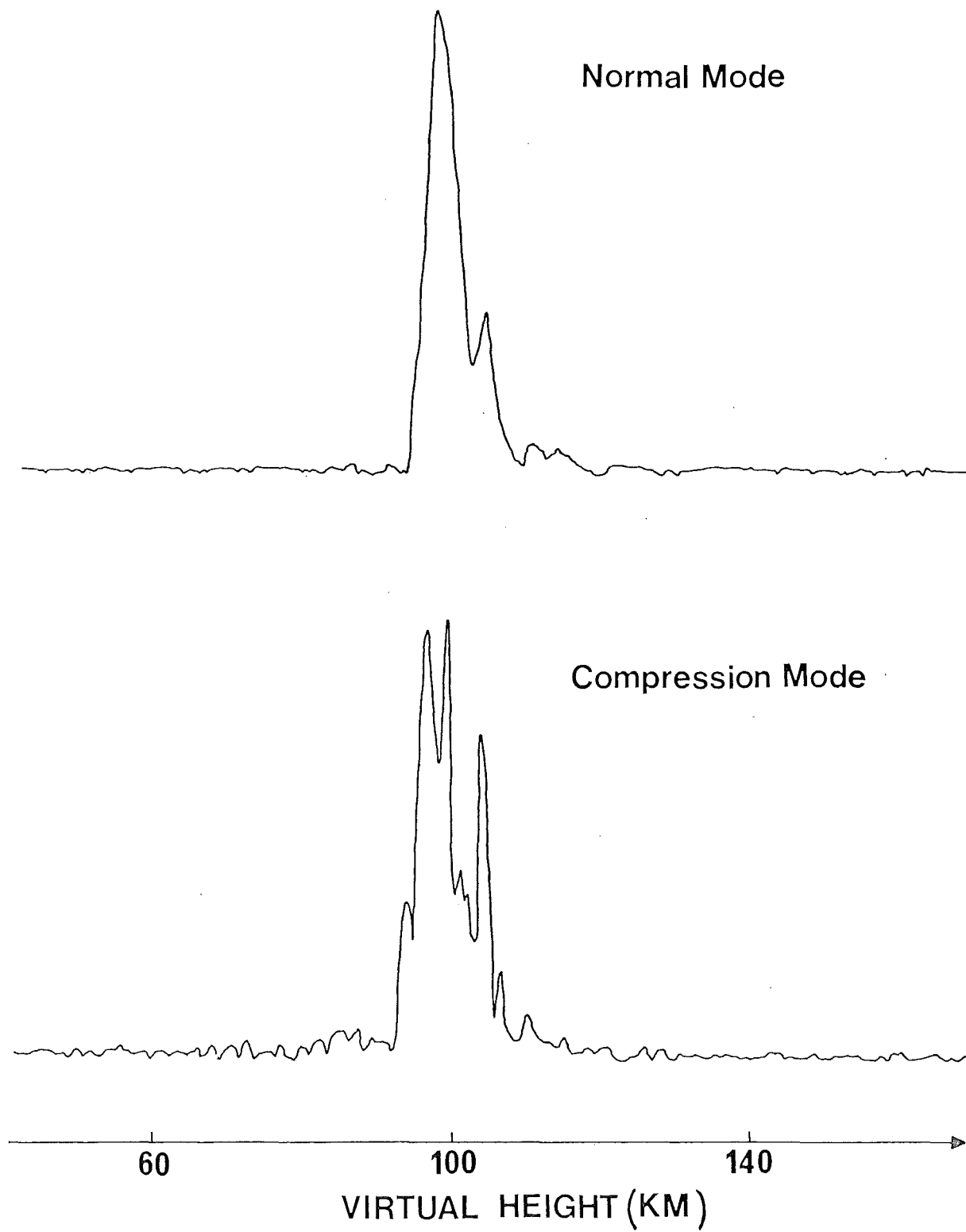
Fig. 10.7: Ionospheric   returns, D- and E-regions.

Normal Mode

Compression Mode

60 100 140

VIRTUAL HEIGHT (KM)
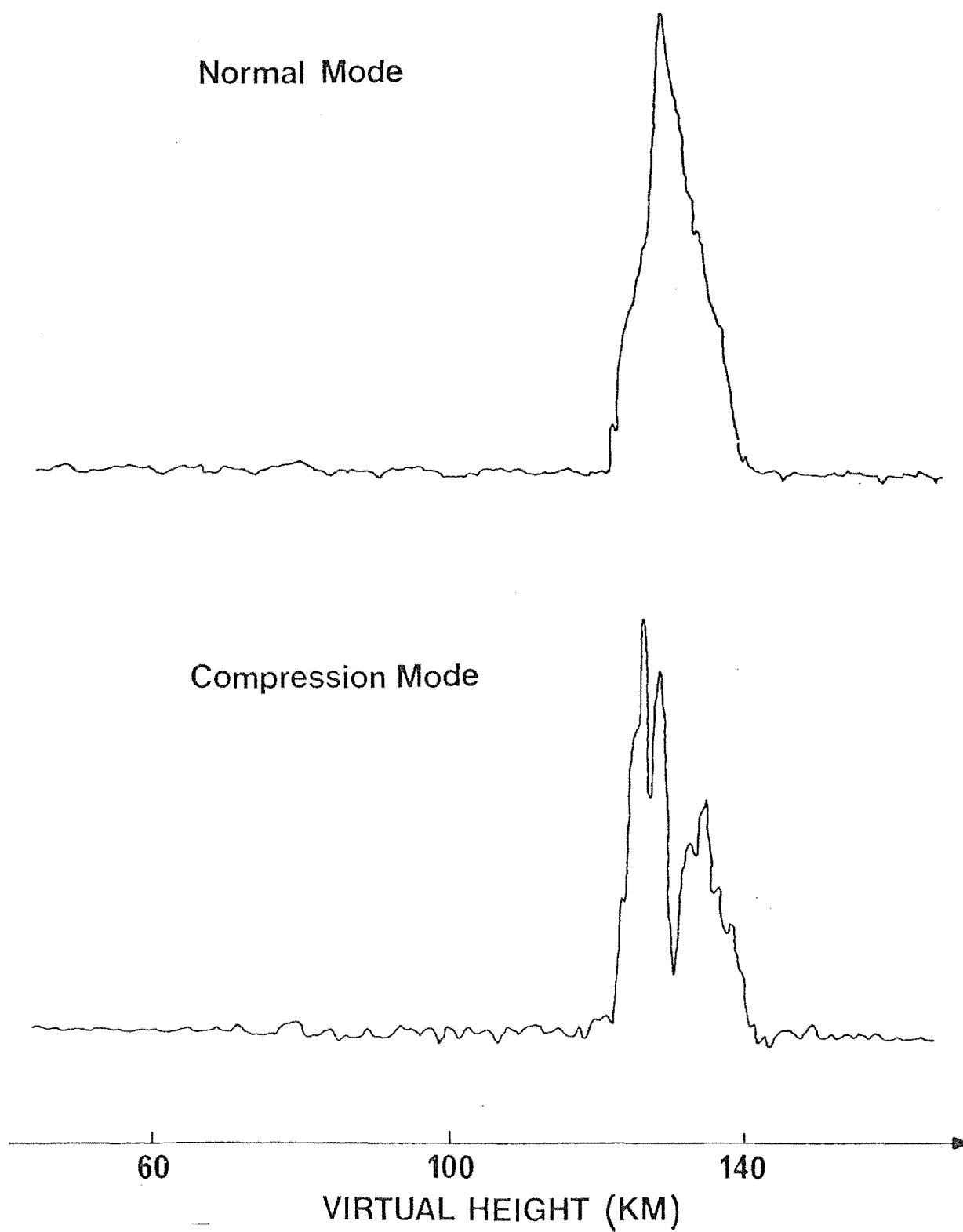
Fig. 10.8: Ionospheric returns, D- and E-regions.

Normal Mode

Compression Mode

260 300 340

VIRTUAL HEIGHT (KM)

Fig. 10.9: Ionospheric returns, F-region.

Normal Mode

Compression Mode

VIRTUAL HEIGHT (KM)
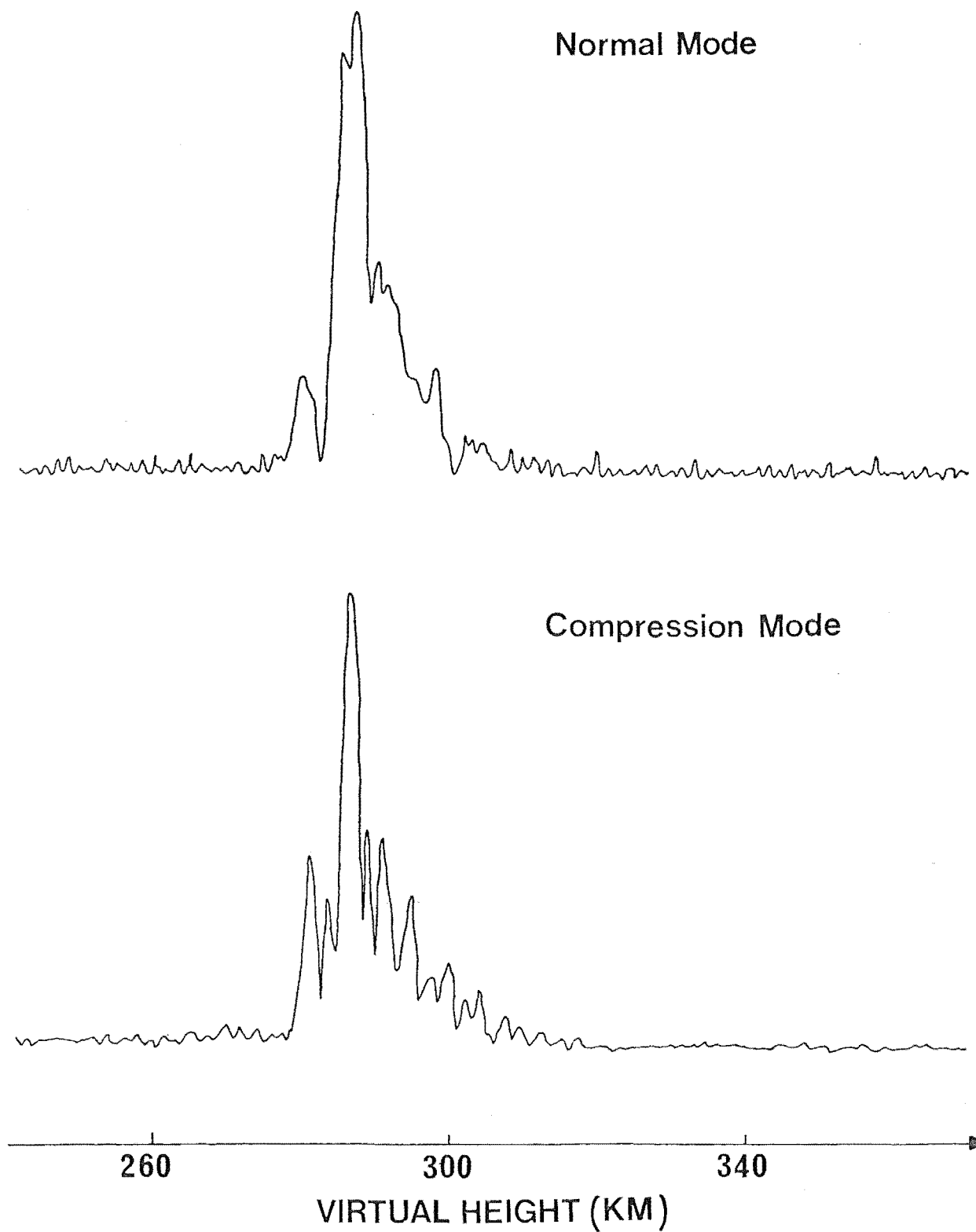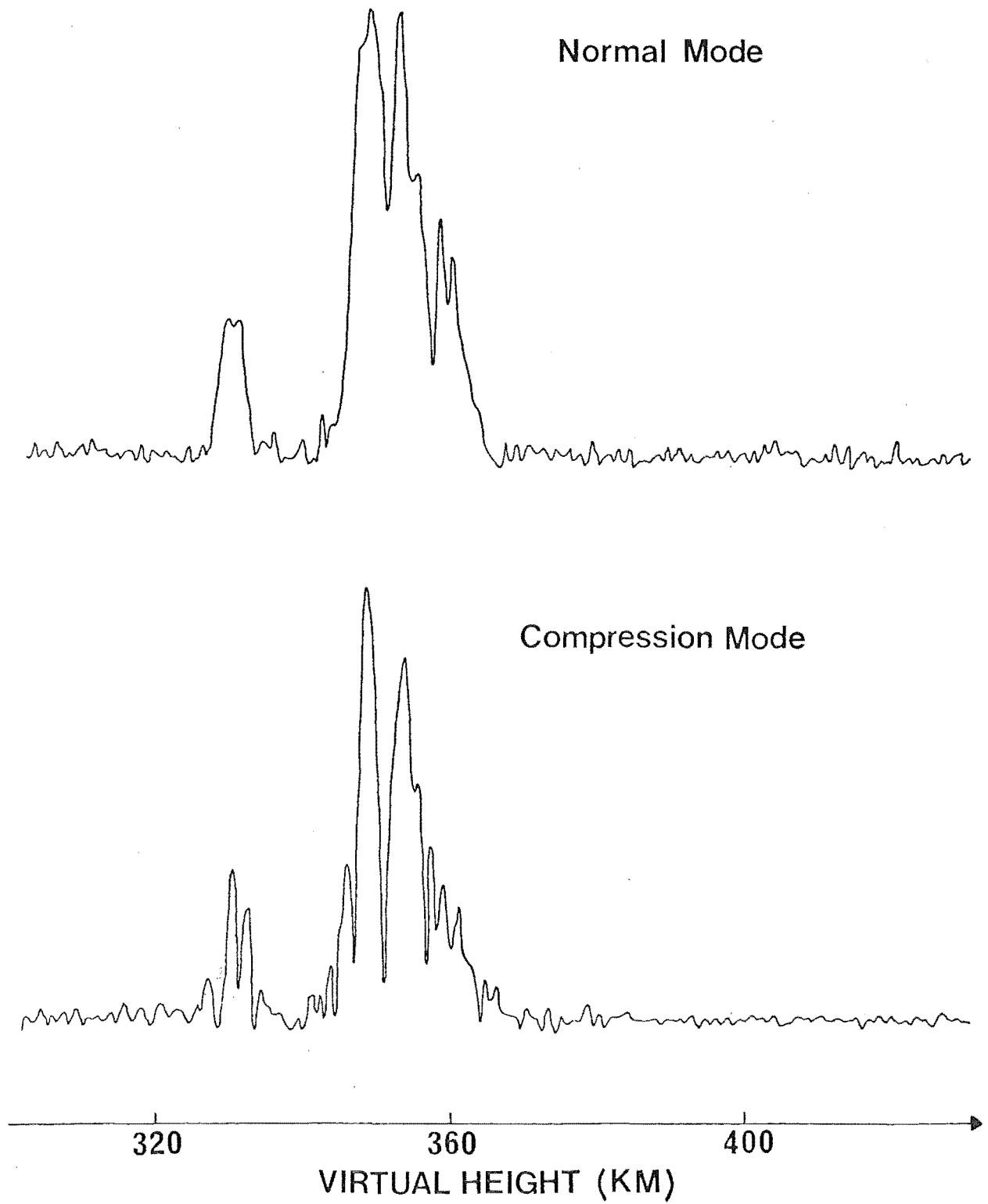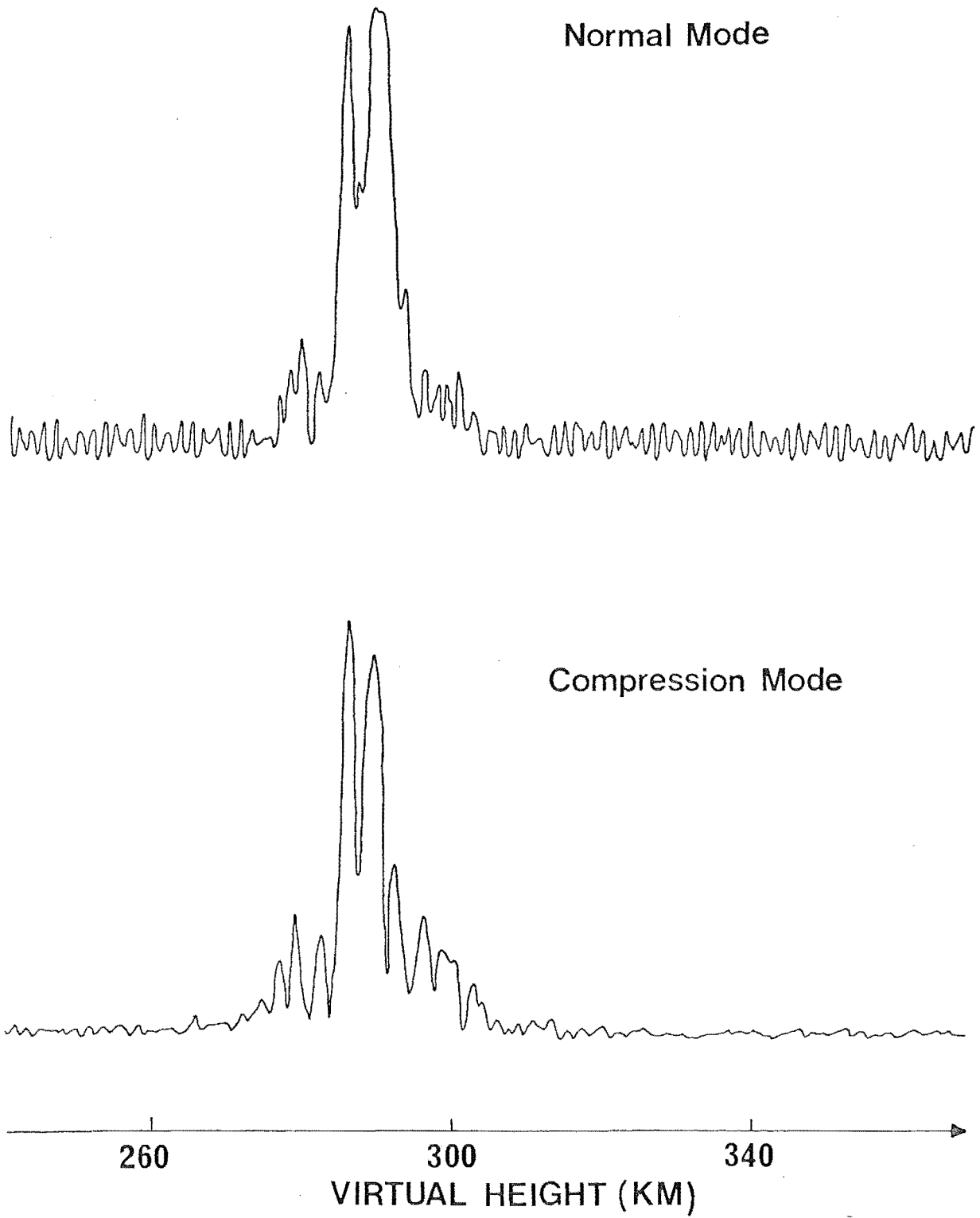
Fig. 10.10: Ionospheric returns, F-region.

Fig. 10.11: Ionospheric returns, F-region.

Figs 10.9 to 10.11 show soundings of the F-region taken between 4 am and 6 am on 15th May, 1978. Fig. 10.9 again indicates that the pulse compression system can show fine structure in the target which is otherwise invisible. Fig. 10.10 is interesting as it shows an example of F-region 'mode-splitting'. Both peaks in this scan in fact originate from the same target; the extraordinary wave always shows greater atten-uation, and is thus the echo which appears to be located about 16 km below the main target. Notice how the essential structure of the target is visible in both the ordinary and extraordinary returns.

Fig. 10.11 is an important plot, in that it shows positive-ly the increased noise-rejection obtainable with the pulse compression system. The periodic noise in the 'normal' scan is actually interference from a communications link operating on a nearby frequency. It can be seen from the 'compression' mode scan that this interference is heavily rejected by the compression filter.

10.4 GENERAL COMMENTS

Results of the system evaluation tests are in general good. There is, however, one area in which the system perfor-mance is well below the design objectives: the overall dynamic range. The degradation of this parameter is fundamentally caused by the system requiring the A-D converter to operate at twice its original design speed. This results in there being insufficient time available for the analogue signals to settle fully after multiplexing, causing a high noise level to be introduced during the conversion process. This noise level is the limiting factor in the system dynamic range. Some means

of circumventing this problem should be found before the pulse
compression radar system is seriously used as a tool for
obtaining ionospheric data. Two possible solutions have been
proposed to date:

1. That the receiver be provided with a separate A-D
converter in each channel - this would remove the necessity for
multiplexing the analogue signals.

2. That the outputs from the receiver be first sampled
and stored by an analogue shift register (charge-coupled device)
(Fairchild, 1977), and later processed by the A-D converter at
a slower rate.

The first of these alternatives would probably be the most
straight-forward and reliable direction to follow; it would,
however, require rather more development and finance to
implement than the second suggestion.

This completes the testing and evaluation of the pulse
compression radar system. Whereas it is presently installed
and operational at Birdling's Flat, some attention should be
paid to the A-D converter in order that the system may realise
its full capabilities.

CHAPTER 11

CONCLUSION

The principal aim of this project has been the development of a radar system capable of resolving the fine structure present in weak ionospheric returns. The pulse compression system described in this thesis does exhibit an overall performance consistent with this requirement, in that it achieves a level of enhancement of both spatial resolution and peak signal power that is in close agreement with that predicted by theory. In addition, the records of ionospheric returns presented in chapter 10 give a direct indication of the effectiveness of the system as a tool for ionospheric observation. In this respect, the present work supports qualitatively the findings of previous workers utilizing pulse compression techniques in the observation of the ionosphere. The work described here may therefore be considered successful. Further, this thesis contains a description of some previously unreported techniques which may have potential significance.

One section of the work which could have a broader application is the development and implementation of the signal processing method. Using the techniques described in chapters 4 and 9, a filter may be realised which can be matched to <u>any</u> signal configuration, without a knowledge of the mathematical form of the signal or its spectrum. Furthermore, this same filter will compensate for any distortions in the generating and receiving systems, and may also apply frequency weighting according to any specified function. It should be noted that

these techniques are entirely general, and will not be res-
tricted to the field of radar signal processing. A further
extension of the method is suggested later in this chapter.

Another aspect of this work which may find future
application is the use of digital techniques in the generation
of the chirp signal. It is recognised that the specific
circuitry described in chapter 5 could be improved somewhat,
given the recent increased availability of microprocessor-
orientated components. For example, a more straightforward
means of generating a specific signal may be to store digitized
samples of the signal in a read-only memory, and read them out
sequentially at a fixed rate. Nevertheless, the 'chirp
generator' does stand as an example of how a complex signal
may be synthesized using digital techniques.

With the radar system installed at the Birdling's Flat
field station, the capability exists for making high-resolution
studies of the lower ionosphere. However, as mentioned in the
previous chapter, attention to the analogue-to-digital converters
is necessary before the system can be fully commissioned.
Future users of the system may also wish to consider the follow-
ing proposal. Whereas the signal processing system described
in this thesis does utilize a filter which is matched to the
signal produced by introducing the output of the chirp generator
directly into the receiver, it cannot compensate for distortions
introduced in the transmitter, the transmitting array, and the
receiving antennas. (The magnitude of these effects is at
present unknown.) A possible means of compensating for these
distortions would be to place some small reflecting target at a
height of about 30 km directly above the field station (e.g. a
large aluminised balloon). If the echo received from this

dummy target were used as the sample signal from which the filter function is derived, the filter obtained would then be truly matched to a real radar return. This procedure would eliminate any uncertainty in the linearity and frequency response of the transmitter and antennas, allowing greater confidence in the interpretation of ionospheric returns.

Nonetheless, the system does have adequate performance without this suggested modification, and will provide the signal power and resolution necessary for any experiment involving studies of ionospheric fine structures.

APPENDIX

Ancillary Electronic Equipment

A.1 GENERAL

The design of any large electronic system which is to be installed in an existing station must be influenced to some extent by certain practical factors relating to the present equipment and resources. This section will thus contain a brief description of the instrumentation existing at Birdling's Flat at the commencement of this project.

With the exception of the transmitters, all the station electronics, including receiving, data processing, and control instrumentation is located in one building at the site, known as the 'receiver hut'. Most of the equipment is constructed in rack-mounted modules, of the type shown in Fig. 5.14. Computer control of equipment is achieved by latching a software-generated 6 bit digital word into any of these modules. The transmitter triggering and power switching functions can likewise be placed under computer control.

Also resident in the receiver hut is the station's frequency standard. This is a temperature controlled crystal oscillator operating at 9.6 MHz. From this are derived all frequencies used for signal transmission, receiver oscillators, and timing functions. A time-of-day clock which is computer accessible is also derived from this source.

The transmitters are located in a caravan about 0.5 km from the receiver hut. Since phase coherence between the transmitted signal and receiver local oscillator is required in some applications, the transmitter RF excitation is derived from

the 9.6 MHz clock in the receiver hut, and conveyed to the transmitter caravan through underground co-axial cables. A 25-pair telephone cable serves to conduct control and trigger signals to the transmitters.

A consideration of prime importance was that the installation of the pulse compression instrumentation must not in any way disable the present radar system; at any time, either of the two modes must be available for use. This fact is responsible for the design philospphy behind some of the control equipment described in the following sections.

A.2   FREQUENCY CONVERTER

The chirp generator requires as its principal input a 17.6 MHz square wave, phase locked to the 9.6 MHz master clock. This frequency is obtained by first dividing the 9.6 MHz by 6, and then multiplying this signal by 11. The multiplication is performed using a Signetics NE562 phase locked loop. A block diagram of a phase locked loop is shown in Fig. A.1.

Briefly, its operation is as follows. The divider, shown with a broken line in Fig. A.1, should be ignored for the purposes of this description. The voltage-controlled oscillator (VCO) is set to some 'free-running' frequency, f_0. When a signal of frequency f_i is applied to the phase locked loop input, a phase detector compares the phase of this signal with that of the VCO, resulting in a signal containing frequencies of $f_i \pm f_0$. If the difference frequency, $f_i - f_0$, is low enough to be passed by the low pass filter, this modifies the frequency of
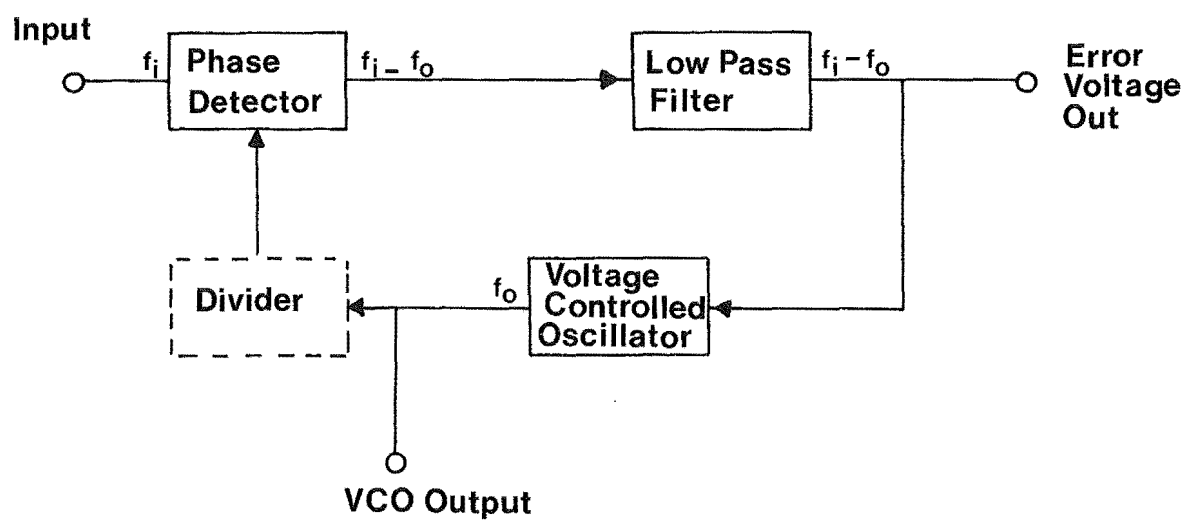
Fig. A.1: A phase locked loop.

the VCO, gradually bringing it closer to that of the input, until it acquires the same frequency. The output of the phase detector is then a DC voltage, which is of sufficient magnitude to keep the VCO locked to the input signal.

A phase locked loop can be made to multiply by n in the following manner. If a divide-by-n circuit is placed between the VCO and the phase detector (see Fig. A.1), the detector 'thinks' that the VCO is operating n times slower than it actually is. Hence, the phase detector can make the VCO lock to an input, or reference frequency, of $f_i = f_0/n$. The VCO will be phase locked to the input signal, but it will be oscillating at n times the frequency.

A circuit of the frequency converter is shown in Fig. A.2, where some of the supporting components around the phase locked loop have been omitted for clarity. The switching transistor in the VCO output provides buffering, and a level shift to TTL voltages. A worst-case drift in the free-running VCO frequency of 5% was assumed; the components for the low pass filter were selected to provide a 'capture range' for the phase locked loop of this magnitude.

A.3 MODE CONTROL AND LINE DRIVER

In order that a change between 'normal' and 'compression' modes of operation be easily instigated, a small piece of circuitry was developed which selects either the chirp generator output, or a continuous 4.8 MHz signal as the RF excitation to the transmitter. Depending on which signal is selected, this circuit also changes the state of a control line (known as the
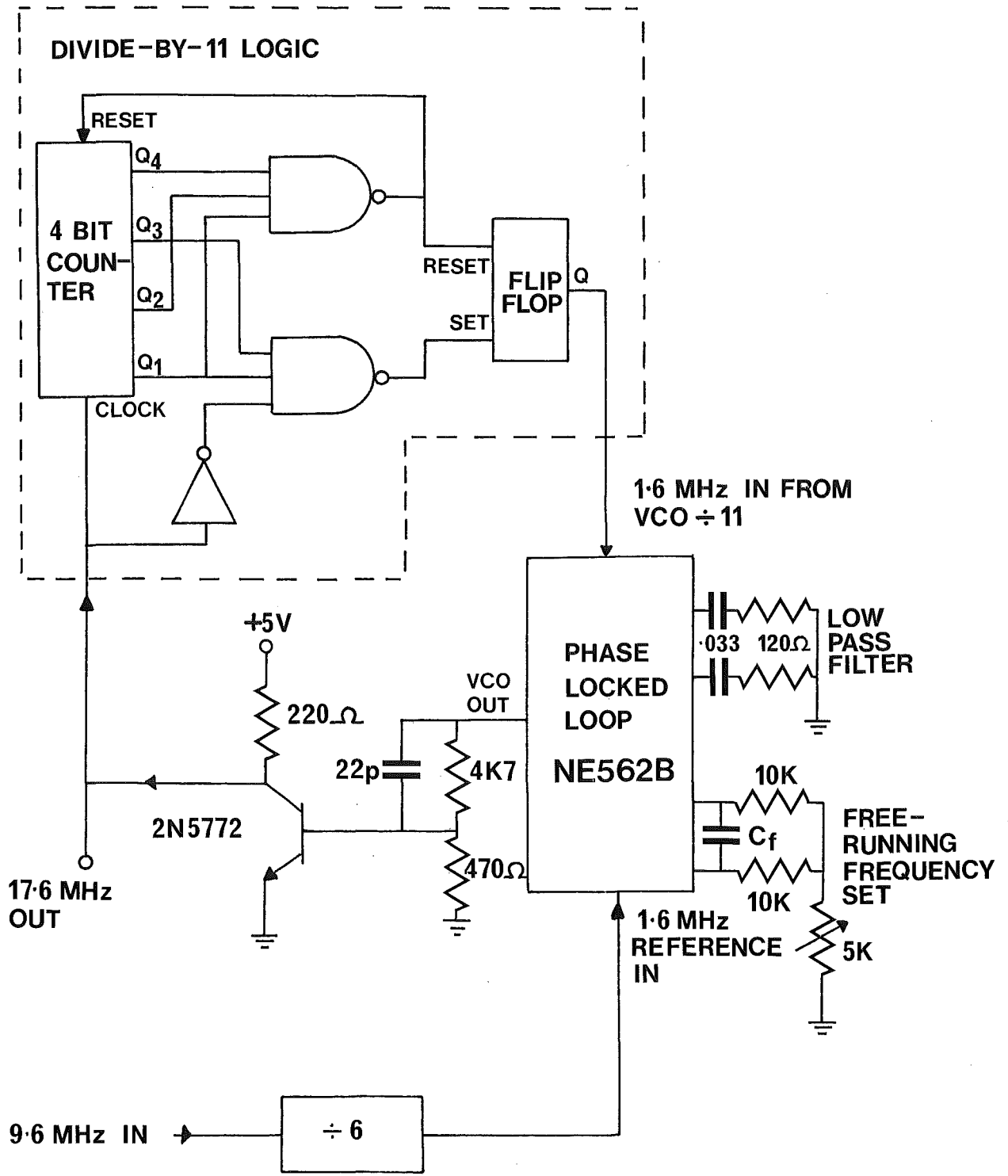
Fig. A.2: Frequency converter circuit.

'mode control' line) to the transmitter gating control, in order that this unit might gate the transmitter accordingly.

The circuit diagram for this device is shown in Fig. A.3. The selection of 'normal' or 'compression' mode may be carried out either manually, or by computer. The mode control line driving circuitry is heavily filtered to suppress any transient signals appearing for any reason on the control line. The line driver for the RF signal is a single integrated circuit (a DM8830) which provides a balanced digital output of 10V peak-to-peak.

A.4 REMOTE PULSE WIDTH CONTROL

During the conceptual design of the transmitter control functions, it was recognised that the ability to change the transmitter pulse width from the receiver hut was a rather desirable feature; since the transmitter gating circuitry was being completely rebuilt, this capability was included.

The pulse width information is conveyed to the transmitter caravan through three control lines, representing 10 μsec, 20 μsec, and 40 μsec respectively. Additive combinations of any of these three lines are permitted, providing pulse widths from 10 μsec to 70 μsec in 10 μsec increments. Each line is asserted, if required, either by switches on the front panel of the 'remote pulse width control' unit, or by computer control. The three lines are driven by circuitry identical to that driving the mode control line described in the previous section.
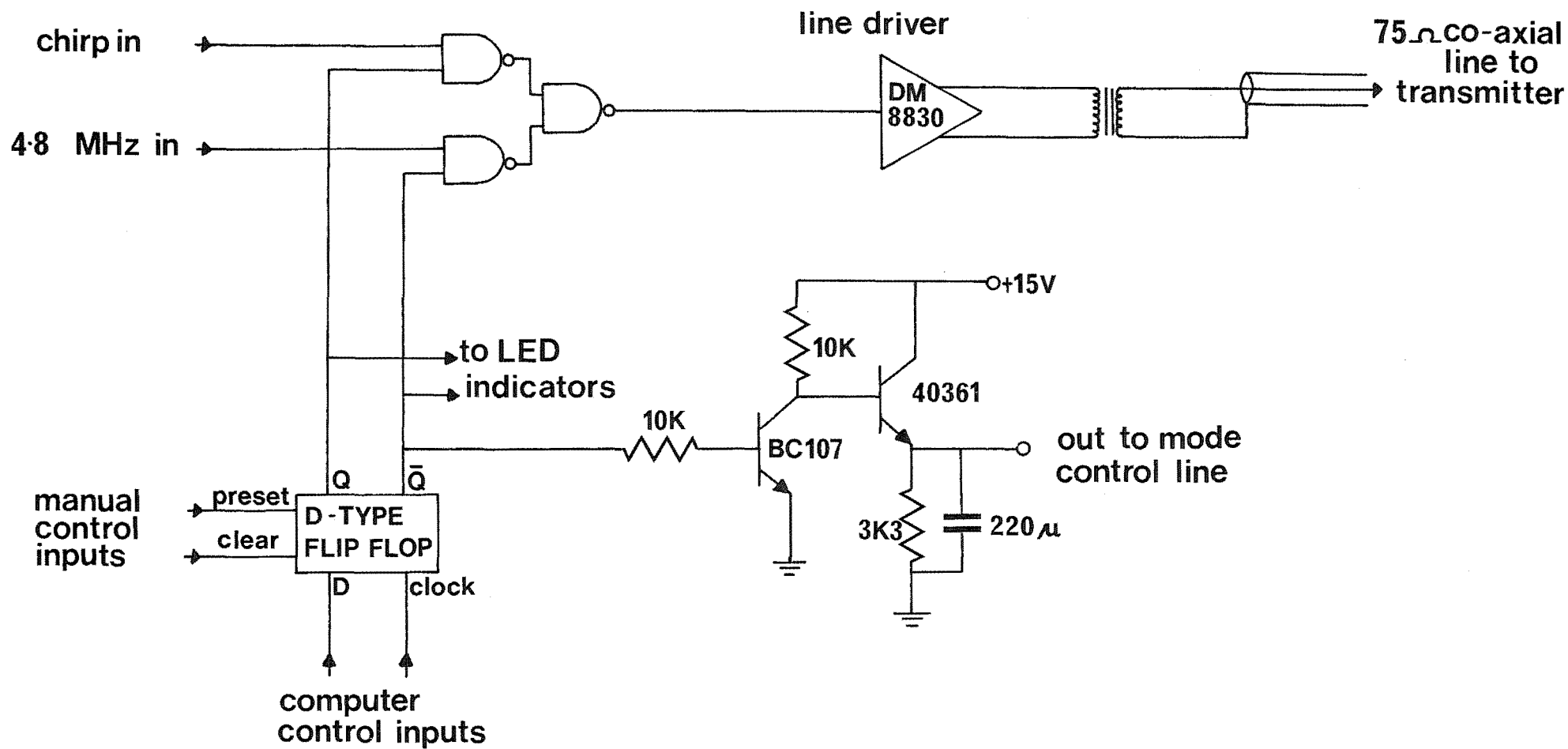
Fig. A.3: Mode control and line driver circuit.

A.5 TRANSMITTER GATING CONTROL

A single unit at the transmitter site, the '2.4 MHz transmitter gating control', decodes the pulse width information, and provides appropriate transmitter gating pulses in both the 'normal' and 'compression' modes. A block diagram of the device is shown in Fig. A.4.

In the 'normal' mode, 4.8 MHz appears continuously at the RF input. The line receiver shapes this input and converts it to TTL levels. After division to 2.4 MHz, this signal is applied to the transmitter exciter input. When a trigger signal (a very short 100 volt pulse) is received, this is shaped and used to trigger a TTL monostable multivibrator, which generates a pulse for gating the transmitter. The width of this pulse is determined by the state of the three pulse width control lines from the receiver hut. If desired, this pulse width may be overridden by switches on the front panel of the unit.

In the 'compression' mode, chirp pulses appear at the RF input. The presence of these pulses is detected by a retriggerable monostable, the pulse width of which is slightly longer than one period of the chirp signal. The output of this monostable will thus be high for the duration of the chirp pulse only; this output is then used as the transmitter gating signal. The falling edge of this signal is also used to reset the $\div 2$ flip-flop in the RF output, to ensure that successive chirps all have the same phase.

A detailed circuit diagram of the RF line receiver is presented in Fig. A.5. The RF signal is at an amplitude of about 100 mV peak-to-peak by the time it reaches the transmitter site. This signal is first amplified by a linear RF
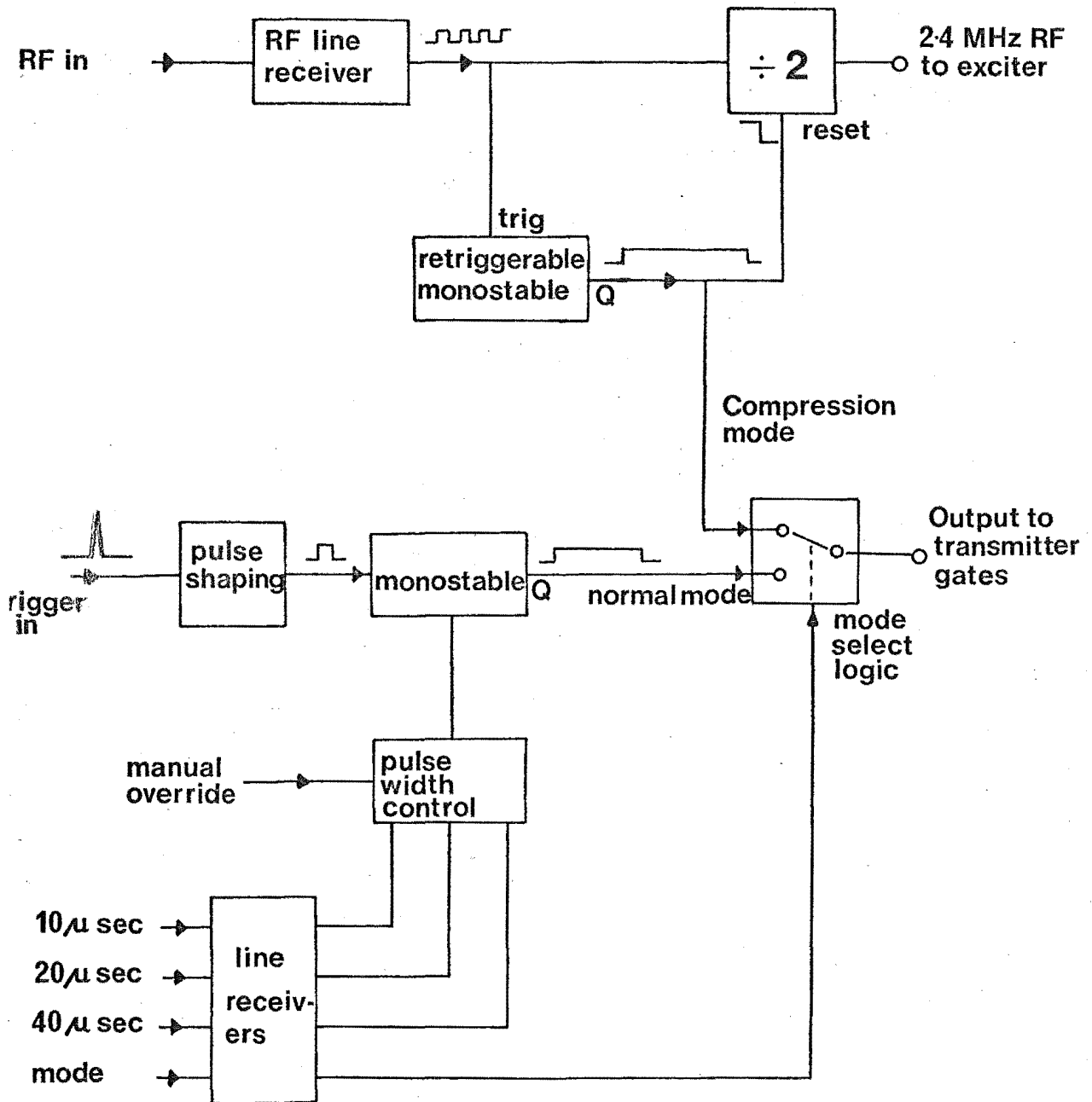
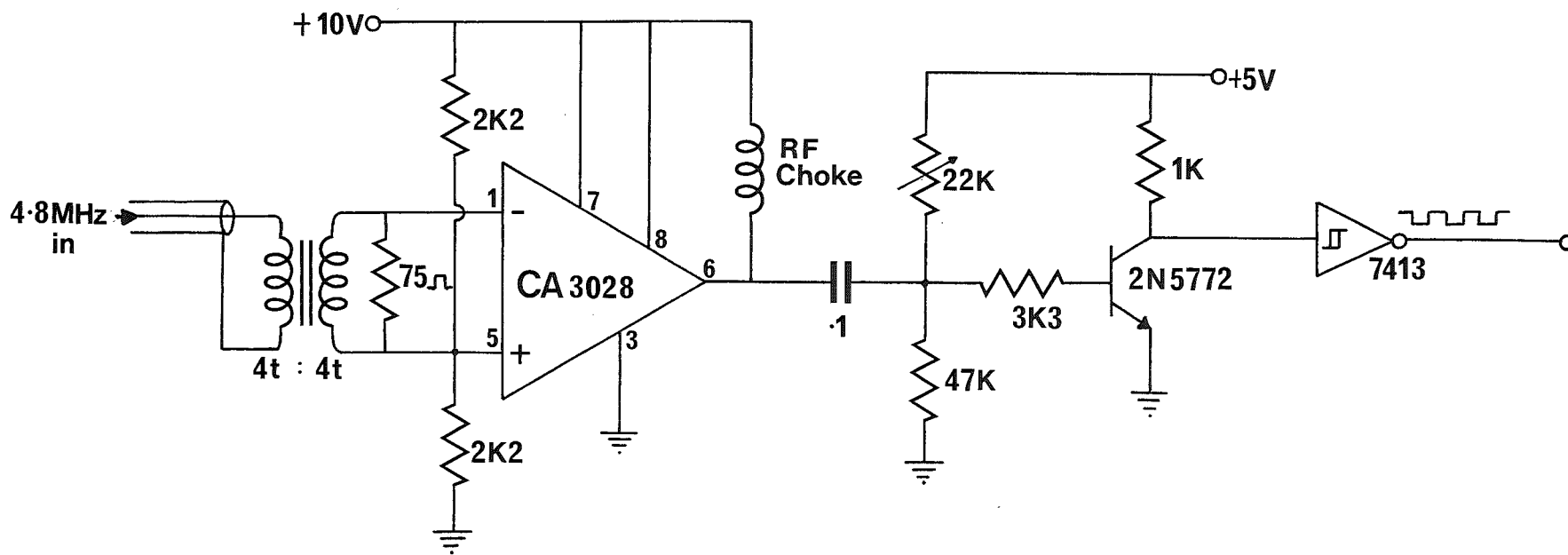Fig. A.4: Block diagram of transmitter gating control.

Fig. A.5: RF line receiver circuit.

amplifier (a CA3028), and the zero crossings detected by a switching transistor. The resulting square wave is then shaped by a Schmidt trigger, and the signal passed into a TTL divider. The complementary outputs of this divider then feed directly the grids of two push-pull pentodes in the transmitter exciter.

Fig. A.6 shows the pulse width control circuitry in more detail. The switching transistor and Schmidt trigger at the 'trigger' input convert the 100V trigger pulse to TTL levels and shape, when it is used to trigger the pulse width mono-stable. Control of pulse width is achieved by switching various capacitors independently into the timing circuit, using a triple analogue switch actuated by the pulse width control lines. In this manner it is possible to select any pulse width from 10 μsec to 70 μsec in 10 μsec steps.
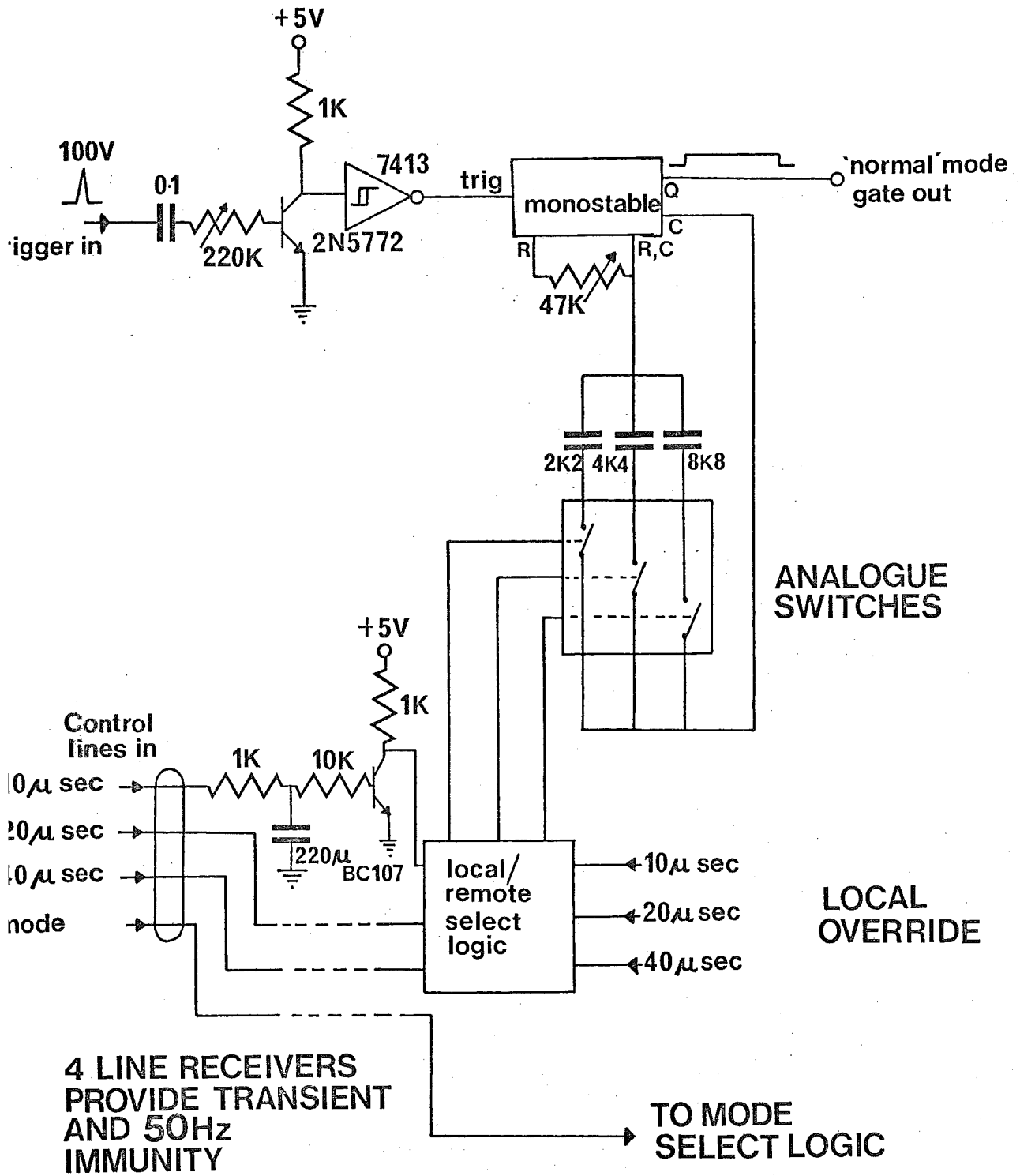
Fig. A.6: Pulse width control circuitry.

REFERENCES

ALTSCHULER, M. 1960: The measurement of self and mutual impedances. IRE Trans. Antennas and Propagation AP-8, p.526.

AUSTIN, G.L. 1966: Measurement of lower ionospheric refractive indices. Thesis, M.Sc., University of Canterbury.

BARRY, G.H. and FENWICK, R.B. 1965: Extraterrestrial and ionospheric sounding with synthesized frequency sweeps. Hewlett-Packard J. 16, no.11, p.8.

BLACK, A.W. 1978: Private communication.

BLACKMAN, R.B. and TUKEY, J.W. 1958: The measurement of power spectra. Dover Publications.

BONGIANNI, W.L. 1971: Pulse compression using non-linear interaction in a surface acoustic wave convolver. Proc. IEEE 39, p.713.

BRANDON, P.S. 1965: The design methods for lumped-constant dispersive networks suitable for pulse compression radar. Marconi Review 28, p.225.

BRIGHAM, E.O. 1974: The Fast Fourier Transform. Prentice-Hall Inc.

BRIGHAM, E.O. and MORROW, R.E. 1967: The Fast Fourier Transform. IEEE Spectrum 4, p.63.

BURROWS, C.R. 1938: The exponential transmission line. Bell System Tech. J. 17, p.555.

CHIN, J.E. and COOK, C.E. 1959: The mathematics of pulse compression - a problem in systems analysis. Sperry Engineering Review 12, p.11.

COLLIN, R.E. 1956: The optimum tapered transmission line matching section. Proc. IRE 44, p.539.

COOK, C.E. 1960: Pulse compression - key to more efficient radar transmission. Proc. IRE 48, p.310.

COOK, C.E. 1961: General matched-filter analysis of linear pulse compression. Proc. IRE 49, p.831.

COOK, C.E. and PAOLILLIO, J. 1964: A pulse compression pre-distortion function for efficient sidelobe reduction in a high power radar. Proc. IEEE 52, p.377.

COOK, C.E., PAOLILLIO, J., BERNFIELD, M. and PALMIERI, C.A. 1964: Matched filtering, pulse compression and waveform design (part 2). Microwave J. 7, p.81.

COOLEY, J.W. and TUKEY, J.W. 1965: An algorithm for the machine computation of complex Fourier series. Math. Comput. 19, p.297.

COOPER, J. 1978: Atmospheric Physics: A study of numerical diffraction models and of F-region travelling ionospheric disturbances. Thesis, Ph.D., University of Canterbury.

CUTRONA, L.J., LEITH, E.N., PALERMO, C.J. and PORCELLO, L.J. 1960: Optical data processing and filtering systems. IRE Trans. Information Theory IT-6, p.386.

DARLINGTON, S. 1954: U.S. patent no. 2, 678, 997.

DICKE, R.H. 1953: U.S. patent no. 2, 624, 876.

DOLPH, C.L. 1946: A current distribution which optimises the relationship between beamwidth and sidelobe level. Proc. IRE 34, p.335.

ECHARD, J.D. and BOORSTYN, R.R. 1972: Digital filtering for radar signal processing applications. IEEE Trans. Audio and Electroacoustics AU-20, p.42.

FAIRCHILD, 1977: An introduction to charge coupled devices.
Fairchild Semiconductor Components division.

FENWICK, R.B. and BARRY, G.H. 1965: Step by step to a linear
frequency sweep. Electronics 38, no. 15, p.66.

FITCH, A.H. 1960: A comparison of several dispersive ultra-
sonic delay lines using longitudinal and shear waves in
strips and cylinders. IRE Int. Conv. Record 8, pt. 6,
p.284.

FRASER, G.J. 1965: The measurement of atmospheric winds at
altitudes of 64-120 km using ground based radio equipment.
J. Atmos. Sci. 22, p.217.

FRASER, G.J. 1968: Seasonal variations of southern hemispheric
mid-latitude winds at altitudes of 71-100 km. J. Atmos.
Terr. Phys. 30, p.707.

FRASER, G.J. 1973: On-line control and data collection for
ionospheric experiments. Paper presented at the 9th N.Z.
National Electronics Conference, Christchurch, August 1973.

GARDNER, F.F. and PAWSEY, J.L. 1953: Study of the ionospheric
D-region using partial reflections. J. Atmos. Terr. Phys.
3, p.321.

GNANALINGUM, S. 1954: An apparatus for the detection of weak
ionospheric echoes. Proc. Inst. Elec. Eng. 101 pt. 3,
p.243.

GRASSE, C.L. 1971: A 400 MHz acoustic surface wave pulse
expansion and compression filter. IEEE Trans. Microwave
Theory and Techniques MTT-19, p.558.

GRAY, G.A. and NATHANSON, F.E. 1971: Digital processing of
radar signals. IEEE EASCON '71 Record, p.208.

GRIFFIN, D.R. 1950: Measurements of the ultrasonic cries of
     bats. J. Acoustical Soc. of America, 22, p.247.

HALPERN, H.M. and PERRY, R.P. 1971: Digital matched filters
     using Fast Fourier Transforms. IEEE EASCON '71 Record, p.
     222.

HART, J.K. and SHEATS, L. 1971: Application of pipeline FFT
     technology in radar signal and data processing. IEEE
     EASCON '71 Record, p.216.

HELMS, H.D. 1968: Non-recursive digital filters: design
     methods for achieving specifications on frequency response.
     IEEE Trans. Audio and Electroacoustics AU-16, p.336.

HUTTMAN, E. 1940: German Patent no. 768,068.

KEIHN, 1974: Applications of the RCA-CA3028A and CA3028B
     integrated-circuit RF amplifiers in the HF and VHF ranges.
     In RCA Linear Application Notes, 1974.

KIBBLER, G.O.T.H. 1968: The CLFM: A method of generating
     linear frequency coded pulses. IEEE Trans. Aerosp.
     Elec. Sys. AES-4, p.385.

KING, R.W.P. and HARRISON, C.W. 1969: Antennas and waves.
     MIT Press.

KLAUDER, J.R., PRICE, A.C., DARLINGTON, S. and ALBERSHEIM, W.J.
     1960: The theory and design of chirp radars. Bell Syst.
     Tech. J. 39, p.745.

KRAUS, J.D. 1950: Antennas. McGraw-Hill.

LILLY, J.C. 1967: The mind of the dolphin. Doubleday and Co.
     Inc.

LYNN, M.P. 1975: Program PLOTARRAY - a Fortran program for
     the B6700. Unpublished.

MANSON, A.H. 1965: Electron densities in the lower ionosphere. Thesis, Ph.D., University of Canterbury.

MOTOROLA, 1971: Linear integrated circuits data book. Motorola.

O'MEARA, T.R. 1959. The synthesis of band-pass all-pass time delay networks with graphical approximation techniques. Hughes Res. Report, no. 114.

PEEBLES, P.Z. and STEVENS, G.H. 1965: A technique for the generation of highly linear FM pulse radar signals. IEEE Trans. Mil. Elec. MIL-9, p.32.

RADER, C. and GOLD B. 1967: Digital filter design techniques in the frequency domain. Proc. IEEE 55, p.149.

REICH, A. and SLOBODIN, L. 1961: Optical pulse expansion/compression. NAECON Proc. 8, p.163.

RINNERT, K., SCHLEGEL, K. and KRAMM, R. 1976: A partial reflection experiment using the FM-CW technique. Radio Sci. 11, p.1009.

ROTHMAN, J. 1968: A Fast Fourier Transform subroutine for complex data. DECUS Program Library, no. 8-144.

RUMSEY, V.H. 1950: The design of frequency-compensating matching sections. Proc. IEEE 38, p.1191.

SHEARMAN, J. 1962: An investigation of atmospheric ionization up to an altitude of 100 kms. Thesis, M.Sc., University of Canterbury.

SHIRLEY, F.R. 1968: A synchronous sweep frequency oscillator. IEEE Trans. Instrum. and Meas. IM-17, p.80.

SLOBODIN, L. 1963: Optical correlation technique. Proc. IEEE 51, p.1782.

TAYLOR, T.T. 1955: Design of line source antennas for narrow beamwidths and low sidelobes. IRE Trans. Antennas and Propagation AP-3, p.16.

TEMES, C.L., CITRIN, A., LAVIOLA, M.A., BOYCE, H.K. and BIGGS, J.P. 1963: Pulse compression system for a down-range tracker. IEEE Int. Conv. Record 11, pt. 8, p.71.

TITHERIDGE, J.E. 1962: The stratification of the lower ionosphere. J. Atmos. Terr. Phys. 24, p.283.

VETTORI, G. 1971: Digital generation of a linear FM pulse of given time-bandwidth product. Alta Frequenza 40, p.140.

VON BIEL, H.A. 1975: Private communication.

WHEELER, H.A. 1939: Transmission lines with exponential taper. Proc. IRE 27, p.65.

WIPPERMAN, D.R. 1967: The application of pulse compression to ionospheric sounding. Aeronomy Report no. 16, University of Illinois, Urbana.

WRATT, D.S. 1974: Atmospheric Physics: Electron density variations in the mesosphere. Thesis, Ph.D., University of Canterbury.

WOODWARD, P.M. 1953: Probability and information theory, with applications to radar. McGraw-Hill, New York.

ACKNOWLEDGEMENTS

I have received assistance from many people during the course of this work. My supervisor, Dr Andreas von Biel, has been particularly helpful, when called upon, in solving the many problems which have arisen from time to time. It is, however, those people who has assisted me 'above the call of duty', to whom this note is primarily addressed. Firstly, my colleagues:

Murray Lynn, who spent considerable time developing and upgrading some of the station hardware at Birdling's Flat, and who also contributed substantially to my knowledge of electronics;

Murray Smith, who pioneered the implementation of the FFT routine on the PDP8, and taught me some advanced programming techniques;

Justin Cooper, who educated me in certain practical aspects of making antenna bridge measurements, including several interesting techniques for clearing sheep from under an antenna prior to making a measurement.

The electronics technicians in the Physics Department, Ian Foster, John de Voil, and Ray Borrell have always been most forthcoming with their assistance in the design of various pieces of electronic equipment, both for this project, and for some of my 'foreigners'.

Dr Grahame Fraser has given me considerable assistance with various aspects of the installation at Birdling's Flat. In particular, he has shown me several good techniques for dealing with a bad-tempered PDP8.

Finally, I wish to thank Dr R.G.T. Bennett. While his direct contribution to this project may not have been great, he has helped me, over the years, to view scientific work, and this thesis in particular, in their correct perspective. An encounter with Bennett is the difference between a mediocre day and a special day.

<div style="text-align: right">

Steve Krenek

June, 1978

</div>